Title
The Supersonic Project: Supersonically Induced Gas Objects in the Early Universe

Author
Chiou, Yeou Shya

Publication Date
2020

Peer reviewed|Thesis/dissertation

UNIVERSITY OF CALIFORNIA

Los Angeles

The Supersonic Project: Supersonically Induced Gas Objects in the Early Universe

A dissertation submitted in partial satisfaction
of the requirements for the degree
Doctor of Philosophy in Physics

by

Yeou Shya Chiou

2020

ABSTRACT OF THE DISSERTATION

The Supersonic Project: Supersonically Induced Gas Objects in the Early Universe

by

Yeou Shya Chiou
Doctor of Philosophy in Physics
University of California, Los Angeles, 2020
Professor Smadar Naoz, Chair

The puzzling origins of globular clusters have been greatly debated over the years. We present a new formation channel for globular clusters, linking them to objects that formed without dark matter (DM) in the early Universe in the presence of a supersonic relative velocity between baryons and DM. This stream velocity arises due to the drop in radiation pressure of baryons from matter-radiation decoupling and induces a physical separation between baryonic and DM overdensity peaks. This effect gives rise to gas dominant objects with little to no DM. These gas-rich structures, called Supersonically Induced Gas Objects (SIGOs), form naturally outside of DM halos as a consequence of the stream velocity. In this thesis, we present a detailed investigation of the physical properties of SIGOs, which leads to a promising connection to globular clusters.

One of the physical parameters often invoked to understand galaxy formation is the spin parameter of halos, which characterizes galaxies' rotational structure. We, thus, first investigate the spins of DM halos and SIGOs with stream velocity. We find that the spin parameter of DM halos follows a lognormal distribution, and the median increases and the misalignment angle between the angular momenta of baryons and DM has a nearly isotropic distribution. We generalize the spin parameter to SIGOs and find that they also have a lognormal distribution. Furthering existing hydrodynamic AREPO simulations by including radiative cooling, we find that this cooling channel has negligible effects on SIGO properties compared to only adiabatic cooling. We find that SIGOs density is high enough to allow stars to form using a simple density threshold criterion based on the balance of gravity and thermal/turbulent energy. Then, we model the star formation process and estimate the luminosity of the first star clusters within a SIGO. We find that SIGOs occupy a different part of the luminosity-mass parameter space than classical DM halos with gas. We further adopt a simple model to evolve the SIGOs to present-day and show that their masses, radii, and luminosities are consistent with present-day (local) globular clusters. Since the stream velocity is coherent over scales of a few Mpc, we predict that if this is the dominant mechanism for globular clusters, the abundances of galaxies hosting global clusters vary significantly over these scales. The upcoming *James Webb Space Telescope* will elucidate the mysteries of the first galaxies and will further shed light on the link between SIGOs as progenitors to globular clusters.

The dissertation of Yeou Shya Chiou is approved.

Steven Furlanetto

Alice Shapley

Tommaso Treu

Smadar Naoz, Committee Chair

University of California, Los Angeles

2020

To my grandmother, Meme,...

who taught me a love of learning

and to always be curious

TABLE OF CONTENTS

LIST OF FIGURES

LIST OF TABLES

ACKNOWLEDGMENTS

I am deeply indebted to my advisor Smadar Naoz, who always believed in me and knew I could accomplish great things. They say your advisor really makes or breaks your grad school career. I didn't truly believe this until I met Smadar. Under her mentorship, I have learned invaluable research and life skills that I will take with me in my next chapter in life.

I would also like to extend my deepest gratitude to my collaborators, Federico Marinacci, Mark Vogelsberger, and Blakesley Burkhart who helped improved my technical and written skills. I am also indebted to Cristina Popa who helped me get up to speed on this project.

I must also thank all the members of the Naoz group, Bao-Minh Hoang, Alexander Stephan, Sanaea Rose, and Jesus Salas, for their support and feedback on presentations. I am also grateful to Rick Mebane and Kevin Hayakawa for helping me fill in some gaps in my astrophysics knowledge.

Many thanks to my committee, Steven Furlanetto, Alice Shapley, and Tommaso Treu for their time and guidance in reviewing this manuscript and and its defense.

Grad school would not have been possible without the support of Justin Faber, Alec Vinson, and Dominic Reiss, my friends since day one of UCLA. Thanks for the crazy nights and enlightening conversations that really helped me grow as a person.

I greatly appreciate Jen Larkin, Kevin Strawn, Sharon Morrison, John Blondin, Stephen Reynolds, Alina Duca and the many teachers, professors, and mentors that taught me so much about the world.

I cannot begin to express my thanks to my grandmother, Joyce Warner, who showed me the value of learning and taught me to never give up in the pursuit my dreams.

I am extremely grateful to my mom, Diana Tran, whose tireless sacrifices and efforts in raising me brought me to where I am today. Mom, I did it! I got my PhD!

Lastly, I want to extend a warm thanks to all of my wonderful friends that saw me through this long, crazy journey to get my PhD!

VITA

2008–2012	B.S in Physics, B.S. in Mathematics, North Carolina State University (NCSU)
2012–2014	M.S. in Physics, NCSU
2014–Present	Ph.D. Candidate in Physics, University of California, Los Angeles (UCLA)
2019–2020	Dissertation Year Fellowship, Graduate Division, UCLA

PUBLICATIONS

Y. S. Chiou, S. Naoz, F. Marinacci, and M. Vogelsberger. The Supersonic Project: rotational effects of supersonic motions on the first structures in the Universe. MNRAS, 481(3):3108–3117, December 2018.

Y. S. Chiou, S. Naoz, B. Burkhart, F. Marinacci, and M. Vogelsberger. The Supersonic Project: Shining Light on SIGOs—A New Formation Channel for Globular Clusters. ApJ, 878(1):L23, Jun 2019.

Y. S. Chiou, S. Naoz, B. Burkhart, F. Marinacci, and M. Vogelsberger. The Supersonic Project: To Cool or Not To Cool SIGOS? (In preparation, 2020)

CHAPTER 1

Introduction

1.1 Background and Motivation

The early Universe was homogeneous and isotropic with perturbations seeded by a period of inflation. Dark matter (DM) overdensities started to grow logarithmically with the scale factor during radiation-dominated era and then linearly during the matter-dominated era. Baryonic matter, on the other hand, was tightly coupled to radiation via Compton scattering and so baryonic overdensities could not grow. As the Universe expanded and cooled, baryons and radiation decoupled giving rise to the period of recombination and hence baryons could start to cluster. Since the baryons were no longer coupled to radiation, they could fall into the deep gravitational potential wells built by the DM overdensities. Without the radiation pressure, the baryonic sound speed dropped precipitously from $c/\sqrt{3}$ to thermal velocities and hence yielding a bulk relative velocity between the DM and baryons. It was shown in Tseliakhovich and Hirata (2010) that this relative velocity was actually supersonic. Below we give a brief pedagogical introduction following Tseliakhovich et al. (2011).

This supersonic relative velocity, also known as the "stream velocity", $v_{\rm bc}$ can be written as

$$\mathbf{v}_{\rm b\mathbf{c}}(\mathbf{k}) = \frac{\hat{\mathbf{k}}}{ik}(\theta_b(\mathbf{k}) - \theta_c(\mathbf{k}), \tag{1.1}$$

where $\hat{\mathbf{k}}$ is the unit vector in the direction of the wave vector k and $\theta = a^{-1}\nabla \cdot \mathrm{v}$ is the velocity divergence (and a is the scale factor, working in comoving coordinates).

The variance is given by

$$\begin{aligned}\langle v_{\rm bc}^2(\mathrm{x})\rangle &= \int \frac{dk}{k}\Delta_\zeta^2(k)\left[\frac{\theta_b(k)-\theta_c(k)}{k}\right]^2 \\ &= \int \frac{dk}{k}\Delta_{v_{\rm bc}}^2(k),\end{aligned} \tag{1.2}$$

where $\Delta_\zeta^2(k) = 2.42 \times 10^{-9}$ is the initial curvature perturbation per ln k. Integrating the variance at the time of recombination $z_{\rm rec} = 1020$ yields that DM moves relative to baryons with an rms velocity of $\sigma_{{\rm v}bc} \sim 30$ km sec^{-1} which corresponds to a Mach number of $\mathcal{M} = v_{\rm bc}/c_s \sim 5$ where c_s is the speed of sound. The consequence of this supersonic relative velocity allows baryons to advect out of the DM potential wells and significantly suppresses the growth of structure at wave numbers higher than

$$k_{\rm vbc} = \left.\frac{aH}{\langle v_{\rm bc}^2(\mathrm{x})\rangle^{1/2}}\right|_{\rm dec} = \frac{k_{\rm J}}{\mathcal{M}} \sim 40\ \mathrm{Mpc}^{-1}, \tag{1.3}$$

where $k_{\rm J}$ is the Jeans wavenumber. Since the stream velocity is coherent over scales of a few comoving Mpc, the velocity in a coherence patch can be described by a three-dimensional Gaussian probability distribution with variance

$$\sigma_{{\rm v}bc}^2 = \langle |v_{\rm bc}(\mathrm{x}|^2)\rangle \tag{1.4}$$

The system of equations needed to solve for the DM and baryon overdensities, $\delta_{c,b} = \rho_{c,b}/\bar{\rho}-1$, (where $\bar{\rho}$ is the average density of the Universe) as well as their velocity divergences, $\theta_{c,b}$, in the presence of a background stream velocity is

$$\begin{aligned}\frac{\partial \delta_c}{\partial t} &= \frac{i}{a}\mathbf{v}_{\mathbf{bc}}\cdot\mathbf{k}\delta_c - \theta_c, \\ \frac{\partial \theta_c}{\partial t} &= \frac{i}{a}\mathbf{v}_{\mathbf{bc}}\cdot\mathbf{k}\theta_c - \frac{3H_0^2}{2}(\Omega_c\delta_c + \Omega_b\delta_b) - 2H_0\theta_c, \\ \frac{\partial \delta_b}{\partial t} &= -\theta_b,\end{aligned}$$

and

$$\frac{\partial \theta_b}{\partial t} = -\frac{3H_0^2}{2}(\Omega_c\delta_c + \Omega_b\delta_b) - 2H_0\theta_b + \frac{k^2}{a^2}\frac{k_\mathrm{b}\bar{T}}{c^2\mu m_\mathrm{H}}(\delta_b + \delta_T), \tag{1.5}$$

where we have included the first-order scale-dependent temperature fluctuations which were shown to be important in Naoz and Barkana (2005a). The temperature fluctuations obey

$$\frac{\mathrm{d}\delta_T}{\mathrm{d}t} = \frac{2}{3}\frac{\mathrm{d}\delta_b}{\mathrm{d}t} + \frac{x_\mathrm{e}(t)}{t_\gamma}a^{-4}\left[\delta_\gamma\left(\frac{\bar{T}_\gamma}{\bar{T}} - 1\right) + \frac{\bar{T}_\gamma}{\bar{T}}(\delta_{T_\gamma} - \delta_T)\right]. \tag{1.6}$$

In the above equations, Ω_c and Ω_b are the present-day DM and baryonic densities, H_0 is the present-day value of the Hubble constant H, m_H is the mass of hydrogen, δ_γ, δ_T, and δ_{T_γ} are the fluctuations of the photon density, mean baryon temperature $\bar{T}$ and mean photon temperature T_γ, $x_\mathrm{e}(t)$ is the electron fraction out of the total number density of gas particles, μ is the mean molecular weight, and $t_\gamma^{-1} = 8.55 \times 10^{-13}$ yr^{-1}.

This effect has often been neglected in the literature mostly because it is a formally second order effect in perturbation theory as seen in Equation 1.5. These are still included because the expansion parameter for these terms is not the density perturbation δ but rather the ratio of the advection terms to the linear terms. This ratio is

$$\frac{v_\mathrm{bc}k}{aH_0}. \tag{1.7}$$

This is a monotonic increasing function of k and is of order unity for $k \sim k_\mathrm{vbc}$. Hence, the v_bc terms are non-perturbative at small scales $k > k_\mathrm{vbc}$ and should be kept when treating small scales. As a result, the stream velocity has nontrivial effects on a wide variety of other cosmological phenomena resulting in the non-negligible suppression of power at mass scales corresponding to the first bound objects in the Universe (Tseliakhovich et al., 2011). To investigate the non-linear effects of the stream velocity on the first structures, one must turn to numerical simulations (e.g., Bovy and Dvorkin, 2013; Fialkov et al., 2012; Greif et al., 2011; Maio et al., 2011; Naoz and Narayan, 2013; Naoz et al., 2012; O'Leary and McQuinn, 2012; Richardson et al., 2013; Stacy et al., 2011; Tanaka and Li, 2014). The stream velocity also has significant implication on the redshifted 21-cm signal (e.g., Bittner and Loeb, 2011; Dalal et al., 2010; McQuinn and O'Leary, 2012; Visbal et al., 2012; Yoo et al., 2011), the formation of primordial black holes (e.g., Hirano et al., 2017a; Latif et al., 2014; Schauer et al., 2017; Tanaka and Li, 2014; Tanaka et al., 2013), and even for primordial magnetic fields (Naoz and Narayan, 2013).

One of the first structures, globular clusters (GCs), are some of the oldest bound objects in the Universe. They have even been used to measure the age of the Universe (Krauss and Chaboyer, 2003). Observations indicate that GC contain practically no gravitationally bound DM (e.g., Bradford et al., 2011; Conroy et al., 2011; Heggie and Hut, 1996; Ibata et al., 2013) Despite decades of investigation, their cosmic origins remain debated. Two of the most popular scenarios are described as follows.

Gunn (1980) proposed that GCs are formed in strong shocks when gas is compressed during galaxy mergers. Many massive young star clusters in the Antennae system have been found (e.g., Whitmore and Schweizer, 1995; Whitmore et al., 1999), giving support to this idea. This formation scenario has also been included in cosmology hierarchical structure formation models (e.g., Ashman and Zepf, 1992; Harris and Pudritz, 1994; Kravtsov and Gnedin, 2005; Muratov and Gnedin, 2010). However, observations of nuclear star clusters (e.g, Böker et al., 2004; Brown et al., 2014; Walcher et al., 2006, 2005) implies that GC-like structure can form inside DM halos and reside in their centers, in direct contrast to this theory.

The other popular scenario proposed by (Peebles, 1984) is that like all structure, GCs formed inside DM halos which were later stripped by the tidal field of their host galaxies, leaving the central parts deficient of dark matter (e.g., Bekki and Yong, 2012; Bromm and Clarke, 2002; Mashchenko and Sills, 2005; Saitoh et al., 2006). However, some GCs are observed to have stellar tidal tails, which is difficult to understand if the objects have extended DM halos (Grillmair et al., 1995; Mashchenko and Sills, 2005; Moore, 1996; Odenkirchen et al., 2003).

A recent scenario which we focus on in this thesis is due to the stream velocity. Naoz and Narayan (2014) showed using linear theory that the stream velocity induces a phase shift between the DM and baryonic overdensities which leads to a spatial separation between the overdensity peaks. For stream velocities over $1\ \sigma_{\mathrm{v}bc}$, the spatial offset can be larger than the virial radius of the DM halo. They also showed that these offset gas-rich structures can form bound, long-lived objects which have masses similar to that of GC. They suggested that these gas-rich structures outside of DM halos may be progenitors of GC.

These "Supersonically Induced Gas Objects" (SIGOs) were subsequently found in simulations by Popa et al. (2016). Using the moving-mesh code AREPO, they ran a suite a adiabatic high resolution simulations. They characterized gas-rich objects ($f_g > f_b$) that appeared outside the virial radius of DM halos and were long lived. Although none lasted to the final redshift $z = 10$, they predict that given star formation, it may be possible. Here, we define a Supersonically Induced Gas Object to be a Gas-Only FOF group fitted to a tight ellipsoid that is outside the virial radius of the closest DM halo and and has a gas fraction above 40%[1].

1.2 Methodology

Our simulations are performed with the AREPO code developed by Springel (2010a). This code uses a finite-volume method to solve the hyperbolic inviscid Euler equations on a moving, unstructured mesh that is able to follow the flow in a Lagrangian fashion. The algorithm is second-order accurate in space and time and does not require any artificial viscosity. The key innovation of the code is the use of a Voronoi tessellation for the construction of the computational mesh, based on the positions of a set of mesh-generating points that define the computational cells. The Voronoi construction allows a continuous deformation of the mesh without the unwanted mesh-tangling or mesh-twisting effects that compromised previous attempts to construct Lagrangian mesh codes. In fact, the mesh can move in an essentially arbitrary fashion. If the points are kept stationary and are arranged on a Cartesian grid, the AREPO code is equivalent to the Eulerian methods employed in other state of the art astrophysical finite-volume codes. However, the mesh can also be moved with the local fluid velocity, which is the most attractive mode of operation as it leads to significant accuracy advantages.

There are three primary reasons why AREPO can be expected to yield superior accuracy in cosmological simulations compared to ordinary mesh codes. Perhaps the most important one is that

[1] This 40% is arbitrary but greater than the cosmic baryon fraction by about a factor of 2.

in its Lagrangian mode of operation the results become Galilean-invariant, meaning that large bulk flows do not introduce large errors, unlike in Eulerian codes. For large velocities, the fixed mesh is not able to resolve the instability anymore owing to large advection errors, while the situation is different for the moving-mesh case, where the numerical result is translationally invariant aside from numerical round-off differences. The drastically reduced advection errors in AREPO mean that astrophysical turbulence can be represented more accurately, that mixing and stripping are followed more faithfully, and that the ubiquitous supersonic bulk motions in cosmology are followed more precisely (e.g., Mocz and Burkhart, 2018; Mocz et al., 2017; Schaal and Springel, 2015).

The second important advantage lies in the continuous and automatic adaptivity of the mesh to the clustering of the mass. This has significant advantages in following self-gravity accurately, as the sudden and discontinuous changes in resolution that occur in Cartesian AMR codes introduce non-Hamiltonian perturbations. It has become clear that the standard refinement criteria used in these AMR codes are often not able to catch the growth of small halos correctly (Heitmann et al., 2008), leading to an artificial truncation of the spectrum of resolved objects.

A third advantage is the complete avoidance of preferred directions for an unstructured mesh, combined with an unsplit hydrodynamic scheme. This eliminates grid alignment effects that are seen in Cartesian mesh codes for small disks, where the disks in these codes invariably tend to align artificially with one of the principal coordinate planes.

In summary, AREPO brings together the advantages of SPH, namely free and unrestricted continuous adjustment of its resolution to local clustering, with those of Eulerian AMR codes, namely high-accuracy treatment of shocks, shear waves and fluid instabilities, and no artificial viscosity for shock-capturing. Furthermore, compared to SPH the scheme implemented in AREPO is less noisy and less diffusive (Springel, 2010b), and compared to AMR codes, AREPO is Galilean-invariant and includes a more accurate treatment of self-gravity. Note that AREPO was compared extensively to the publicly available code GADGET2, and it was demonstrated that AREPO performs much better in a large number of test problems (e.g., Sijacki et al., 2012; Vogelsberger et al., 2012).

As it has been shown in Naoz et al. (2006) and Naoz and Barkana (2007), setting up initial conditions for cosmological simulations on small spatial scales is a delicate issue. High accuracy in the initial conditions is crucial for making meaningful predictions of the halo mass function in the lowest mass regime ($M \lesssim 10^7\ M_\odot$). Following Naoz et al. (2011a), we generate separate transfer functions for DM and baryons as described in Naoz and Barkana (2005a). These initial conditions include the Compton scattering of the CMB photons onto residual free electrons after recombination, which induces scale-dependent temperature fluctuations. The latter translates into a non-uniform speed of sound. As was shown in Naoz and Barkana (2005a) at large wave numbers ($k > 100$ Mpc^{-1}) the growth of baryon density fluctuations is changed significantly by the inhomogeneous sound speed (up to 30% at $z = 100$ and 10% at $z = 20$).

The stream velocities are realized in the initial conditions in a self-consistent way with the transfer functions, which are calculated up to the second order in perturbation theory as described in Tseliakhovich and Hirata (2010), similar to the initial conditions presented in studies by McQuinn and O'Leary (2012) and O'Leary and McQuinn (2012). Unlike previous studies we will not assume the same phases for the dark matter and the baryons, but rather take into account the realistic phase difference.

The thesis is organized as follows. In chapter 2, we study the effect of the stream velocity on the spin parameters DM halos and SIGOs. In chapter 3, we analyze the effect of atomic cooling on these objects with and without the stream velocity. In chapter 4, we use a density threshold criterion to determine the star forming properties of SIGOs and use semi-analytic modeling to argue that SIGOs may be the progenitors of modern day metal-poor globular clusters. Finally in chapter 5, we review a summary of the results and future directions.

Throughout the thesis we assume a ΛCDM cosmology with $\Omega_\Lambda = 0.73$, $\Omega_m = 0.27$, $\Omega_B = 0.044$, $\sigma_8 = 1.7$, and $h = 0.71$. Note the higher value of σ_8 is necessary to achieve more statistical power of small scale objects in simulation (Naoz et al., 2012).

CHAPTER 2

Rotational Effects of Supersonic Motions on the First Structures in the Universe

2.1 Abstract

We introduce the "Supersonic Project," aimed at investigating the effects of the supersonic relative velocity between dark matter (DM) and baryons at high redshift using a combination of analytical calculations and cosmological simulations. In this paper, we study the effect of this stream velocity on the angular momentum of the first structures in the early Universe using simulations. We focus on DM halos and their gas component as well as the recently predicted Supersonically-Induced Gas Objects (SIGOs) that arise as a result of the stream velocity phase shift. We find that the spin parameter of the gas component in these first halos is increased with the stream velocity. Moreover, we find that when the stream velocity is taken into account, the angular momentum vectors of the DM component and the gas component are typically misaligned and this misalignment angle has a nearly isotropic distribution. The spin parameter value of the gas component is higher than in the no stream velocity case, which even in the absence of cooling, may result in more prolate objects. We also generalize the spin parameter to the SIGOs and find that they typically have a larger spin parameter with respect to their dark matter counterparts and that there is no correlation of the spin parameter and the prolateness of such structures. We speculate that SIGOs may be observed as very low luminosity objects in the early Universe and may serve as potential progenitors of Little Blue Dot-like systems.

2.2 Introduction

The Lambda-Cold Dark Matter model (ΛCDM) has had great success in characterizing structure formation and the evolution of the Universe. Using this model, numerical simulations have been able to accurately describe structure on the largest of scales ($\sim$ (100 Mpc)^3, e.g., Schaye et al., 2015; Springel, 2005; Vogelsberger et al., 2014a,b). The currently accepted paradigm suggests that present-day galaxies evolved from primordial inhomogeneities in the density distribution at very early times (e.g., Blumenthal et al., 1984; Rees and Ostriker, 1977; Silk, 1977; White and Rees, 1978). Dark Matter (DM) over-densities had been evolving logarithmically with the scale factor during the radiation-dominated era and linearly during matter-dominated era. However, baryons decoupled from the radiation only at the time of recombination, and thus were free to start growing (e.g., Padmanabhan, 2002). This resulted in a significant difference between the over-density amplitudes of DM and baryons at the time of recombination (Naoz and Barkana, 2005b), and in a relative velocity between the two components as well. Tseliakhovich and Hirata (2010) showed that the relative velocity between these over-densities was supersonic at the time of recombination as a consequence of the sudden drop in baryonic temperature. In particular, it had an rms velocity of ~ 30 km s^{-1} and was coherent on scales of less than a few comoving Mpc. This effect was coined the "stream velocity" effect. In terms of cosmological perturbation theory, the relative velocity coupling to the over-densities is formally a second-order effect and is often neglected in analytical work and in simulations.

Although second-order, the supersonic nature of the stream velocity has been shown to have non-trivial effects on the evolution of the over-densities within those patches such as lowering the number density of halos (e.g., Asaba et al., 2016; Bovy and Dvorkin, 2013; Fialkov et al., 2012; Maio et al., 2011; Naoz et al., 2012; O'Leary and McQuinn, 2012; Stacy et al., 2011; Tanaka and Li, 2014; Tanaka et al., 2013; Tseliakhovich et al., 2011; Tseliakhovich and Hirata, 2010). Naoz et al. (2013), showed that the stream velocity also increases the minimum halo mass that is capable of retaining most of its baryons throughout its formation epoch, yielding first structures that are deprived of gas. Overall, the gas fraction in the first DM halos decreases (e.g., Asaba et al., 2016; Dalal et al., 2010; Fialkov et al., 2012; Greif et al., 2011; Maio et al., 2011; Naoz et al., 2012, 2013;

O'Leary and McQuinn, 2012; Richardson et al., 2013; Tseliakhovich et al., 2011). As a result, star formation in halos is delayed because halos are not capable of accreting enough gas at early times (e.g., $z \lesssim 10$ Ahn, 2016; Bovy and Dvorkin, 2013; Fialkov et al., 2012; Greif et al., 2011; Liu and Wang, 2011; Maio et al., 2011; O'Leary and McQuinn, 2012; Richardson et al., 2013). It was also shown that the stream velocity, in combination with spatial fluctuations in the speed of sound (Naoz and Barkana, 2005b), can cause the formation of coherent large-scales magnetic fields (Naoz and Narayan, 2013). Moreover, it was suggested that the delayed star formation can result in black hole formation via direct collapse and largely affect primordial black hole evolution (e.g., Hirano et al., 2017a; Latif et al., 2014; Schauer et al., 2017; Tanaka and Li, 2014; Tanaka et al., 2013). Finally, the stream velocity has important implications for 21-cm cosmology since the stream might enhance the hydrogen signal from the different patches in the sky (e.g., Visbal et al., 2012) and might also be related to the trough in 21-cm via DM-baryon scattering (Barkana, 2018; Barkana et al., 2018).

Naoz and Narayan (2014) demonstrated, analytically, that the supersonic nature of the relative velocity results in a physical off-set between the DM and baryonic over-densities. This leads to the formation of Supersonically-Induced Gas Objects (SIGOs) outside the virial radius of dark matter halos. They conjectured that these structures could be the progenitors of globular clusters, which tend to be devoid of DM. Additionally, the parent gas-deprived dark matter halos could potentially explain some of the dark satellite galaxies. Popa et al. (2016), using simulations performed with the moving-mesh code AREPO (Springel, 2010a), revealed that these SIGOs do indeed exists outside the virial radius of DM halos. SIGOs also tend to have an ellipsoidal structure, in contrast to the roughly spherical nature of the DM halos. Recently, Hirano et al. (2017b) also confirmed the existence of these structures in a cosmological simulations using the SPH code GADGET-2 (Springel, 2005). Utilizing a zoom-in method, they followed the fragmentation of gas clouds into SIGOs and suggested that these clumps are the progenitors of the first star clusters.

SIGOs are therefore of great interest; they might be the first star clusters and/or represent the present day globular clusters. One potentially promising observable of these SIGOs in particular, and the stream velocity as a whole, is the angular momentum of these objects. Both SIGOs and

DM halos are affected by the stream velocity. Thus, one expects a notable signature on their angular momentum and specifically on the so-called spin parameter, which is a normalized angular momentum. The angular momenta of the DM and the gas component of halos are directly related to their formation history (e.g., Fall and Efstathiou, 1980; Mo et al., 1998; Peebles, 1969). Within the context of the hierarchical structure formation picture, baryons lose their angular momentum to the DM as they spiral into the centre. In the presence of the stream velocity, there is a preferred directionality that is expected to increase the spin parameter.

Furthermore, the angular momentum distribution of an object is correlated with the formation of a gaseous disk. Earlier studies of disk formation typically assume that early tidal torques endow the same angular momentum to DM and baryons (e.g., Barnes and Efstathiou, 1987; Fall and Efstathiou, 1980; Mo et al., 1998). However, such an assumption breaks down when considering the non-linear Universe. The inclusion of baryonic processes and feedback further complicates the problem. Given the importance of the topic, several studies have investigated the angular momentum distributions of DM halos and baryons and have had great success in describing disk formation (e.g., Maller and Dekel, 2002; Rodriguez-Gomez et al., 2017; Teklu et al., 2015; van den Bosch et al., 2002). Since the spin parameter gives a measure of the rotational support of an object, it was suggested that this quantity may serve as an observational signature of the parent halo at low redshift for high-mass halos (e.g., Somerville et al., 2017; Teklu et al., 2015; Zavala et al., 2016). In particular, Somerville et al. (2017) showed that ratio of the half-light radius to the virial radius of the halo is proportional to the DM spin parameter value. However, as pointed out by Jiang et al. (2018), there is still no clear correlation between the DM spin parameter and the corresponding gas component spin parameter. Somerville et al. (2017) found that the stellar radius-halo radius correlation is roughly independent of stellar mass at $z \sim 1$, but at higher redshift ($z \sim 2$) there is a mass dependence with high mass galaxies having a 50% smaller ratio of stellar radius to halo radius than low mass galaxies. This correlation informs on the way that galaxies at high redshift interact. In particular, major mergers and violent disk instabilities may drive the loss of angular momentum from these halos. However, observations in high redshift regimes ($z \gtrsim 10$) are beyond current technological reach. Detailed numerical simulations can provide the necessary insight into the complex physical processes that take place at these high redshift regimes.

The goal of the "Supersonic Project" is to understand the stream velocity effect and how it affects structure formation in the early Universe. Future papers in this series will address the stream velocity effect with star formation and feedback prescriptions taken into account. In this first paper of the "Supersonic Project", we specifically investigate the consequences of the stream velocity at high redshift ($20 < z < 10$) on the morphology and spin of DM and gas inside halos, as well as the SIGOs, using a suite of AREPO simulations (see Popa et al., 2016).

This chapter is organized as follows. In section 2.3, we briefly describe the simulation setup. We review the spin parameter and the numerical methods that were employed in section 2.4. We then present our results about the effects of the stream velocity on the spin parameter and misalignment angle between gas and DM for halos in our simulations in section 2.5. Finally, we wrap up with a summary and conclusions in section 2.6.

2.3 Numerical simulations

We study the AREPO simulations presented in Popa et al. (2016). The transfer functions of the initial conditions are calculated via a modified CMBFAST code (Seljak and Zaldarriaga, 1996) to take into account the first-order correction of the scale dependent temperature fluctuations (following Naoz and Barkana, 2005b). These corrections were shown to have a significant effect in determining the gas fraction in halos at high redshift (e.g., Naoz et al., 2009, 2011b, 2013). The transfer functions also include the stream velocity evolution (these are second-order corrections to the equations Tseliakhovich and Hirata, 2010). We chose to work with the 2 Mpc box size presented in Popa et al. (2016). The box has 512^3 DM particles with associated mass resolution of $m_{\rm DM} = 1.9 \times 10^3\ M_\odot$. The gas component is represented by 512^3 Voronoi mesh cells which corresponds to a particle mass of $m_{\rm gas} = 360\ M_\odot$. These simulations include only gravitational physics and non-radiative hydrodynamics, i.e., no radiative cooling or (sub-grid) galaxy formation physics (star formation, stellar feedback, etc.) is considered. The box was run from $z = 200$ to $z = 0$ twice, once with no stream velocity, and once with stream velocity $v_{bc} = 2\ \sigma_{v_{bc}} = 11.8\ {\rm km\ s^{-1}}$, where $\sigma_{v_{bc}}$ is the rms velocity. Stream velocity values of 2 $\sigma_{v_{bc}}$ were chosen because such values are able to produce gas-rich structures outside the virial radius of DM halos with masses near that of globular clusters (Naoz and Narayan, 2014). Both DM and gas structures in Popa et al. (2016) were identified using the Friends-of-Friends (FOF) algorithm with a linking length of 0.2 times the mean particle separation to identify halos and their corresponding virial radius. Following Popa et al. (2016) we defined two different structures with the FOF algorithm:

1. *DM-Primary/Gas-Secondary* objects are those for which FOF was run on the DM first. Gas cells were then linked in a secondary stage (Dolag et al., 2009) in order to investigate gaseous substructure in the DM halos. A spherical overdensity (SO) calculation is performed to obtain the virial radius from these FOF groups.

2. *Gas-Primary* objects are found by running the FOF algorithm only on the baryonic component[1]. The Gas-Primary structures tend to be more filamentary in nature, thus, we adopt the ellipsoidal fitting algorithm from Popa et al. (2016) to each FOF group. Since some of these structures tended to be very sparse, we implement a "tightly fitting ellipsoid" to each object in the following manner: keeping the axis ratios constant, the ellipsoid is progressively shrunk in decrements of 0.5% until the the ratio of the lengths of the axis of the shrunken ellipsoid to the original is greater than the ratio of the number of gas cells in the shrunken ellipsoid to the original or until 20% of the particles have been removed. Note that many of these Gas-Primary structures reside inside DM halo, as they are simply the gas components of the DM-Primary/Gas-Secondary structures.

Our definitions of structures are summarized in Table 2.3. In the analysis that follows, we focus on the morphology and angular momentum of these high-redshift $(20 < z < 10)$ structures.

[1] One important question is if these objects are bound. These objects may be falling into a bigger potential well. Furthermore, numerical effects (see below) tend to disperse these objects.

DM-Primary/Gas-Secondary	Gas-Primary	Supersonically Induced Gas Objects (SIGOs)
Objects for which FOF was run on the DM first, then gas was linked in a secondary stage	Objects for which FOF was run on the gas only	Gas-Primary objects that are outside the virial radius of the closest DM halo and have gas fractions greater than 40%

Table 2.1: Table of structure definitions used in the thesis.

2.4 Structure and Morphology

The spherically averaged density profiles of DM halos are typically well described by an NFW (Navarro et al., 1996) profile. One can associate a radius, R_{200}, to these halos, which corresponds to the radius of a sphere with overdensity 200 times the critical density for closure of the Universe[2]. Note that DM halos show clear triaxiality (e.g., Lithwick and Dalal, 2011; Schneider et al., 2012; Sheth et al., 2001; Vogelsberger et al., 2011), and are assumed to be spherically symmetric here for simplicity. As depicted in Figure 8 of Popa et al. (2016), the NFW profile is preserved even with the introduction of the stream velocity. In contrast to the DM profile, Popa et al. (2016) showed that Gas-Primary components tend to be more ellipsoidal in nature. Typical density profiles for Gas-Primary objects are displayed in Figure 2.1, top row. Estimating the density in ellipsoid shells demonstrates that the profile deviates from an NFW profile for these objects. We also consider density profiles as a function of the longest axis of the ellipsoid which describes the concentration of mass along the axis. We have smoothed the density along the longest axis using a moving average filter to minimize particle discretization effects. We find three typical cases. The first, shown in solid red in Figure 2.1, demonstrates a relatively flat distribution in the middle of the ellipsoid corresponding to the left panel in the bottom row of Figure 2.1. The second, shown in dotted green, exhibits multiple peaks, which might suggest a merger or a breakup, corresponding to the middle panel in the bottom row. Lastly the third, in dot-dashed blue, shows an increasing density towards one direction, corresponding to the right panel in the bottom row. This could be

[2]It has been suggested that R_{200} does not accurately describe a physical boundary for a halo. In particular, processes such as further mass accretion may cause the actual radius of the halo to be larger than R_{200}. This was the motivation for the "splash back" radius (Diemer et al., 2017; More et al., 2015). Although there are possible disadvantages of R_{200}, here we us it as a simple normalization which allows us to compare to previous studies.

caused by gravitational attraction to the closest dark matter halo. At large distances (i.e., $r > R_{\rm max}$ for SIGOs and $r > r_s$ for DM halos, where r_s is the scale radius of NFW) the distribution drops sharply. However, the inner slope is different, and tends to be flatter for the Gas-Primary objects. The gas density projections (Figure 2.1, bottom row) show asymmetric gas distributions inside the these objects.

To properly analyze SIGOs, we will define them to be Gas-Primary structures whose centre of mass lies outside the virial radius of the closest dark matter halo and that have gas fraction $> 40\%$[3].

To characterize the ellipsoidal morphology of Gas-Primary objects, we define a prolateness factor as

$$\xi = \frac{R_{\rm max}}{R_{\rm min}} \,, \tag{2.1}$$

where $2R_{\rm max}$ ($2R_{\rm min}$) refers to the length of the maximum (minimum) axis of the ellipsoid. In Figure 2.2 we show the distribution of $R_{\rm max}/R_{\rm min}$ for our gas ellipsoids with and without the stream velocity. As can be seen in this Figure the stream velocity tends to produce more prolate systems.

Naoz and Narayan (2014) used analytical calculations to show that SIGOs originated from a corresponding DM over-density mode that is shifted by a physical distance which can be larger than the virial radius of the DM halo. Thus the gas-deprived parent DM halo (i.e., the fiducial halo corresponding to the DM over-density mode) simply has a mass of $M_{\rm DM} \sim 6M_{\rm gas}$ since DM is on average 5 times as massive as gas. One might naively expect that the closest DM halo of a SIGO will be the parent halo. However, due to dynamical interactions, we find that the closest DM halo is not necessarily the host halo, as can be seen in Figure 2.3. In other words, SIGOs move around and tend to cluster around more massive DM halos. In Figure 2.3, SIGOs are represented by star symbols and show no correlation with $M_{\rm gas}$.

The suppression of the gas component in DM halos from the stream velocity effect can be evaluated analytically from the power spectrum. The typical mass at which the gas fraction is

---

[3]The choice of 40% is somewhat arbitrary, we note that it is above the cosmic baryon fraction and close to 50%, i.e., the stellar fraction of globular clusters (Bradford et al., 2011; Conroy et al., 2011; Heggie and Hut, 1996; Ibata et al., 2013)

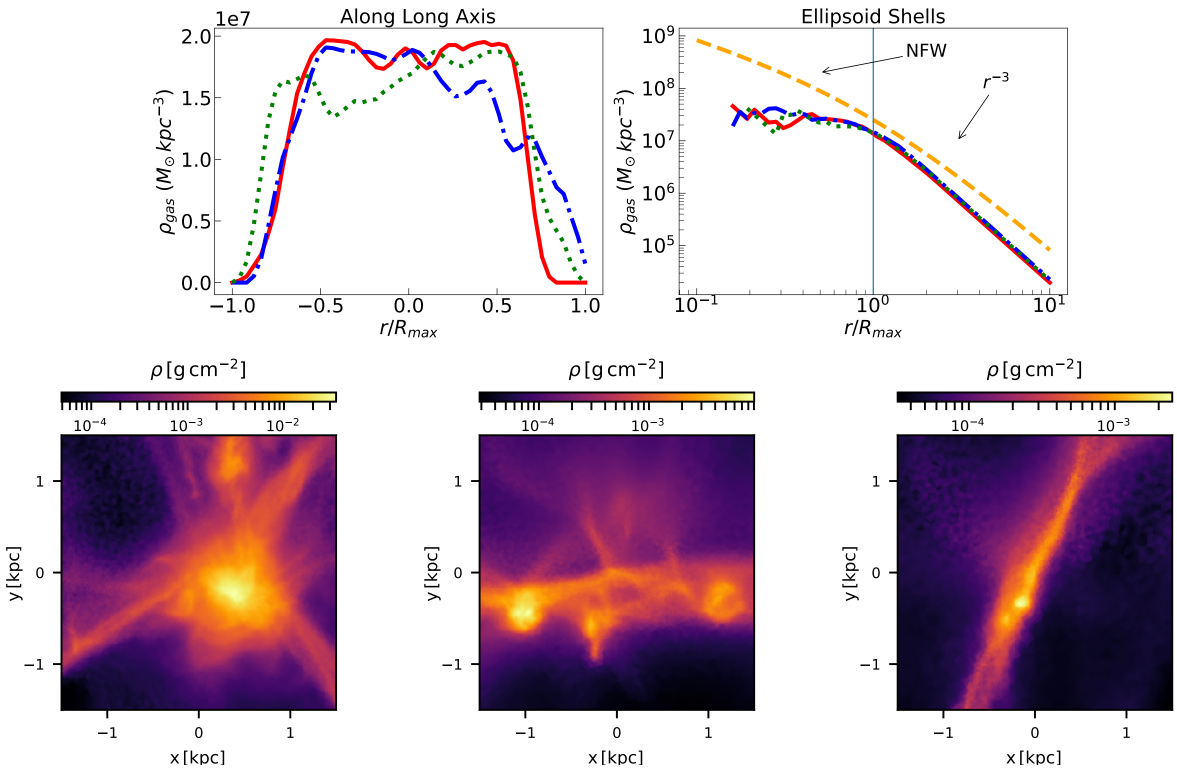

Figure 2.1: **Top row:** Three examples of the density profiles of Gas-Rich Objects The left panel depicts the density along the long axis of ellipsoid, while the right panel shows the density in increasing ellipsoidal shells. For illustration purposes, in the right panel, we present a typical NFW profile, with $\rho_0 = 10^8\ \mathrm{M}_\odot\ \mathrm{kpc}^{-3}$, and replacing $r/r_s \to r/R_{\max}$ (dashed orange line). The left panel densities have been smoothed with a moving average filter. **Bottom row:** Projected density profiles (in $\mathrm{g\ cm}^{-2}$) for the three example ellipsoids from the top row at $z = 20$. In particular, the left panel corresponds to the red (solid) line in the top row, while the middle panel corresponds to the green (dotted) line in the top row, and finally the right panel corresponds to the blue (dot-dashed) line in the top row.

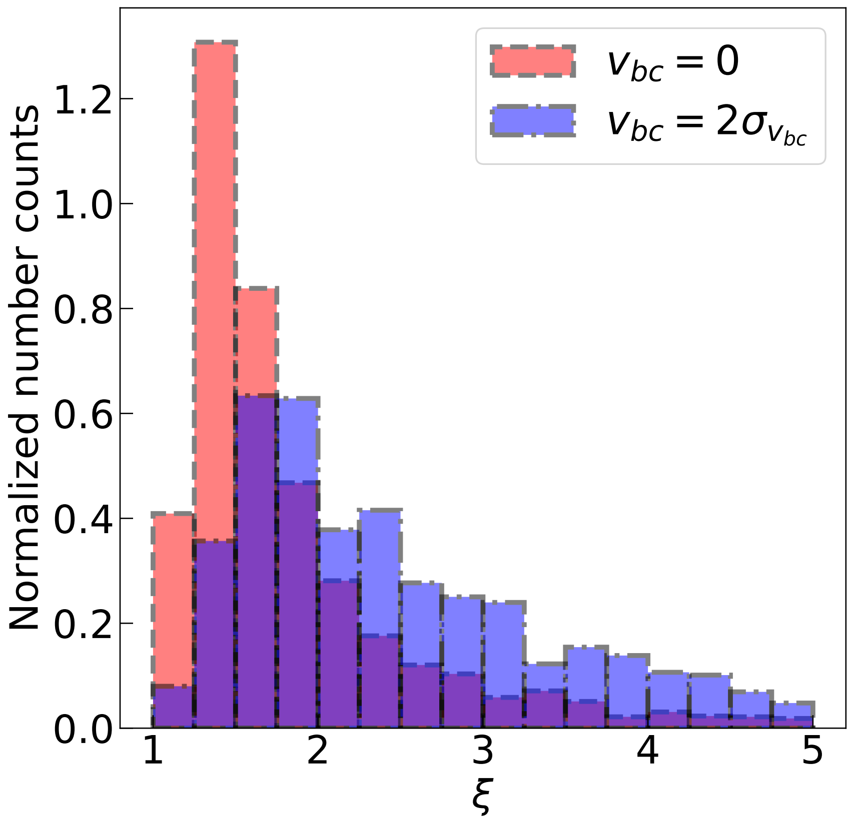

Figure 2.2: A histogram of the prolateness factor, ξ (see Eq. 2.1) for Gas-Primary objects at $z = 20$. The zero stream velocity case is shown in dashed red, whereas the $v_{\rm bc} = 2\sigma_{v_{\rm bc}}$ in dot-dashed blue. The stream velocity shifts the prolateness of Gas-Primary objects towards higher values.

substantially suppressed, when estimated from such calculations (for both $v_{\rm bc} = 0$ and $v_{\rm bc} \neq 0$), agrees with the fits from simulations (the so called characteristic or filtering mass, e.g., Gnedin, 2000; Naoz and Barkana, 2007; Naoz et al., 2009, 2011b, 2013; Popa et al., 2016). Thus, we can find a simple correlation between the gas mass in a DM halo and the DM mass of that halo, using the characteristic mass M_c:

$$M_{\rm gas} = f_{b,0} M \left[1 + (2^{\gamma} - 1) \left(\frac{M_c}{M} \right)^{\beta} \right]^{-1/\gamma} , \qquad (2.2)$$

where we adopt the following fit parameters: $\gamma = 8$, $\beta = 1$, $M_c = 6 \times 10^5\ M_{\odot}$ (e.g., Popa et al., 2016). Note that $f_{b,0}$ is defined as the gas fraction of the top 5% massive halos realized. For the nonzero stream velocity run, we have $f_{b,0} = 0.07$. This fit is depicted in Figure 2.3 (orange line) and shows an agreement with the apparent correlation of the gas components inside their DM halos. The SIGOs exhibit scatter and do not lie on this line and therefore do not display the classical behaviour of gas clumps inside DM halos.

Note that the relatively small number of SIGOs, with 18 (98) objects at redshift 10 (20) is probably numerical in nature. In AREPO, gas cells interact as gravitationally softened particles. Thus, the gas component in a SIGO has a velocity distribution, with a tail of particles' velocities above the escape velocity of the SIGO. These particles then become unbound, and the SIGO slowly evaporates. To estimate the timescale of this evaporation, we adopt a crude collisionless approach (Gieles et al., 2011; Gnedin et al., 2014; Naoz and Narayan, 2014). This collisionless process results in the unbinding (evaporation) of star clusters (e.g., Gieles et al., 2011) as well as the low mass SIGOs in our simulation. Specifically, Gnedin et al. (2014) showed that the evaporation timescale of a 2×10^5 $\rm M_{\odot}$ star cluster is approximately 17 Gyr, if all the stars are 1 $\rm M_{\odot}$. From the point of view of gravitationally softened interacting particles, a 2×10^5 $\rm M_{\odot}$ SIGO mass object has about 555 particles (for our mass resolution of $M_{\rm gas} = 360$ $\rm M_{\odot}$). The evaporation timescale for this object is 0.045 Gyr, which is much shorter than the time passed between $z = 20$ to $z = 10$. Therefore our insufficient resolution results in the numerical loss of many SIGOs (which implies that the SIGOs are marginally bound). In follow up investigations we plan to use a zoom-

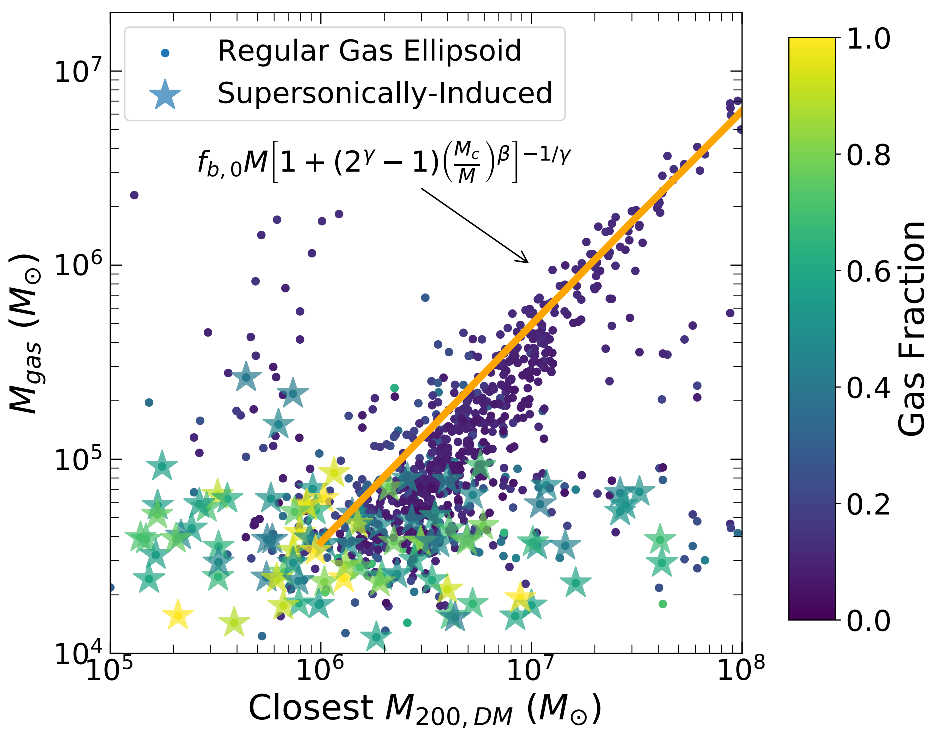

Figure 2.3: Comparison of the gas mass inside ellipsoids and the virial mass of the closest dark matter halo at redshift 20 for the nonzero stream velocity run. Stars refer to SIGOs. The orange line refers to the fit to gas mass derived from an initial DM halo (see Equation 2.2). This characteristic mass fit describes the fact that smaller DM halos will have less gas. The fit parameters are $\gamma = 8$, $\beta = 1$, $M_c = 6 \times 10^5\ M_\odot$, and $f_{b,0} = 0.07$. We fit only objects that are not SIGOs.

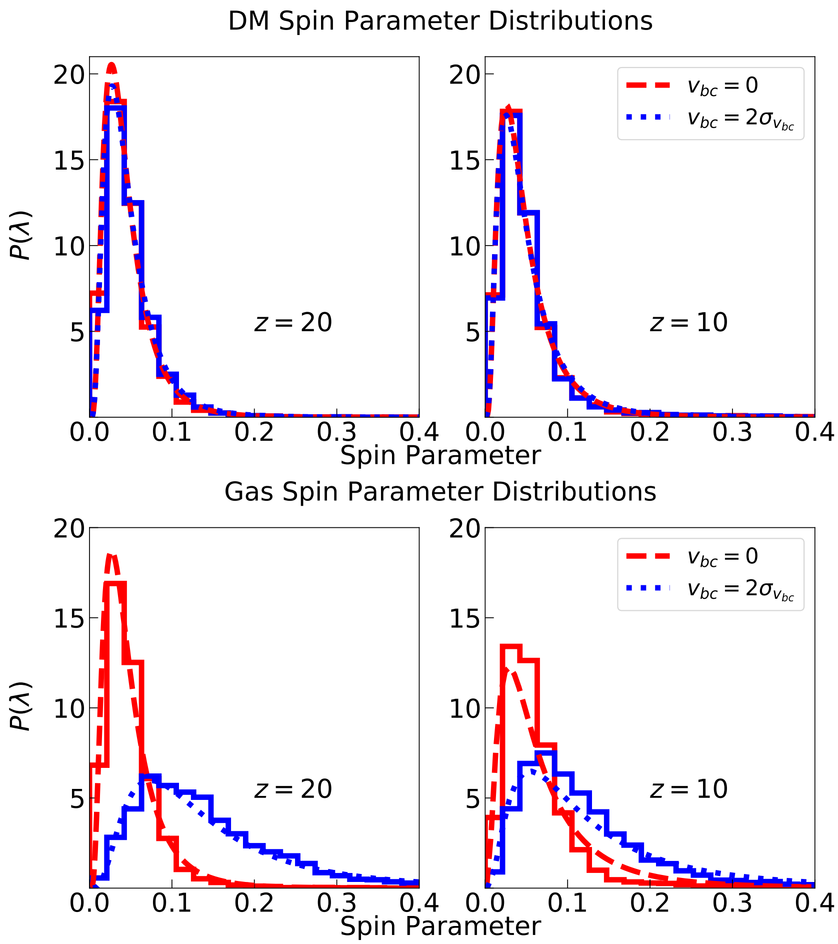

Figure 2.4: Spin parameters distributions of DM (top panels) and gas in the DM halos (bottom panels). We consider the zero stream velocity case (dashed red lines) and the $v_{\rm bc} = 2\sigma_{\rm vbc}$ (dotted blue lines), for two redshift examples ($z = 10$ and $z = 20$). We also provide a lognormal fit to the distribution. The fit parameters are available in Table 2.2.

in methodology to increase the resolution.

2.5 The Angular momentum of Gas-rich and Gas-poor structures

2.5.1 The spin parameter

The angular momentum, J, of a DM halo is typically estimated by using the spin parameter that was originally defined as (Peebles, 1969),

$$\lambda_P = J \frac{E_{\rm DM}^{1/2}}{G M_{\rm DM}^{5/2}} \,, \tag{2.3}$$

where $E_{\rm DM}$ is the binding energy associated with the DM halo with mass $M_{\rm DM}$, and G is the gravitational constant. For practical purposes, a more feasible measure of the angular momentum was defined by Bullock et al. (2001) as

$$\lambda = \frac{j_{\rm sp}}{\sqrt{2} v_{200} R_{200}} \,, \tag{2.4}$$

where

$$\mathbf{j}_{\rm sp} = \frac{\mathbf{J}}{M} = \frac{1}{M} \sum_{i=1}^{N} m_i \mathbf{r}_i \times \mathbf{v}_i \,, \tag{2.5}$$

$j_{\rm sp} = |\mathbf{j}_{\rm sp}|$, $v_{200} = \sqrt{G M_{200}/R_{200}}$, and $M = \sum_i^N m_i$. The sums are over any set of particles $\{\rm gas, DM, total\}$. The expression in Eq. (2.4) allows for the definition of separate spin parameters for the DM and gas component of a halo. Non-radiative hydrodynamical simulation studies have shown that the spin parameter of the gas component is typically higher than that of the DM component (e.g., Sharma and Steinmetz, 2005; Zjupa and Springel, 2017, but see van den Bosch et al. (2002) for a different conclusion). Below we adopt Eq. (2.4) as our definition of the spin parameter. We note that the two alternative definitions for the spin parameter are not entirely equivalent. Analytically, for NFW halos, the different definitions are related to each other via $\lambda_P = f(c)^{1/2}\lambda$, where $f(c)$ depends on the concentration c of the halo (Mo et al., 1998). The spin parameter is well described by a log-normal distribution (e.g., Bullock et al., 2001)

$$P(\lambda) = \frac{1}{\lambda\sqrt{2\pi}\sigma} \exp\left(-\frac{\log^2(\lambda/\lambda_0)}{2\sigma^2} \right) \,, \tag{2.6}$$

where the fit parameters are: $\lambda_0 = 0.035$ and $\sigma = 0.5$ (Bullock et al., 2001, similar fits were found by Hetznecker and Burkert (2006); Rodriguez-Gomez et al. (2017); Zjupa and Springel (2017)). In this work, we focus on smaller mass structures $\lesssim 10^8\ M_\odot$, and separate our discussion to the DM halos with a gas component and Gas-Primary objects. We assume spherical symmetry and the same normalization for each of the halo's component (i.e,. M_{200} and v_{200}).

2.5.2 DM-Primary/Gas-Secondary Objects

Recall that DM-Primary/Gas-Secondary objects were found via the FOF algorithm. Using a spherical overdensity algorithm, one can compute an associated virial radius. We then restrict to the spherical overdensity halo and study its properties. These halos in general contain both DM and gas particles. Note that the Bullock et al. (2001) definition of the spin parameter (Eq. 2.4) is appropriate for such halos given their inherent spherical symmetry assumption.

As depicted in the top panels of Figure 2.4, the spin parameter distribution of these small-size, high-redshift ($z = 10,\ 20$), DM halos ($\leq 10^8\ M_\odot$) follows a log-normal distribution, consistent with massive halos at low redshift. Both the zero and non-zero stream velocity cases give similar results for the DM component in the halo. The fit parameters of the distribution are given in Table 2.2, and they also agree with the low-redshift, massive DM halos parameters (e.g., Bullock et al., 2001).

In the bottom panels of Figure 2.4, we display the spin parameter of the gas components of these halos, for $v_{\rm bc} = 0$ (dashed red lines) and $v_{\rm bc} = 2\sigma_{\rm bc}$ (dotted blue lines). As before, the two representative examples are for $z = 10$ and $z = 20$. We note first that the gas component distribution of the $v_{\rm bc} = 0$ case, has a slight evolution in time (see Table 2.2). This evolution is to be expected since more gas is being accreted onto the DM halos as the Universe evolves. Notably, while the stream velocity has a negligible effect on the DM, it has a significant effect on the spin parameter distribution of the gas component. The gas spin parameter distribution has become flattened leading to a larger median. In comparison to the DM, the gas has spun up by an amount $\lambda_{\rm gas}/\lambda_{\rm DM}$ of 3.5 at $z = 20$ and of 2.7 at $z = 10$ in the presence of the stream velocity. As time goes by, the DM angular momentum torques the gas angular momentum and re-aligns it.

$\lambda_{\rm DM}$	$z = 20$		$z = 10$	
	λ_0	σ	λ_0	σ
$v_{\rm bc} = 0$	0.04	0.61	0.04	0.68
$v_{\rm bc} = 2\sigma_{v_{\rm bc}}$	0.04	0.62	0.04	0.70
$\lambda_{\rm gas}$	$z = 20$		$z = 10$	
	λ_0	σ	λ_0	σ
$v_{\rm bc} = 0$	0.04	0.65	0.06	0.82
$v_{\rm bc} = 2\sigma_{v_{\rm bc}}$	0.12	0.70	0.11	0.82
$\lambda_{\rm ellip}$	$z = 20$		$z = 10$	
	λ_0	σ	λ_0	σ
$v_{\rm bc} = 0$	0.07	0.68	0.07	0.74
$v_{\rm bc} = 2\sigma_{v_{\rm bc}}$	0.12	0.65	0.11	0.73

Table 2.2: Lognormal fit parameters for DM component, the gas inside the DM halos, and the gas ellipsoid structures.

Smaller mass halos are more sensitive to stream velocity effects. This is depicted in the top panels of Figure 2.5, where we present the combined spin parameter of both gas and DM as a function of the total halo mass. The first row is for $z = 20$ while the second is for $z = 10$. The colors represent the gas fraction in each halo. As expected, the stream velocity decreases the gas fraction of a halo (e.g., Popa et al., 2016). In the bottom panels of Figure 2.5, we plot the gas component of the spin parameter but split the objects into those that were above and below $f_{\rm b,0}$ to distinguish between gas-rich and gas-poor halos. This shows that the gas spin parameter distribution of gas-poor halos is more extended in the stream velocity case as compared to the zero stream velocity simulation. We see that the objects below the threshold in $f_{\rm b,0}$ exhibit slightly higher median gas spin parameter. The gas content in these objects is smaller due to the presence of the stream velocity, which corresponds to higher spin parameter for the gas-poor halos. Gas-rich halos represent those objects that are less sensitive to $v_{\rm bc}$, i.e., typically DM halo mass larger than a few $\times 10^6$ M$_\odot$ (e.g., Naoz and Narayan, 2014), and thus results in the nominal, $v_{\rm bc} = 0$ spin parameter peak value, (see blue lines in the bottom panels and green dots in the top panels in Figure 2.5). On the other hand, smaller mass objects are more sensitive to $v_{\rm bc}$ and thus, are gas deficient and have higher spin parameter peak value, compared to the gas-rich ones (see red lines in the bottom panels and dark blue dots in the top panels in Figure 2.5). In the nonzero stream velocity case, the gas-poor halos accumulate gas preferentially from the stream flow which causes the excess of angular momentum compared to the $v_{\rm bc} = 0$ case.

We calculate the misalignment angle θ between the DM and gas particle angular momentum:

$$\cos(\theta) = \frac{\boldsymbol{J}_{\rm DM} \cdot \boldsymbol{J}_{\rm gas}}{|J_{\rm DM}||J_{\rm gas}|} \, . \tag{2.7}$$

Previous simulation studies have shown that there is a moderate misalignment of $\sim 30^\circ$ between the DM and baryons (e.g., van den Bosch et al., 2002; Zjupa and Springel, 2017). As depicted in Figure 2.6, we find a similar median misalignment angle in the zero stream velocity case as in previous studies. However, the stream velocity effect results in a nearly isotropic distribution of the misalignment angle and increases the median to about 81° (72°) at $z = 20$ ($z = 10$). The DM did not have enough time to torque the gas component into alignment as the gas accretes at later times onto these halos.

2.5.3 Gas-Primary and Supersonically-Induced Gas Objects

We define a Gas-Primary object by running the FOF algorithm only on the baryonic component and tightly fitting an ellipsoid around them (see Section 2.4). We also note that some of these structures are, in fact, the gas component in a DM halo. We refer to those that lie beyond the virial radius of their parent dark matter halo and also have a gas fraction larger than 40% as SIGOs.

We extend the spin parameter definition to the Gas-Primary structures. Since these structures are ellipsoidal in nature (e.g., Popa et al., 2016, and see Figure 2.1), the spherical symmetry associated with the spin parameter normalization does not hold. Furthermore, as shown in Figure 2.1 the gas inside the Gas-Primary structures does not have an NFW distribution. In particular, Gas-Primary structures, tend to have a flatter inner distribution, unlike the DM halos. Therefore, in order to compare between the DM-Primary/Gas-Secondary and Gas-Primary (and SIGOs), we need to choose a self-consistent normalization. We choose a normalization in accordance with the physics picture described in Naoz and Narayan (2014), in which Gas-Primary structures originated from the corresponding overdensity mode of their DM counterparts. These are simply defined by

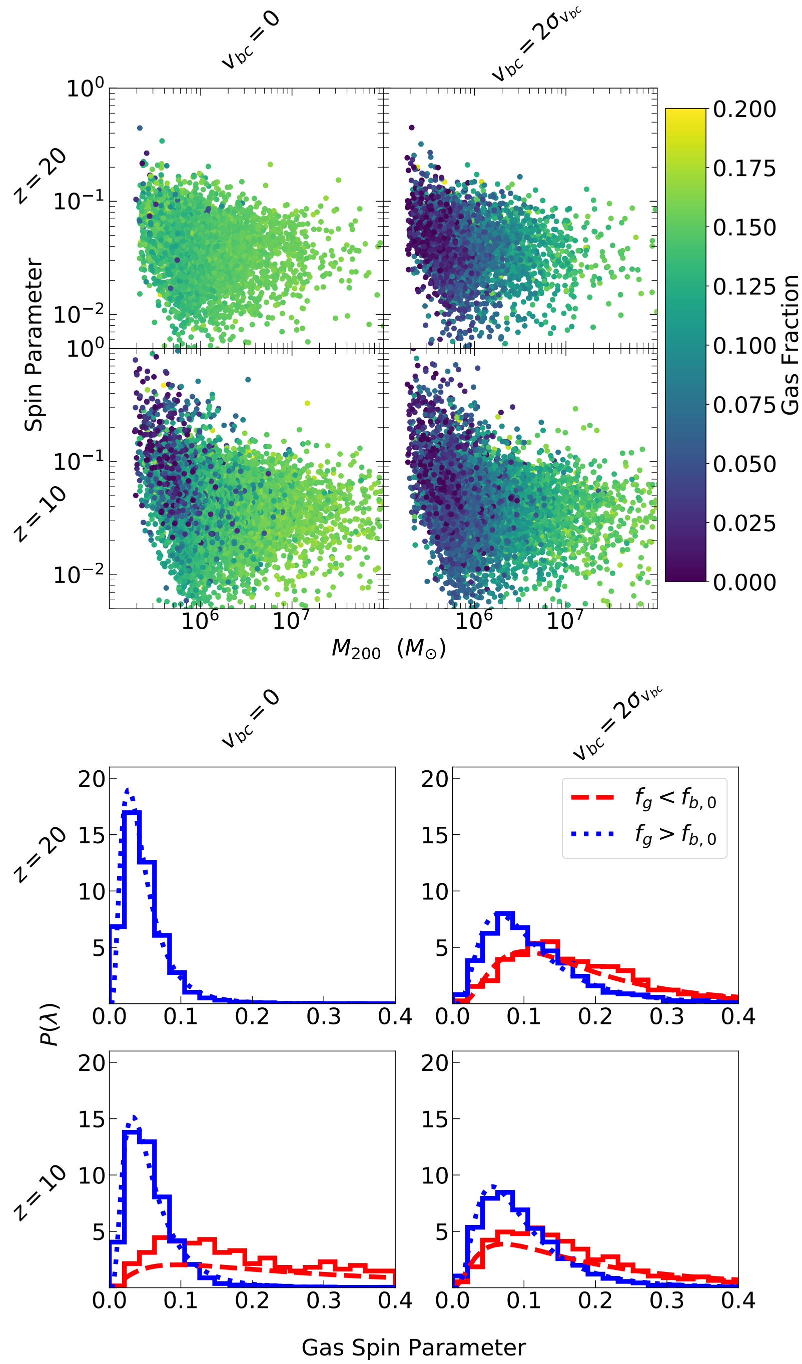

Figure 2.5: The top panels depict distributions of halo spin parameters (including both DM and gas components) as a function of halo mass colored by gas fraction. The bottom panels show the (lognormal) distributions where we have separated the populations between gas poor ($f_g < f_{\mathrm{b},0}$, dashed red lines) and gas rich ($f_g > f_{\mathrm{b},0}$, dotted blue lines) structures, where $f_{\mathrm{b},0}$ is the gas fraction of the top 5% massive halos realized. The stream velocity effect increases the median spin parameter more for gas poor halos than gas rich halos.

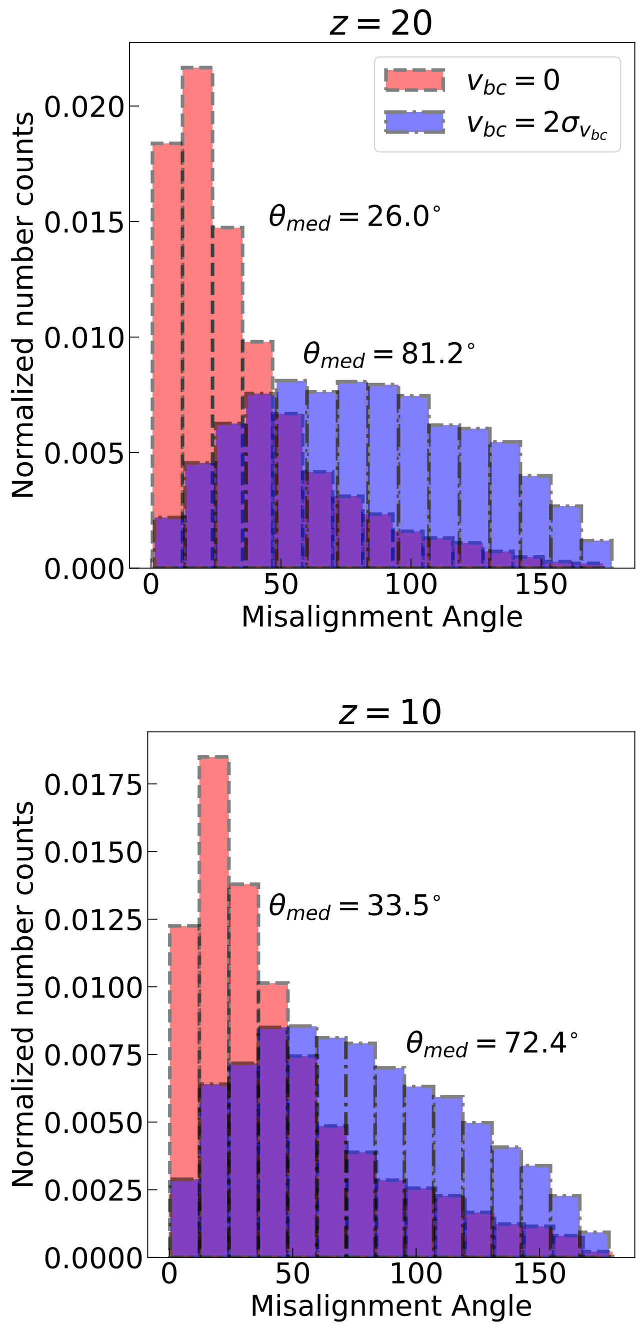

Figure 2.6: Histogram of misalignment angle between the DM and baryonic component (see Eq. 2.7) . We consider the zero $v_{\rm bc}$ case in dashed red and the $v_{\rm bc} = 2\sigma_{v_{\rm bc}}$ in dot-dashed blue. The $v_{\rm bc} = 0$ result is in agreement with previous studies (van den Bosch et al., 2002; Zjupa and Springel, 2017). Note the nearly isotropic distribution at early times with stream velocity (i.e., $z = 20$).

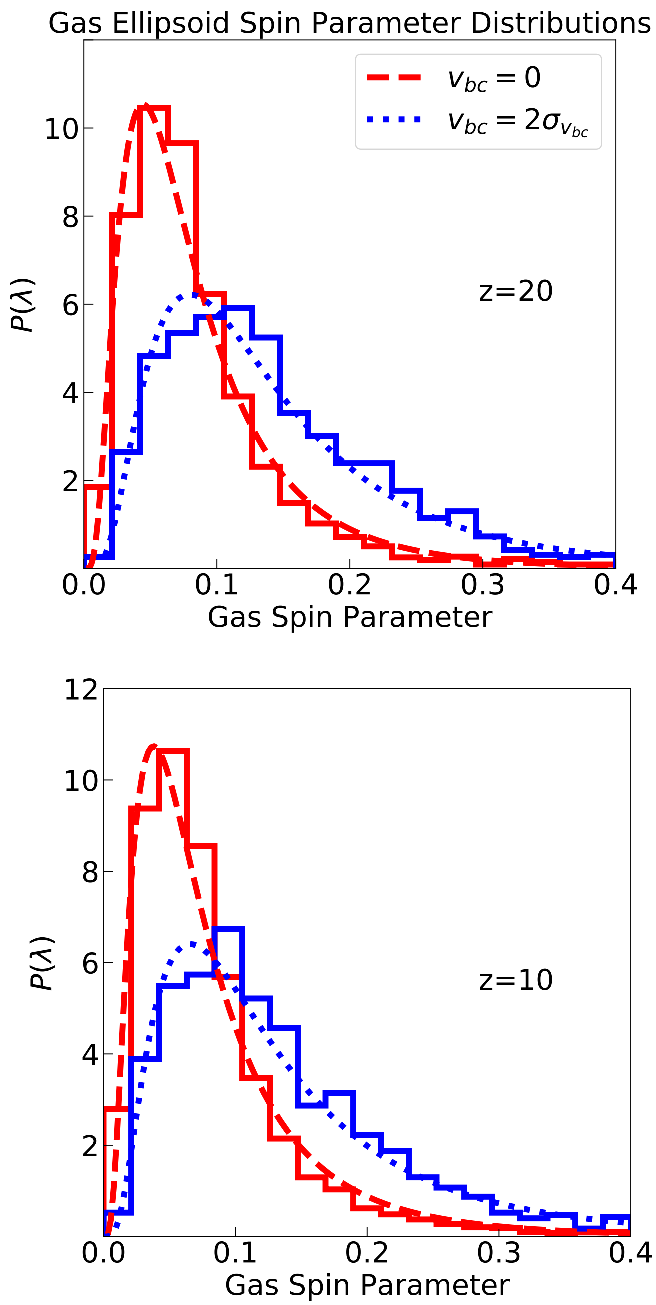

Figure 2.7: Lognormal distribution of generalized spin parameters for Gas-Primary objects at different redshifts. We consider the zero $v_{\rm bc}$ case in dashed red and the $v_{\rm bc} = 2\sigma_{v_{\rm bc}}$ in dotted blue.

$\sim 6 \times M_{\rm gas}$, where $M_{\rm gas}$ is the mass of the gas structure. Furthermore, as it can be seen in Figure 2.1, the complex dynamical evolution of these systems, resulted in having the gas-rich clumps concentrated around a larger halos. In other words they have not stayed with the parent DM halo. Hence, we define a spin parameter for the ellipsoidal Gas-Primary objects as

$$\lambda_{\rm GP} = \frac{J_{\rm gas}}{6\sqrt{2} M_{\rm gas} v_{\rm GP} R_{\rm max}} \ , \tag{2.8}$$

where $R_{\rm max}$ is half of the longest axis of the fitted ellipsoid, and $v_{\rm GP}$ is the circular velocity at this distance. This choice of similar normalization for the Gas-Primary objects, allows us to have one-to-one comparison with the definition of the spin parameter (Eq. 2.4). As shown in Figure 2.7, the extended spin parameter definition also follows a lognormal distribution and the stream velocity effect shifts the median higher. This is expected because a majority of the Gas-Primary objects are just the gas components of a corresponding DM-Primary/Gas-Secondary object.

Similar to our presentation of the spin-mass relationship of the DM-Primary/Gas-Secondary objects (see Figure 2.5), we analyze the spin-mass behavior of the Gas-Primary objects in Figure 2.8. We mark the SIGO subset of objects in stars. As shown in the Figure, SIGOs have typically smaller masses (as expected from the analytical analysis, Naoz and Narayan, 2014), and systematically larger spin parameter.

Another question one can ask is how the ellipsoidal morphology is affected by the spin parameter. Under the stream velocity effect, the ellipsoidal Gas-Primary structures, (see Figure 2.9), become more prolate. There is also a small positive correlation between the prolateness and the spin parameter that decreases with redshift. We suspect that this correlation exists because the baryonic components are collapsing on to disks, which gives higher spin. However, with the stream velocity effect included, this correlation disappears at high redshift, where the stream velocity has a greater effect. The weak correlation is restored at low redshift, but in this case the objects are prolate ellipsoids in shape. The SIGOs, however, do not seem to show any correlation between spin parameter and prolateness.

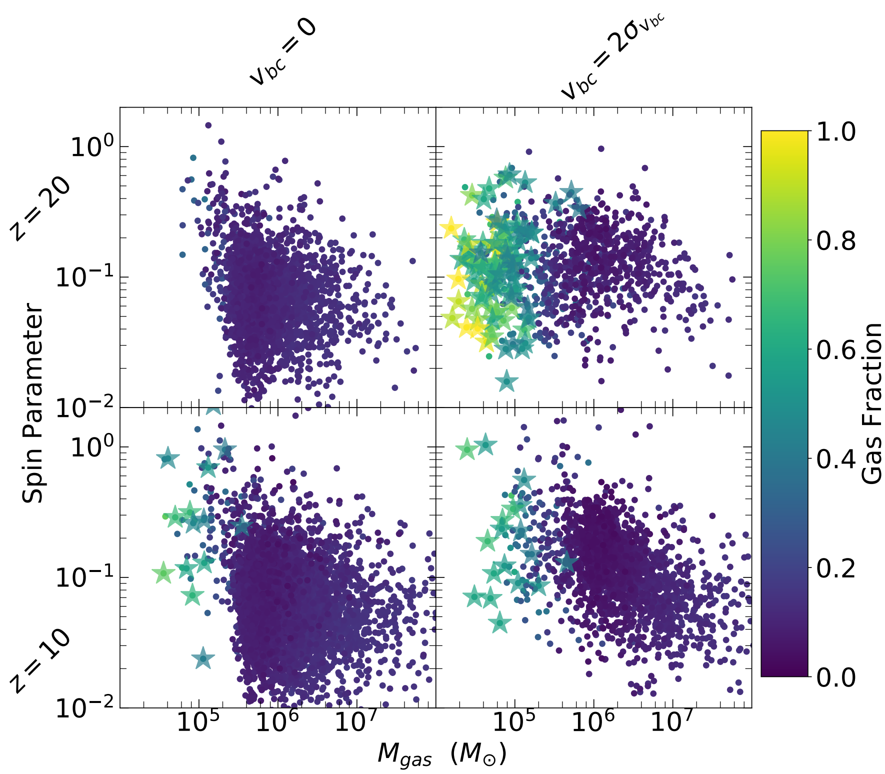

Figure 2.8: Spin parameter distributions for Gas-Primary objects with and without stream velocity at different redshifts. We mark the Supersonically-Induced Gas Objects (SIGOs) as stars. Note that SIGOs occupy a large range of spin parameters, and as predicted in (Naoz and Narayan, 2014), are typically below 10^6 $M_\odot$. The color code describes the gas fraction in these structures.

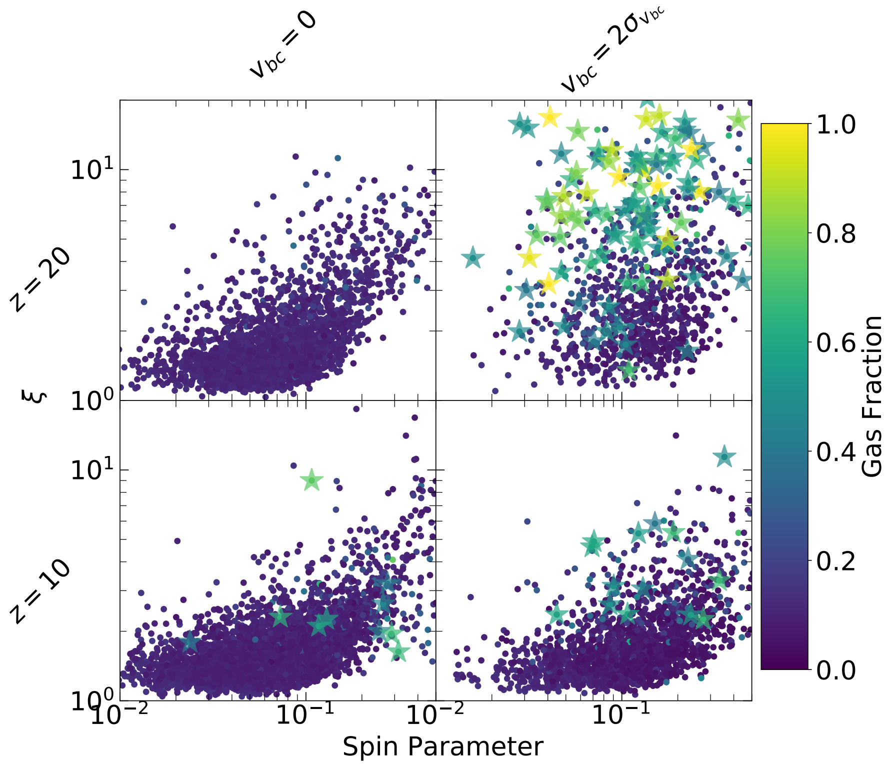

Figure 2.9: The prolateness of ellipsoids (see Eq. 2.1) as a function of spin parameter. $R_{\max}$ and $R_{\min}$ refer to the largest and smallest axis of the ellipsoid in question. Stars refer Supersonically-Induced Gas Objects (SIGOs). The colour code indicates the gas fraction in each object. Note that $\zeta \to 1$ means a spherical system. Rotationally supported systems have large prolateness and large spin parameter.

2.6 Summary and Conclusions

The supersonic relative velocity between the DM and baryons in the early Universe has been shown to shift the positions of baryonic and DM over-densities (e.g., Naoz et al., 2012), and in some cases the baryonic over-densities may collapse outside the virial radius of their parent DM halo, forming the so-called *Supersonically-Induced Gas Objects* (e.g., Naoz and Narayan, 2014; Popa et al., 2016). We identified two significant structures (see Section 2.3). The first structures are the classical DM halos, with a gas component. These were found in the simulation by using a DM-Primary/Gas-Secondary linking in the FOF groups. The other structures were identified in the simulation using only gas particles in the FOF groups, namely the Gas-Primary objects. The stream velocity effect further produces SIGOs (which are a subset of Gas-Primary objects). This new class of objects is defined by lying outside the virial radius of DM halos and also have a gas fraction of over 40%. At $z = 20$, $\sim 11\%$ of the gas-rich objects ($f_g > f_{\rm b,0}$) are in fact SIGOs.

We have investigated the angular momentum of all preceding objects through the spin parameter. To our knowledge, this is the first study of spin parameters of simulated halos at the low mass range ($10^{5-8}\ M_\odot$) at high-redshift.

We began by investigating the DM halos and their baryonic counterparts. We found that the spin parameter of the DM halos is described by a lognormal distribution, just as the low-redshift, high-mass counterparts. Moreover, the fit parameters are consistent with those obtained for high-mass, low redshift halos (see Table 2.2, and see for example, Bullock et al. (2001)). The relative velocities between baryons and DM produce non-trivial consequences to the spins parameters of these objects. In particular, the stream velocity effect increases the median spin parameter of the gas components of DM halos, as seen in Figure 2.4.

We have demonstrated in Figure 2.6 that the angular momenta of the gas and DM components are highly misaligned, due to the stream velocity effect. The angle between the angular momentum vectors of the DM and gas component of the halo has a nearly isotropic distribution. The standard picture of galaxy formation posits that both baryons and DM inherit the same initial angular momentum from tidal torques. However, baryonic effects in the case of zero stream velocity still produce about $30°$ misalignment (e.g., Jiang et al., 2018; Liao et al., 2017; van den Bosch et al., 2002; Velliscig et al., 2015). Notably, the stream velocity effects yields a larger misalignment that can occur in high-redshift galaxies. In particular, at high redshift the misalignment angle roughly follows an isotropic distribution.

We then generalized the spin parameter to accommodate the ellipsoidal Gas-Primary objects which also include the new class of Supersonically-Induced Gas Objects (SIGOs) that arise from the stream velocity effect. The spin parameter traditionally normalizes the angular momentum to with the virial parameters of the DM halo. Since SIGOs do not live inside a DM halo[4], we normalize spin parameters for Gas-Primary objects to a fiducial host DM halo of mass $6M_{\rm gas}$. The majority of the Gas-Primary objects (90% at $z = 20$) are gas components of DM halos, as such they are expected to follow a log normal distribution as expected (e.g., Bullock et al., 2001; Zjupa and Springel, 2017) The lognormal distribution in the classical objects are shown in Figure 2.4, and the log-normal distribution of the Gas-Primary ellipsoids is demonstrated in Figure 2.7. Thus, although these are classified differently, they represent the same component. Focusing on the SIGOs, we found that their morphology, in particular, their prolateness is uncorrelated with the spin parameter, in contrast to typical disk galaxies which would exhibit a positive correlation (as depicted in Figure 2.9).

We showed that in the presence of stream velocity, even in the non-radiative case, the spin parameter the gas component of DM halos is increased, and is misaligned with respect to the DM's angular momentum. Moreover, we showed that the SIGOs have higher spin parameters in the presence of the $v_{\rm bc}$ compared to Gas-Primary in the case of $v_{\rm bc} = 0$. The spin parameter already serves as a valuable measurable quantity for higher mass galaxies ($\lesssim 10^{10}$ $M_{\odot}$), and lower redshift ($z \sim 1-3$) formation histories (e.g., Burkert et al., 2016).

These SIGOs are likely to form stars from their gas concentrations and are typically small (about a few kpc, which expected to be even smaller when cooling is introduced e.g., Hirano et al., 2017b). Therefore they might explain the low luminosity, small-sized objected recently reported

[4]Note that the gas ellipsoids with gas fraction lower then 40% are dominated by DM, but not necessarily in the centre of a DM halo (Naoz and Narayan, 2014).

by (Bouwens et al., 2017). Furthermore, JWST may be able to detect SIGOs and low luminosity DM halos at their formation sites, $z \sim 20$. The large spin parameter, if inferred from observational data, might serve as an indication for a high stream velocity patch. Recently, HST has observed a potentially promising candidate, the so-called "Little Blue Dots" (Elmegreen and Elmegreen, 2017). These objects are thought to be gas-dominated systems in the early Universe, with high specific star formation rates. Based on the gas fraction and the scale of the structures, we speculate SIGOs are a possible formation channel for these observed objects.

CHAPTER 3

SIGOs – To Cool or Not to Cool?

3.1 Abstract

Supersonically Induced Gas Objects (SIGOs) form in the early Universe, before reionization outside of dark matter halos due to the presence of a relative stream velocity between baryons and dark matter. These structures may be the progenitors of globular clusters. Since SIGOs are made out of pristine gas, we investigate the effect of atomic cooling on their properties. We run a set of four simulations by using the moving-mesh code AREPO, with and without baryon-dark matter relative velocity and with and without the effects of atomic cooling. We show that SIGO's density, temperature, and prolateness are determined by gravitational interactions rather than cooling. The cold gas fraction in SIGOs is much higher than that of dark matter halos. Specifically, we show that the SIGO's characteristic low temperature and extreme high gas density forges a nurturing site for the earliest star formation sites.

3.2 Introduction

One of the fundamental tenets of the Lambda cold dark matter (ΛCDM) cosmology is the hierarchical buildup of structure in a bottom-up fashion (e.g., Blumenthal et al., 1984; Rees and Ostriker, 1977; Silk, 1977; White and Rees, 1978). Smaller structures collide and build bigger structures. After inflation, dark matter (DM) in the Universe started this buildup by clustering gravitationally. However, since baryonic matter and radiation were tightly coupled, it was not until after the time of recombination that baryonic overdensities could grow. After decoupling, the baryons felt the gravitational potential wells of DM overdensities, as well as their own, and subsequently their overdensities grew.

Tseliakhovich and Hirata (2010) noted that the evolution during these early times yielded a relative velocity between the DM and baryons, the so called "stream velocity." Although a formally second order, the stream velocity has far-reaching consequences on a wide variety of cosmological phenomena (e.g., Fialkov et al., 2012; Greif et al., 2011; Maio et al., 2011; Naoz et al., 2011b, 2012; O'Leary and McQuinn, 2012; Richardson et al., 2013; Stacy et al., 2011; Tanaka and Li, 2014). For example, this relative velocity may have nontrivial effects on the cosmological 21-cm signal (e.g. Dalal et al., 2010; Fialkov and Barkana, 2014; McQuinn and O'Leary, 2012; Muñoz, 2019; Visbal et al., 2012), the formation of primordial black holes (e.g., Hirano et al., 2017a; Latif et al., 2014; Schauer et al., 2017; Tanaka and Li, 2014; Tanaka et al., 2013), and even for primordial magnetic fields (Naoz et al., 2013).

In particular, it was recently suggested that the stream velocity can result in a gas-dominated structure Naoz and Narayan (2014), and that these Supersonically Induced Gas Objects (SIGOs) could be the progenitors of globular clusters (Chiou et al., 2019, 2018; Naoz and Narayan, 2014; Popa et al., 2016). These SIGOs arise naturally as a consequence of the stream velocity effect (Tseliakhovich and Hirata, 2010). In particular, this relative velocity introduces a phase shift between DM and baryons, which can lead to baryon overdensity peaks collapsing outside the virial radius of their parent DM halo (Naoz and Narayan, 2014).

We previously suggested that SIGOs may be a viable nurturing ground for star formation (Chiou et al., 2019). Specifically, we used a combination of simulation and semi-analytical modeling to follow the SIGOs from birth to present day. We showed that present day SIGOs share characteristics with observed globular clusters. One physical process we included was cooling. While in (Chiou et al., 2019) we studied star formation and the connection between SIGOs and globular clusters, here we focus specifically on the effect that atomic cooling has on SIGOs and run detailed comparisons between simulations with cooling turned on versus turned off.

Cooling plays a vital role in the formation of the first stars in the Universe, the so called Population III (Pop III) stars (see Wise (2012), Bromm (2013) and references within for a review). These stars formed in pristine gaseous clouds that were heated and shocked as they fell into dark matter minihalos ($10^5 - 10^7 M_\odot$). These objects would become pressure supported unless cooling via atomic and molecular hydrogen allowed them to collapse to such densities that stars could form.

In the context of cosmological simulations, cooling has been taken into account in a variety of ways with different cooling channels (e.g., Abel et al., 2002; Bromm and Clarke, 2002; Glover, 2013; Reed et al., 2005; Sarmento et al., 2018; Stacy et al., 2011; Vogelsberger et al., 2013; Xu et al., 2016; Yoshida et al., 2006). The standard assumptions are that hydrogen and helium are in photo-ionisation equilibrium with a uniform, but time-varying, UV background and that metals are in collisional ionisation equilibrium.

The first stage of cooling for pristine, non-molecular, gas is the so-called atomic hydrogen cooling. This cooling channel is typically more effective for gas with temperatures $> 10^4$ K (e.g., Barkana and Loeb, 2001). Metal-enriched gas cools via molecular cooling. H_2 cooling becomes effective for a gas cloud when the number density reaches above 10^4 cm^{-3} and further allows cooling down to temperatures of 300 K (Wise, 2012). Since we focus on the very first gas statures, which include pristine gas, we target the atomic cooling channel.

Recently, Schauer et al. (2019) incorporated the stream velocity effect between DM and baryons in the early Universe with an advanced chemistry network. Focusing on classical DM halos, they showed the minimum halo mass that allows star formation is significantly increased and that the cooling of gas is suppressed. They however, did not investigate the effect of cooling on SIGOs properties.

In this chapter, we investigate the effect of cooling on SIGO morphology and potential star forming properties by analyzing the cosmological simulations in Chiou et al. (2019) with cooling and UVB shielding taken into account. This chapter is organized as follows: in Section 3.3 we detail the simulations. In Section 3.4 we describe how cooling affects the characteristics and morphological properties of SIGOs. and we wrap up with a discussion and our conclusions in Section 3.5.

3.3 Simulations

3.3.1 Cooling and non-cooling runs

We perform a suite of cosmological simulations using the moving-mesh code AREPO (Springel, 2010a). Below we briefly describe the main aspects of the simulations and we refer the reader to Chiou et al. (2018) and Chiou et al. (2019) for a complete overview of the simulations, with and without cooling, respectively. We employ a modified version of the CMBFAST (Seljak and Zaldarriaga, 1996) code to generate the transfer functions used for the creation of the initial conditions. These transfer functions take into account the first-order correction of the scale dependent temperature fluctuations (as shown in Naoz and Barkana, 2005b). We note that our simulations naturally include different transfer functions for the DM and baryon components, which play an important role in determining the gas fraction and overdensity growth rate (e.g., Naoz and Barkana, 2007; Naoz et al., 2011b, 2013; Park et al., 2020).

We include radiative cooling with a 2 cMpc^3 box size, with and without stream velocity effects, however, we do not include explicit star formation or feedback. AREPO's basic cooling module is composed by a primordial chemistry and cooling network of the evolution of species H, H^+, He, He^+, He^{++} and e^- in equilibrium with a photoionizing background. The background is assumed to be spatially constant, but redshift dependent. The gas cooling and heating rates are calculated as a function of gas density, temperature,[1] and redshift (See Vogelsberger et al., 2013, and references therein for further details on the numerical implementation of these processes).

As a control, we also ran simulations without cooling, and with and without stream velocity effects [2]. We perform a simulation with a stream velocity of 2 $\sigma_{\mathrm{v}bc}$ and one without stream velocity. The stream velocity effect is implemented as a uniform boost in the x-direction for the baryons. The box has 512^3 DM particles associated with a mass resolution of $m_{\mathrm{DM}} = 1.9\times10^3 M_\odot$. We represent the gas as mesh of 512^3 Voronoi cells that correspond to a particle mass of $m_{\mathrm{gas}} = 360 M_\odot$. We

[1]Note that while all cooling rates include self-shielding corrections, these do not apply above redshift of 6, and thus do not contribute for the cooling of the $z = 20$ objects.

[2]We note that the simulations in (Chiou et al., 2019) are denoted here as V0Cool and V2Cool

Name	$v_{\rm bc}(\sigma_{\rm vbc})$	Cooling
v0Cool	0	Yes
v2Cool	2	Yes
v2Uncool	2	No

Table 3.1: Details of the simulations performed. For all simulations we have 2 cMpc box, 512^3 DM particles, and 512^3 gas cells. For this set of parameters we have that the mass of the DM particle is $m_{\rm DM} = 1.9 \times 10^3 M_\odot$ whereas the mass of a gas cell is $m_{\rm gas} = 360 M_\odot$.

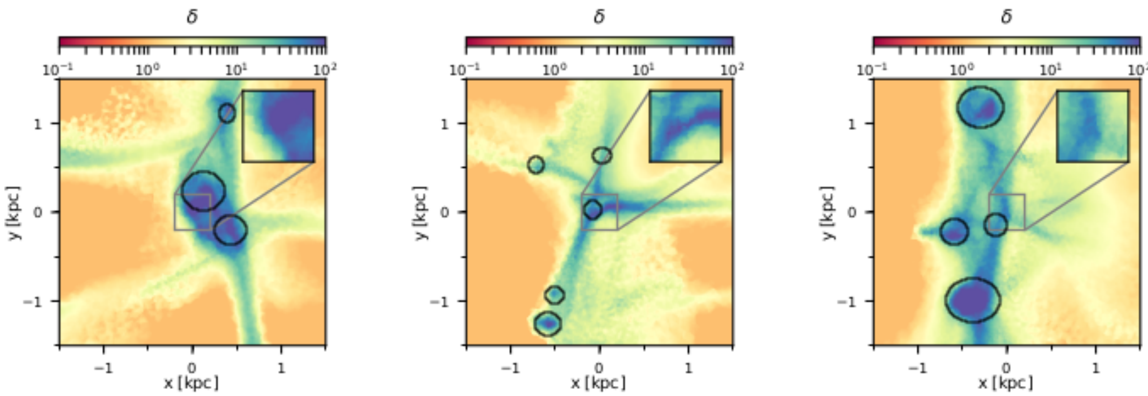

Figure 3.1: Projected overdensities of various SIGO environments in v2Cool. SIGOs are located in the center of each panel with a zoom-in to the center region showed in each subpanel. Notice that in regions at which the SIGOs are nested, large by a factor of a few, have projected $\delta > 1$, already at $z = 20$. DM/G are identified by the black circles. In the left and right panels we detect one SIGO, while the middle panel depicts a "binary" SIGO configuration. Note that in projection the SIGOs seem to overlap the classical DM/G. However, as shown in Figure 3.2, these SIGOs are detached from the DM/G.

note that, while the $2\sigma_{\rm vbc}$ with cooling simulation is presented in Chiou et al. (2019), here we focus on the comparison between cooling and not cooling and with and without the stream velocity.

Overall we present here a total of 3 simulation results at $z = 20$, with and without cooling, and with and without stream velocity, with the aforementioned parameters [3]. A summary of the simulations performed is given in Table 3.1. The naming convention is as follows. 0 or 2 represents $v_{\rm bc} = 0, 2\ \sigma_{\rm vbc}$ and 'Cool' or 'Uncool' denote whether cooling was turned on or switched off.

[3] v0Uncool has been the subject of previous studies (Chiou et al., 2018; Popa et al., 2016)

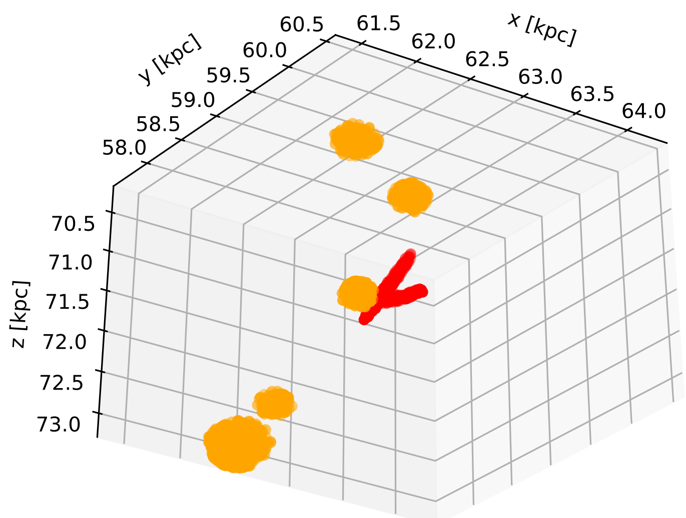

Figure 3.2: SIGOs corresponding to the middle panel in Figure 3.1. There are two SIGOs in red and the surrounding DM/G are in orange. Note the deviation form sphericity as shown in Popa et al. (2016) and Chiou et al. (2018). To generated this Figure we ignore ambient particles and only consider DM and gas particles that are bound to an object.

3.3.2 Object classification

Following Popa et al. (2016) and Chiou et al. (2019, 2018), we define the following objects in our simulation: DM-Primary/Gas-Secondary (DM/G) and Supersonically Induced Gas Objects (SIGO). These objects come from a Friends-of-Friends (FOF) halo finding algorithm with a linking length of 0.2 times the mean particle separation. We define the DM/Gs by running the FOF algorithm first on the DM, and then adding gas cells in a secondary linking step (Dolag et al., 2009). We only consider the DM/G to be all particles within a sphere of radius of R_{200} of the center of mass the FOF group with the further constraints that that they contain over 300 DM particles and over 100 gas cells. SIGOs are gas-only FOF groups whose center of mass is outside the virial radius of the closest DM/G and have gas fractions $> 40\%$. SIGOs must contain more than 32 gas cells and are fitted to tight ellipsoids. Notice that by definition, SIGOs only appear in runs with nonzero stream velocity.

The SIGOs overdensities are much larger than unity and thus in the process of collapsing, (as noted in Popa et al., 2016, Figure 2). We define overdensities as $\delta = (\rho_{\rm gas} - \bar{\rho})/\bar{\rho}$, where $\rho_{\rm gas}$ is the density of the gas cells composing the SIGO and $\bar{\rho}$ is the average density of the Universe. Interestingly we find that the large filaments around the SIGOs have overdensities that are much larger than unity, as depicted in Figure 3.1. While the typical size of a SIGO is about $10-50$ pc, it seems that in projection already a larger regime (by a factor of a few) has an overdensity larger than unity, (see Figure 3.3 for the 3-D overdensity of SIGOs). This is a complex neighbouring environment, which includes both DM halos (with little to no gas component in them) and SIGOs in between (as shown in see Figure 3.2).

In Figure 3.1, the black circles are projected dark matter halos in the vicinity of the SIGO. SIGOs tend to be found in the gas streams between dark matter halos. All SIGOs are collapsing at $z = 20$, with the smallest SIGO having an overdensity of ~ 400 at $z = 20$. We note that Figure 3.1 shows the results of the simulation with cooling. We find similar results without cooling.

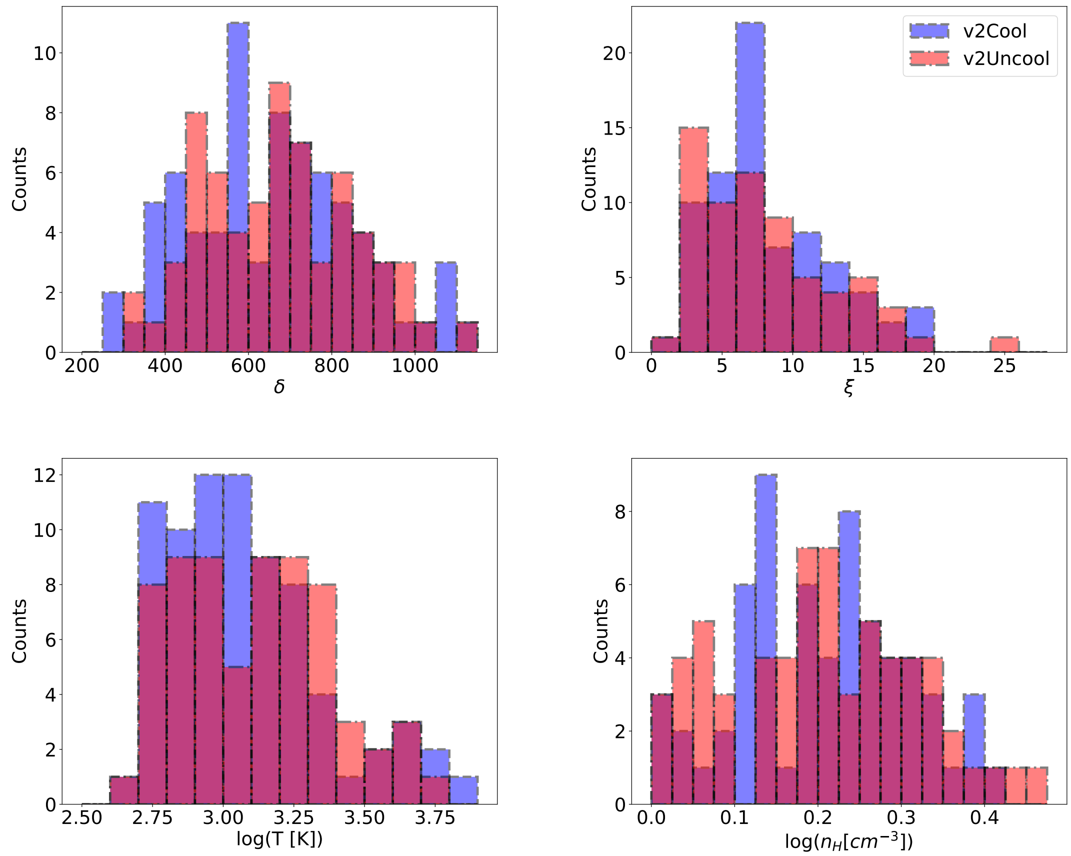

Figure 3.3: Histograms of SIGO properties in v2Cool (purple, dashed) and v2Uncool (pink, dot–dashed). Cooling does not dramatically affect SIGO properties.

3.4 The relevance of cooling on SIGOs properties

3.4.1 Physical properties

It is well established that cooling affects the properties of DM/G objects (e.g., Hartwig et al., 2015; Katz et al., 1996; Vogelsberger et al., 2013) even in the presence of stream velocity (e.g., Druschke et al., 2019; Schauer et al., 2019, 2017). We discuss these results in Appendix 3.6.2. In this section, we investigate the effect of cooling on SIGOs properties such as morphology, temperature, density and environment. Most of the previous investigations of SIGOs were conducted in simulations with no radiative cooling (Chiou et al., 2018; Popa et al., 2016). In Chiou et al. (2019) for the first time, we studied the evolution of SIGOs while including atomic cooling. Here we examine in details the effect that cooling has on SIGOs and compare to the no cooling realization. Considering the temperature of SIGOs in the case of no cooling (v2Uncool), their temperatures range from about ~ 400 K to $\sim 6 \times 10^3$ K (as shown in purple, dot-dashed in the bottom left panel in Figure 3.3). Thus, since atomic cooling is rather inefficient for temperatures below 10^4 K, we expect that atomic cooling will have little to no change on the SIGOs temperature, as shown in Figure 3.3 bottom left panel. In fact, because of this inefficiency of atomic cooling, we further expect that other SIGO properties, such as overdensity, prolateness, and number density will be similar between the case of with and without cooling. Histograms of these properties are shown in Figure 3.3 on the top left, top right, and bottom right respectively. The KS test we conducted between the two runs found that there was not enough evidence to conclude that the SIGO properties came from different distributions at 95% confidence. The p-values, means, medians, and standard deviations can be found in the right column of Table 3.4.1.

The distributions of overdensities (top left panel of Figure 3.3) are roughly normal in both runs, and all SIGOs have greater than 200 overdensity. The prolateness $\xi = R_{\rm max}/R_{\rm min}$(top right panel) is shifted to slightly higher due to cooling, but statistically indistinguishable. Similarly, the temperature distribution of SIGOs (bottom left panel) is shifted to slightly lower values, but again, as expected, is statistically indistinguishable from the non-cooling run. Furthermore, cooling does not affect the hydrogen number density (bottom right panel). Performing two-sample KS tests between v2Cool and v2Uncool all yield p-values $> .05$, implying that there is not enough information to reject the null hypothesis at 95% confidence that these two simulations come from the same property distributions.

We note that in the v2Cool we have removed one outlier SIGO that has an overdensity (density) of 1.3×10^6 $M_\odot$ (5.2×10^{-21} g cm^{-3}), mass of 3×10^6 $M_\odot$ and a temperature of 3100K. It is 1.1 kpc away from the closest DM/G. There is no corresponding massive SIGO in v2Uncool [4]. While massive, this is not unexpected. Naoz and Narayan (2014) found an upper limit for a 2σ density fluctuation to be $\sim 10^6 M_\odot$. We further explore this object in Appendix 3.6.1.

To illustrate further the consistency between the v2Cool and v2Uncool, we consider three rep-

[4]The most massive SIGO in the v2Uncool is 1.9×10^5 $M_\odot$ (Chiou et al., 2019; Popa et al., 2016)

		v2Cool			v2Uncool		KS p-value
	mean	median	σ	mean	median	σ	
δ	657	660	197	690	670	200	0.58
ξ	8.33	7.23	4.30	9.47	7.81	8.79	0.50
T (K)	1429	1064	1127	1696	1421	1370	0.17
n_H (cm^{-3})	1.52	1.53	0.46	1.60	1.53	0.46	0.58

Table 3.2: Table of summary statistics of SIGOs for v2Cool. We use a two sample Kolmogorov Smirnov (KS) test to compare the distributions of the SIGO parameters in v2Cool and v2Uncool. Cooling does not significantly alter the distributions of SIGO properties. We note that in this statistics we dropped one major SIGO outlier, and we discuss its properties in appendix 3.6.1.

resentative examples of SIGOs in Figure 3.4, with and without cooling (bottom and top panels, respectively). As can be seen in the Figure, the morphology, the environment as well as the turbulent velocity field in the inner region of the SIGOs seems consistent between the two scenarios.This turbulent energy, driven by the supersonic stream velocity, must be overcome for star formation to occur. We note that the left panels correspond to the same SIGO between runs. In this Figure we zoom in to the innermost 1 kpc part of the SIGO as shown in the inset of each panel. We can visually identify the shock in this Figure, where the gas density jumps dramatically, corresponding to a transition from subsonic to supersonic. SIGOs in these simulations are highly nonlinear and dense objects, with a mean overdensity in v2Cool and v2Uncool of 657 and 690 and n_H of 1.52 cm^{-3} and 1.60 cm^{-3} (see Table 3.4.1).

Given that the morphologies and attributes remain similar with and without cooling, it stands to reason that atomic cooling may not significantly affect the star forming ability of SIGOs. Further inclusion of molecular hydrogen cooling should only increase the star formation potential.

3.4.2 The Effect of Cooling on Star Formation in SIGOs

Star formation requires the gas within a DM/G or SIGO to be very cold and dense so that it can collapse gravitationally. In a previous paper (Chiou et al., 2019), the cooling simulations that we ran did not explicitly follow star formation. To study the star forming properties, we used a simple stability argument similar to the Jeans criteria. However, due to the supersonic nature of the stream velocity, turbulence must also be considered. Equating the Jeans length with the sonic

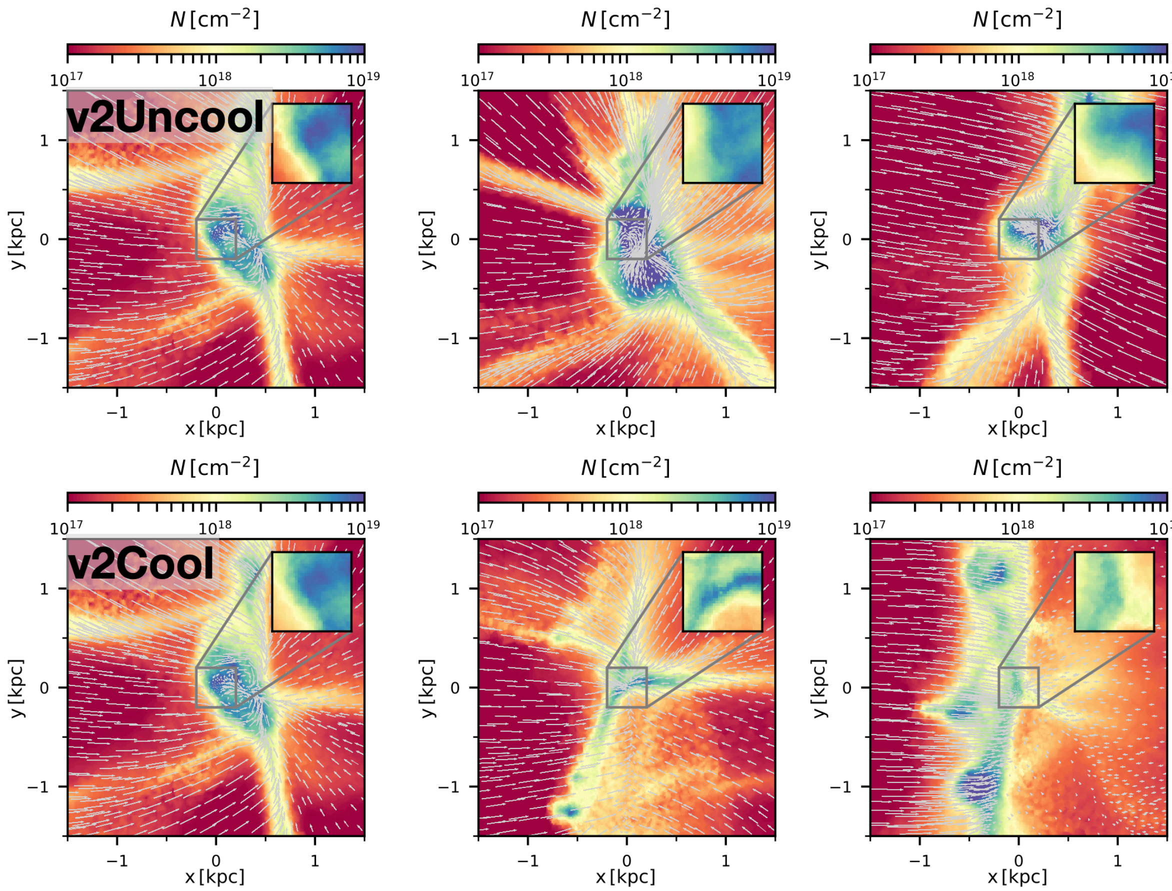

Figure 3.4: Column densities of a SIGO and its surrounding environment. A slice of the velocity field is also shown. Gas is accreting onto the SIGO. The top row contains SIGOs from the v2Uncool run and the bottom contains three from the v2Cool run.

length (i.e., the length scale at which gas transitions from supersonic to subsonic), Krumholz and McKee (2005) defined a critical density for collapse, $\rho_{\rm crit}$. This critical density is given as

$$\rho_{\rm crit} = \frac{\pi c_{\rm s}^2 \mathcal{M}^4}{GL^2}, \tag{3.1}$$

where $c_{\rm s}$ is the sound speed, $\mathcal{M}$ is the Mach number, G is the gravitational constant and L is the scale at which turbulence is driven, and as demonstrated visually in Figure 3.4, it coincides with the diameter of the SIGO along the longest axis. This critical density represents the balance between gravity and turbulent/thermal kinetic energy (in the absence of magnetic fields), above which the gas in the object will become unstable to collapse and the object will likely form stars. (Burkhart, 2018) related this critical density to the transition between a turbulent density distribution and one that is experiencing gravitational collapse and hence it is a natural consequence of the continuity of the density distribution function (see also Burkhart and Mocz, 2019; Girichidis et al., 2014; Guszejnov et al., 2018). Here we use this critical density as an indicator of star formation.

In Chiou et al. (2019) we have shown that SIGOs are ripe sites for start formation. Notably, 88% of the SIGOs were star forming in the cooling simulations performed there (v2Cool). This is comparable to the v2Uncool run in which 91% of SIGOs were star forming. Moreover, while classical small scale structures in the early Universe, i.e., DM/G, are less likely to form stars, SIGOs' critical density typically is much higher than unity (as shown in Chiou et al., 2019, Figure 2). In Figure 3.5, we show the cooling runs overlayed with the no cooling results in grey. As expected, the cooling tends to lower the average temperatures to below $10^4\ K$ of DM/G as expected (Figure 3.6), but the SIGOs' temperatures are not significantly affected.

As can be seen in Figure 3.5, a few SIGOs in the no-cooling realization, have a temperature about 10^4 K (grey stars at the left top corner - left to the red vertical line). These SIGOs indeed cooled via atomic cooling, reduced their temperature and slightly increased the density. But we note that these SIGOs are not expected to form stars, unlike the majority of the SIGOs (to the right of the red vertical line). Cooling does not significantly affect the scatter of SIGOs in the temperature - density plane. Although the SIGOs in v2Uncool seem achieve in general higher densities, it is not statistically significant (as shown in table 3.4.1). However, the scatter remains

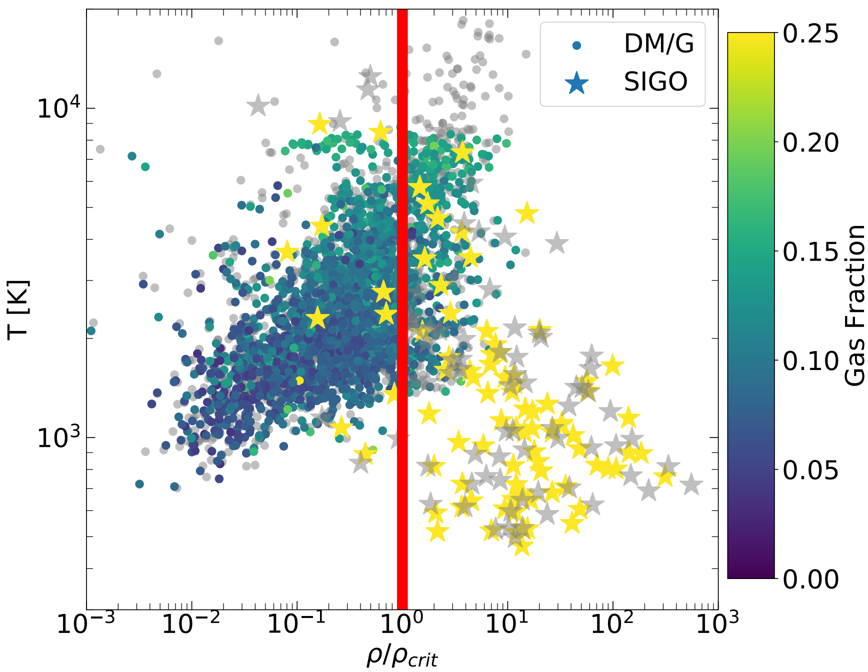

Figure 3.5: Temperature of objects as a function of as a function of $\rho/\rho_{\rm crit}$ at $z = 20$ with stream velocity. All objects to the right of the red line are star forming (see Chiou et al. (2019). The gray points are from v2Uncool, whereas the colored points are from v2Cool. The temperatures decrease a bit due to cooling, however the overall shape of the distributions stay the same indicating that gravity is dominating.

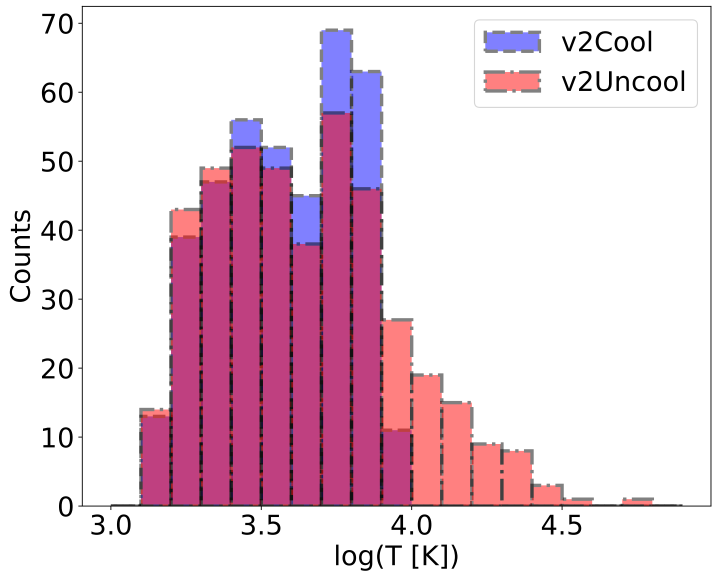

Figure 3.6: Histogram of temperatures of DM/Gs in v2Cool (purple, dashed) and v2Uncool (pink, dot-dashed)

similar suggesting that gravity is the dominating mechanism for the onset of star formation in SIGOS (not so dissimlar to modern star formation (e.g., Burkhart and Mocz, 2019)).

In the literature, the fraction of the cold gas in an object compared to the total gas fraction is often used as a tracer to star formation (e.g., Davis et al., 2019; Schauer et al., 2019; Wang et al., 2017). Here, we define a cold gas cell to be one with a temperature $< 500\,\mathrm{K}$ and define as a cold object a structure that contains at least one cold gas cell following Schauer et al. (2019).

In Figure 3.7, we plot the cold gas fraction, $f_{\rm cold} = M_{\rm cold}/(M_{\rm gas} + M_{\rm DM}) = M_{\rm cold}/M_{\rm tot}$, as a function of total mass of the object for v2Cool and v0Cool in the top and bottom panels. The points are colored by gas density. We find that 29% of DM/G and 43% of SIGOs contain cold gas in v2Cool. In v0Cool, only 24% of DM/G contain cold gas (and of course no SIGOs are present).

A clear feature for the zero stream velocity cooling run (v0Cool) is an increasing trend of cold mass fraction for masses $M_{\rm tot} \geq 10^7 M_\odot$. This kink corresponds to a virial temperature of about 10^4 K. Above this temperature, atomic cooling dominates (Barkana and Loeb, 2001). The stream velocity generally increases the scatter in the cold gas fraction in the DM/G. This is expected as the

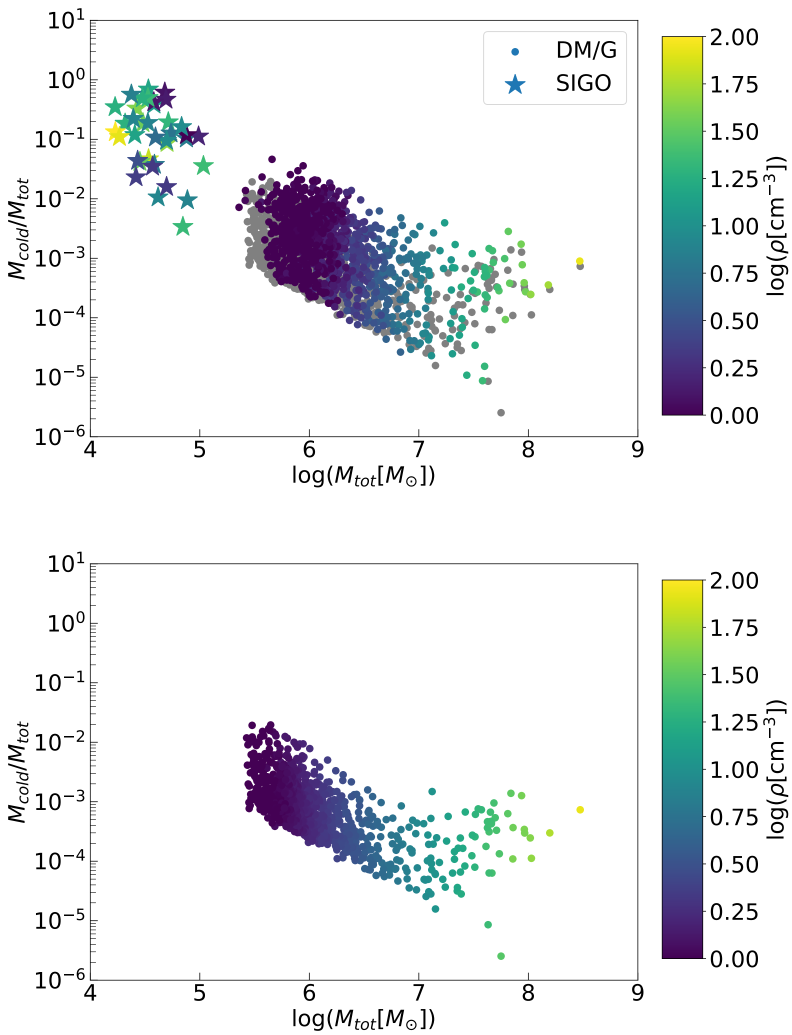

Figure 3.7: Ratio of cold gas mass to halo gas mass as a function of halo mass. Here we define a cold gas cell to have a temperature of < 500K. The color code is by gas density of the object. The top panel corresponds to v2Cool and the bottom panel corresponds to v0Cool. 29% of DM/G and 43% of SIGOs contain cold gas. In no stream velocity case, 24% of DM/G contain cold gas. The gray points in the top panel correspond to the v0Cool points in the bottom panel.

stream velocity acts as an additional pressure, enhancing collisions and diffusing the kink-feature at $10^7 M_\odot$.

The SIGOs have overall higher cold gas fraction than the DM/G. Furthermore, as empathized in Figure 3.4, SIGOs generally have lower temperature and high gas densities compared to their DM/G counterparts. Thus, it is not surprising that they present a high cold mass fraction (as depicted in Figure 3.7, top panel).

3.5 Summary and conclusions

We have investigated the nature of Supersonically Induced Gas Objects (SIGOs) under the influence of atomic cooling in cosmological simulations. In previous simulations (e.g., Chiou et al., 2018; Popa et al., 2016) with only adiabatic cooling due to the expansion the Universe, SIGOs were shown the be gas-rich ellipsoidal objects residing outside of dark matter halos. SIGOs at $z = 20$ generally have overdensities well above 200 indicating collapse.

We find that cooling does not dramatically alter the SIGO environment, though it does contribute to a more diffuse IGM, as shown in the density projections examples in Figure 3.4. We find that are no ≥ 3 neighboring SIGOs within ~ 2 ckpc^3 box. However, rarely we find 2 neighboring SIGOs (see Figure 3.2). As was noted in Chiou et al. (2019), SIGOs live in highly turbulent environments (e.g., Figure 3.4) which assist with star formation.

SIGOs form in the very early universe, where the gas is pristine, before high abundance of molecular hydrogen formed, therefore we consider the effects of atomic cooling. However, atomic cooling is inefficient below 10^4 K, thus since SIGOs' temperatures due to adiabatic cooling is generally lower than 10^4 K we expect only a marginal effect of this cooling channel on SIGOs temperatures (see Figure 3.5). Similarly, the overdensities, prolateness, and hydrogen number densities are not substantially affected, as shown in Figure 3.3. The physics behind the SIGOs properties is thus, mostly determined by gravity and the gravitational collapse.

The combination of high densities and low temperatures yield promising nurturing ground for star formation for the SIGOs, as illustrated in Figure 3.5 and in Chiou et al. (2019). The classical objects, (DM/G) on the other hand, not only have less gas fraction due to the stream velocity effects, but also have a too high temperature ($T \sim 10^3 - 10^4\ K$) to have efficient star formation. We speculate that molecular hydrogen cooling will further decrease the temperatures and clump SIGOs in a more pronounced way to produce more favorable sites for star formation which will be discussed in a future paper.

SIGOs have been purported as a novel formation channel for globular clusters (Chiou et al., 2019; Naoz and Narayan, 2014). The further addition of realistic physics in simulation such as molecular cooling, star formation, and feedback will allow for a more accurate modeling of these possible progenitors. As the *James Webb Space Telescope* comes online, future observations will further verify the link between SIGOs and globular clusters.

3.6 Appendix

3.6.1 The biggest SIGO

In this section we discuss the properties of the outlier SIGO in v2Cool shown in Figure 3.8. The SIGO (in red) is 1.1 kpc away from the closest DM/G, clearly out of the virial radius. Surrounding DM/G are shown in orange. The largest DM/G displayed here is the second largest in the simulation. This SIGO was the most dense (5.2×10^{-21} g cm^{-3}) and massive (3×10^6 M$_\odot$) SIGO found in v2Cool, an order of magnitude more massive than the most massive found in V2Uncool (which was $1.9 \times 10^5 M_\odot$). It was also an order of magnitude more massive than the next most massive SIGO in v2Cool. The temperature was 3100 K. Although there is no corresponding object in v2Uncool, we conjecture that this object is a result of Poisson statistics and not a sole result of cooling. Using linear theory, Naoz and Narayan (2014) showed that a 2σ overdense patch could form SIGOs as big as $\sim 10^6 M_\odot$.

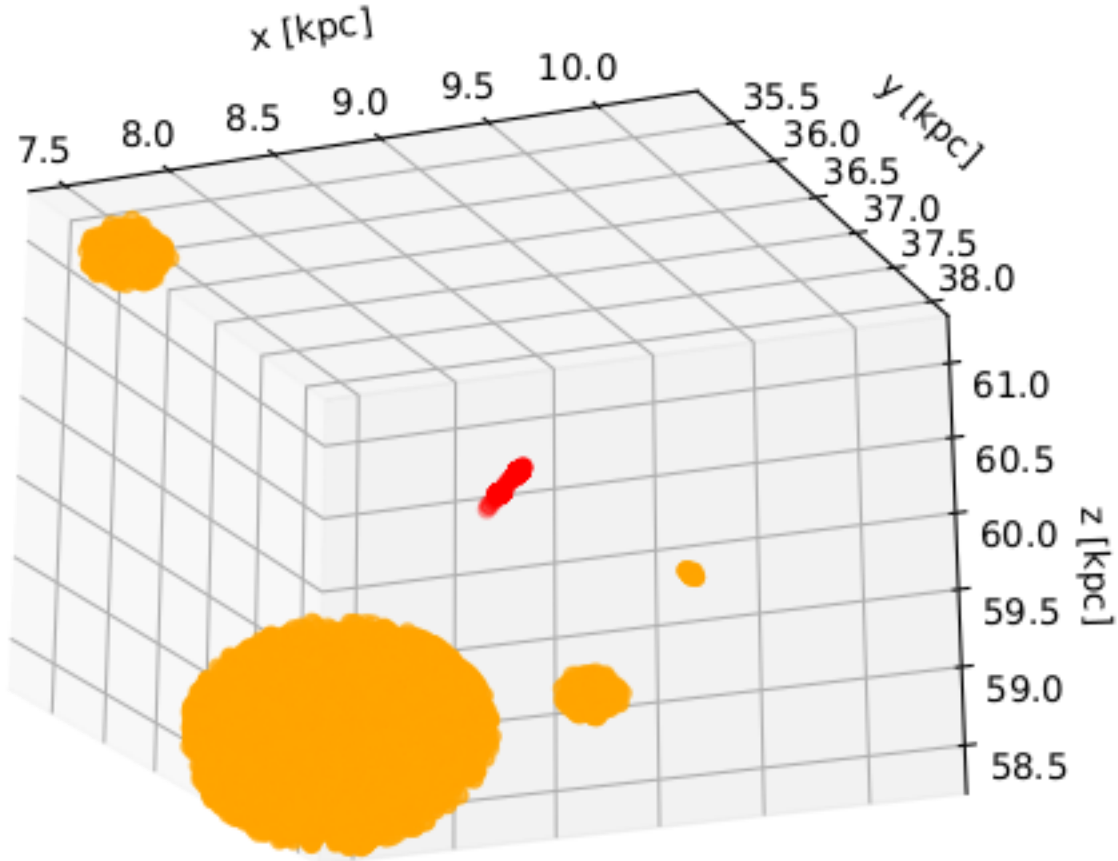

Figure 3.8: The largest SIGO (red) in v2Cool with mass $M_{\rm tot} \sim 3 \times 10^6$ $M_\odot$ Surrounding DM/G are in orange. The largest DM/G shown here is the second most massive in the simulation. The SIGO is 1.1 kpc from the closest DM halo.

3.6.2 DM/G

In this section we briefly reproduce several aspects of the effects of cooling on classical DM halos such as density projections and temperature distributions.

Several gas density projections of DM/Gs are shown in Figure 3.9. The top panels are from the v2Uncool run and the bottom are from v2Cool run. The circles represent the virial radius of the DM/G. The white arrows are velocity maps showing accretion onto the DM/G. The left DM/G is the most massive DM/G in each simulation and has similar large scale features. The cooling serves to compactify the DM/G as expected. The outer environments of the DM/G are less dense overall due to the gas condensing on the halo. The velocity field within the DM/Gs is more turbulent in the v2Uncool run since in general the DM/Gs in v2Cool have lower average temperature.

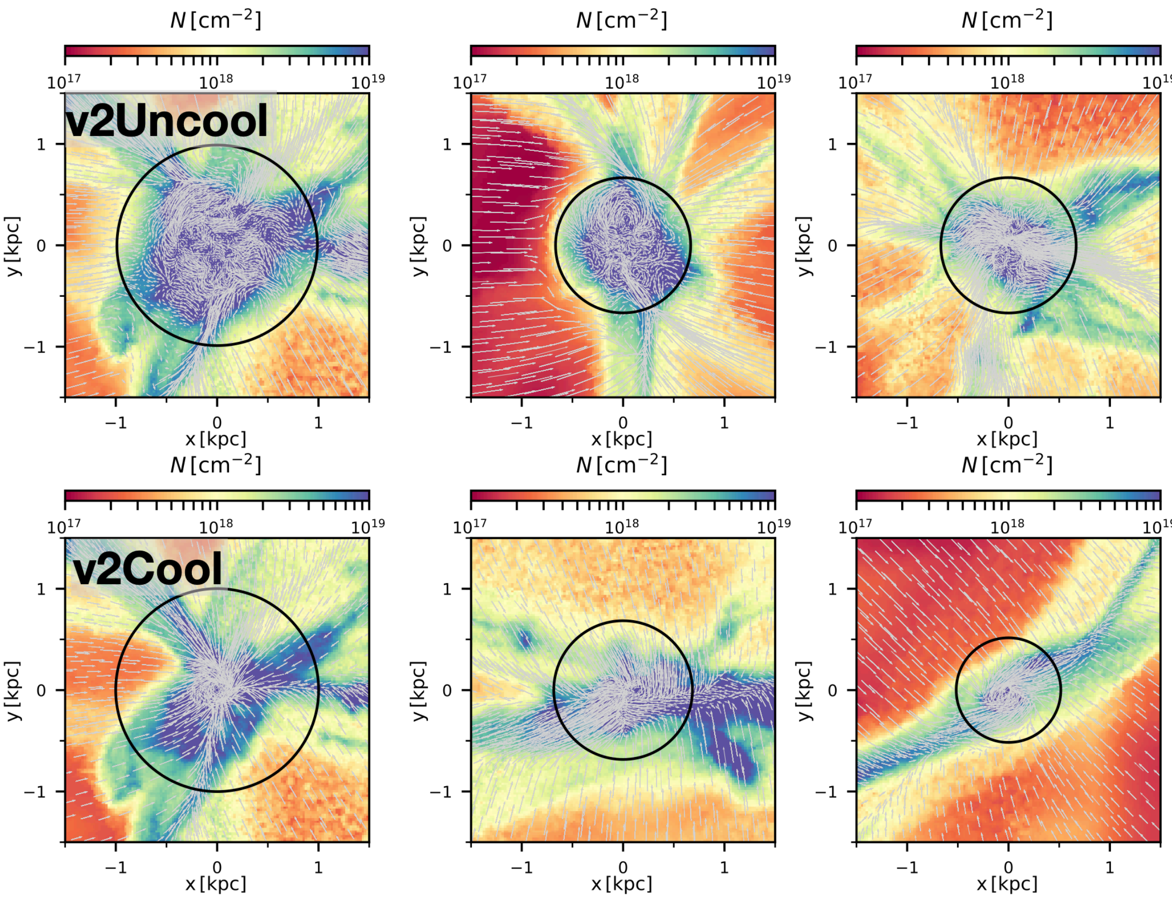

Figure 3.9: Column densities of a DM/G and its surrounding environment. A slice of the velocity field is also shown. Gas is accreting onto the DM/G. The top row contains DM/Gs from the v2Uncool run and the bottom contains three from the v2Cool run. The black circle indicates R_{200} of the DM/G.

CHAPTER 4

Shining Light on SIGOs - a New Formation Channel for Globular Clusters

4.1 Abstract

Supersonically induced gas objects (SIGOs) with little to no dark matter component are predicted to exist in patches of the Universe with non-negligible relative velocity between baryons and the dark matter at the time of recombination. Using AREPO hydrodynamic simulations we find that the gas densities inside these objects are high enough to allow stars to form. An estimate of the luminosity of the first star clusters formed within these SIGOs suggests that they may be observed at high redshift using future HST and JWST observations. Furthermore, our simulations indicate that SIGOs lie in a distinct place in the luminosity-radius parameter space, which can be used observationally to distinguish SIGOs from dark-matter hosting gas systems. Finally, as a proof-of-concept, we model star formation before reionization and evolve these systems to current times. We find that SIGOs occupy a similar part of the magnitude-radius parameter space as globular clusters. These results suggest that SIGOs may be linked with present-day metal-poor local globular clusters. Since the relative velocity between the baryons and dark matter is coherent over a few Mpc scales, we predict that if this is the dominant mechanism for the formation of globular clusters, their abundance should vary significantly over these scales.

4.2 Introduction

The puzzling origins of globular clusters (GCs) have been greatly debated over the years (Ashman and Zepf, 1992; Bekki and Yong, 2012; Bromm and Clarke, 2002; Grillmair et al., 1995; Gunn, 1980; Harris and Pudritz, 1994; Kravtsov and Gnedin, 2005; Kruijssen, 2015; Mandelker et al., 2018; Mashchenko and Sills, 2005; Moore, 1996; Muratov and Gnedin, 2010; Peebles, 1984; Renaud et al., 2017; Saitoh et al., 2006). These objects serve as the testing grounds for early structure formation since they are very old (~ 13 Gyr, e.g., Trenti et al., 2015). For example, they have even been used to estimate the age of the Universe (Krauss and Chaboyer, 2003). Observations suggest that GCs contain practically no gravitationally bound dark matter (e.g., Bradford et al., 2011; Conroy et al., 2011; Heggie and Hut, 1996; Ibata et al., 2013, although see Taylor et al. (2015) for evidence to the contrary). Although direct observations of high redshift GCs is difficult, statistical studies with strong gravitational lensing have enabled the investigation of high redshift star-forming GC candidates (e.g., Elmegreen et al., 2012; Vanzella et al., 2017). There has even been some direct evidence of possible GC progenitors (e.g., Bouwens et al., 2017; Vanzella et al., 2019, 2016). Furthermore, GCs and their progenitors may also play a large role in reionizing the Universe (e.g., Boylan-Kolchin, 2018; Schaerer and Charbonnel, 2011). The upcoming *James Web Space Telescope* (JWST) offers an exciting chance to observe GCs and their progenitors at early times. These observations will give insight to the formation of the very early building blocks in the Universe.

In the standard model of structure formation, due to the baryon-radiation coupling, baryon over-densities at the time of recombination ($z \sim 1020$) were about 5 orders of magnitude smaller than dark matter (DM) over-densities. Tseliakhovich and Hirata (2010) showed that not only were the amplitudes of the DM and baryonic density fluctuations different at early times (e.g., Naoz and Barkana, 2005b), but so were their velocities. After recombination, the baryons decoupled from the photons and their subsequent evolution was dominated by the gravitational potential of the DM. In the period following recombination, the baryons underwent rapid cooling. At this point, their relative velocity with respect to the DM, which at recombination was of the order of ~ 30 km sec^{-1}, became supersonic. Tseliakhovich and Hirata (2010) also showed that this relative velocity between the baryons and the DM remained coherent on scales of a few Mpc and in these regions it can be modeled as a stream velocity.

The stream velocity effect has previously been overlooked because the velocity terms are formally second order in perturbation theory and are therefore neglected in the linear approximation. However, this second-order effect is unusually large, resulting in the non-negligible suppression of power at mass scales that correspond to the first bound objects in the Universe (Tseliakhovich et al., 2011). The non-linear effects of the stream velocity on the first structures were subsequently investigated using numerical simulations (e.g., Fialkov et al., 2012; Greif et al., 2011; Maio et al., 2011; Naoz et al., 2011b, 2012; O'Leary and McQuinn, 2012; Richardson et al., 2013; Stacy et al., 2011; Tanaka and Li, 2014). The stream velocity also has significant implication on the redshifted cosmological 21-cm signal (e.g. Dalal et al., 2010; McQuinn and O'Leary, 2012; Visbal et al., 2012), the formation of primordial black holes (e.g., Hirano et al., 2017a; Latif et al., 2014; Schauer et al., 2017; Tanaka and Li, 2014; Tanaka et al., 2013), and even for primordial magnetic fields (Naoz et al., 2013). See Fialkov and Barkana (2014) for a detailed review.

Recently, Naoz and Narayan (2014) proposed that metal-poor GCs may be linked to objects that can be formed without DM in the early Universe in the presence of the stream velocity. These supersonically induced gas objects (SIGOs) were later found in numerical simulations by Chiou et al. (2018); Popa et al. (2016). However, their connection to GCs is still uncertain. Specifically, the ability of SIGOs to form stars was not addressed in those simulations. If these objects indeed form stars, these first star clusters will host little to no DM component.

The formation of the first stars from pristine gas was addressed in length in the literature focusing on the detailed chemistry and equation of state (e.g., Abel et al., 2002; Bromm and Clarke, 2002; Glover, 2013; Reed et al., 2005; Sarmento et al., 2018; Schauer et al., 2019; Stacy et al., 2011; Xu et al., 2016; Yoshida et al., 2006). In this chapter, we take a global, statistical approach through an investigation of the conditions for star formation in SIGOs via a simple density threshold argument. In particular, stars will form if the global gas density within a given SIGO is above the predicted critical value for star formation in pristine and low-metallicity gas (e.g., Burkhart and Mocz, 2019; Christlieb et al., 2002; Krumholz and McKee, 2005). We then use semi-analytical calculations to determine the luminosities of objects in our simulations. We note that, although we study these objects at $z = 20$, they still exists at lower redshifts (e.g., Chiou et al., 2018; Naoz and Narayan, 2014; Popa et al., 2016). Thus, their expected luminosities could possibly be detectable with JWST.

This chapter is organized as follows: we begin by describing our simulations in Section 4.3 then we discuss the star formation model (Section 4.4) and the subsequent luminosity (Section 4.5). Finally we offer our discussion and qualitative predictions in Section 4.6.

4.3 Simulation details and object classification

We run two cosmological simulations with the moving-mesh code AREPO (Springel, 2010a) in a 2 Mpc box with 512^3 DM particles of mass $M_{\rm DM} = 1.9 \times 10^3 M_\odot$ and 512^3 Voronoi mesh cells with $M_{\rm gas} = 360 M_\odot$. One run has a stream velocity value of $v_{\rm bc} = 2\sigma_{v_{\rm bc}}$, where $\sigma_{v_{\rm bc}}$ is the rms value of the stream velocity (i.e., the relative velocity between the gas and the dark matter component), while the other, which we use for comparison, has no such stream velocity. Both runs include radiative cooling (see Chiou et al., 2019). The cooling module in AREPO is based on a self-consistent primordial chemistry and cooling network, which includes the evolution of species H, H^+, He, He^+, He^{++} and e^- in equilibrium with a photoionizing background that is spatially constant but redshift dependent. The gas cooling and heating rates are calculated as a function of redshift, gas density, temperature and (for the metal line part) metallicity[1] See (Vogelsberger et al., 2013, and references therein) for further details on the numerical implementation of these processes. The simulations do not include explicit star formation or feedback.

We note that our simulations do not include H_2 cooling. Molecular cooling was shown to be important for early star formation (e.g. Glover and Jappsen, 2007; Hartwig et al., 2015; Schauer et al., 2019, 2017). Nonetheless, the densities in our simulations (as we show below) reach the necessary high densities and low temperatures to trigger star formation. Thus, inclusion of molecular

[1] Note that while all cooling rates include self-shielding corrections, these corrections do not apply above redshift of 6, and thus do not contribute for the cooling of the $z = 20$ objects.

cooling in followup simulations will yield even higher densities, further facilitating star formation.

The initial conditions adopted different transfer functions for the DM and baryon components as described in Naoz and Barkana (2005b); Naoz et al. (2009, 2011b, 2012, 2013). The runs were performed from a redshift of $z = 200$ to $z = 20$. The stream velocity is implemented as a uniform boost for the gas in the x-direction. The choice of $v_{\rm bc} = 2\sigma_{v_{\rm bc}}$ allows us to gain a larger effect, however the same physical picture is applicable for $v_{\rm bc} = 1\sigma_{v_{\rm bc}}$, (as noted by Naoz and Narayan, 2014). Furthermore, we gain more statistical power by adopting $\sigma_8 = 1.7$ (e.g., Chiou et al., 2019, 2018; Popa et al., 2016).

We follow the structure definitions suggested in Chiou et al. (2018). In particular, DM-Primary/Gas-Secondary (DM/G) objects are spherical overdensity DM halos that also contain gas. The Gas-Primary objects are gas objects obtained through running a Friends-of-Friends (FOF) algorithm on only the gas component and subsequently fitted to a tight ellipsoid. Both DM/G and Gas-Primary objects are identified by using the FOF algorithm with a linking length of 0.2 times the mean particle separation. Finally, the SIGOs are Gas-Primary objects that are outside the virial radius of the closest DM halo and also have gas fractions greater than 40%. These objects have little to no DM component. The advantage of our small simulation box is that it allows us to resolve SIGOs, however, it prevents us from following the detailed evolution of SIGOs to smaller redshift. Thus, in order to investigate the evolution of SIGOs at $z < 20$ we employ semi-analytical modeling.

4.4 Star formation model

We estimate the plausibility that a dense gas clump (either a SIGO or within a DM/G) may form stars. Primordial star formation may be the most suitable epoch during the evolution of the Universe for the application of the Jeans criterion since the level of turbulence and strength of the magnetic field are expected to be significantly lower (Bromm et al., 1999, 2002). The Jeans criterion (Jeans, 1902) and the related Bonnor-Ebert mass describes the balance between gravity and

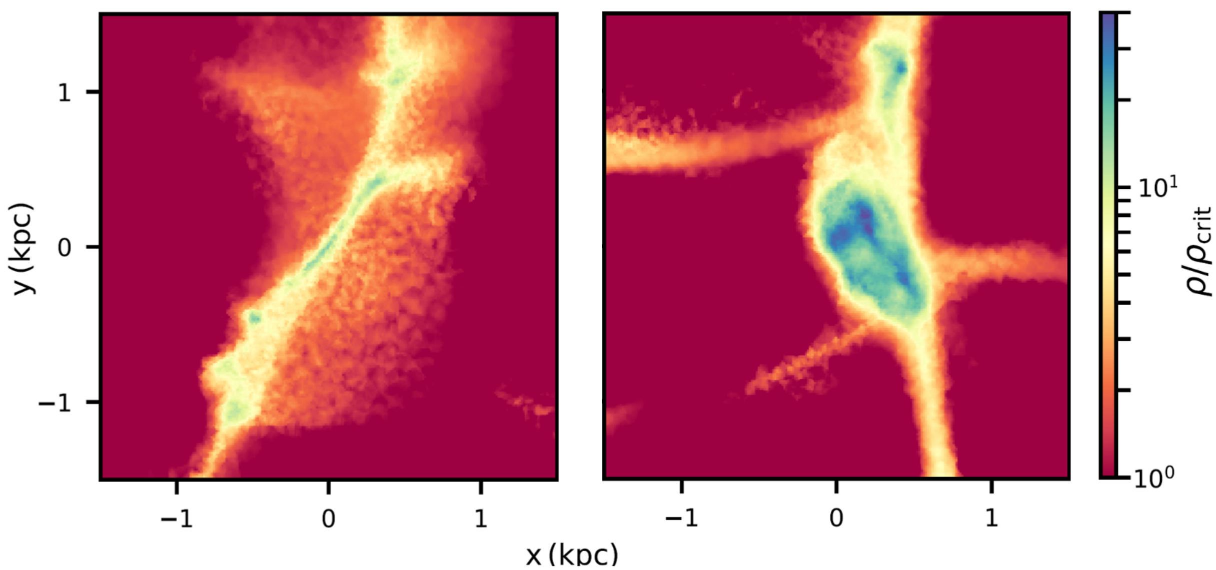

Figure 4.1: Density projections of two representative SIGOs at $z = 20$. The density has been normalized to $\rho_{\rm crit}$ for each SIGO. The highest density ratio here is ~ 40, corresponding to dark blue color. Note the filamentary nature with multiple high, smaller scale density peaks. The SIGO is embedded at the center of the region with a scale of $(R_{\rm min}, R_{\rm max})$ of (.01, .03) kpc and (.08, .14) kpc for the left and right panels, respectively.

thermal pressure and is given by:

$$M_{\rm BE} = 1.18 \frac{c_{\rm s}^3}{\sqrt{G^3 \rho}} = \frac{1.18}{\pi^{3/2}} \rho \lambda_{\rm J}^3 \,, \tag{4.1}$$

where $c_{\rm s}$ is the isothermal sound speed in the region, G is the gravitational constant, ρ is the density of the gas, and $\lambda_{\rm J}$ the Jeans length. The mass in Equation (4.1) is the largest mass that an isothermal gas sphere embedded in a pressurized medium can have while still remaining in hydrostatic equilibrium (Bonnor, 1956; Ebert, 1955). This depends on the Jeans length, defined as follows:

$$\lambda_{\rm J} = \sqrt{\frac{\pi c_{\rm s}^2}{G \rho}} \,. \tag{4.2}$$

The Jeans length is therefore the critical radius of a cloud where thermal energy is counteracted by gravity.

Since we are dealing with a supersonic medium the other length scale of interest for defining a critical density for star formation is the sonic scale[2]:

$$\lambda_{\rm s} = \left(\frac{L_{\rm drive}}{\mathcal{M}^2}\right) . \quad (4.3)$$

$\lambda_{\rm s}$ is defined as the length scale such that $\sigma_l = c_{\rm s}$, $\mathcal{M}$ is the mach number on the driving scale, $L_{\rm drive}$, of the turbulence, and σ_l is the one-dimensional velocity dispersion computed over a sphere of diameter l within a turbulent medium. The sonic scale physically represents the scale at which turbulence in the gas transitions from supersonic to subsonic.

As discussed in Krumholz and McKee (2005), if $\lambda_{\rm J} \leq \lambda_{\rm s}$, gravity is approximately balanced by thermal plus turbulent pressure, and the object is at best marginally stable against collapse. Here we assume that the magnetic field is dynamically unimportant relative to turbulence and gravity. If $\lambda_{\rm J} \gg \lambda_{\rm s}$, turbulent/thermal kinetic energy greatly exceeds gravitational potential energy and the object is stable against collapse. Since $\lambda_{\rm J}$ is a function of the local density, the condition $\lambda_{\rm J} \leq \lambda_{\rm s}$ for collapse translates into a minimum local density required for collapse (in the absence of magnetic fields). Equating the two length scales yields a critical density

$$\rho_{\rm crit} = \frac{\pi c_s^2 \mathcal{M}^4}{G L_{\rm drive}^2} , \quad (4.4)$$

which can be rewritten in terms of the virial parameter, and assuming that the driving scale of the turbulence is the characteristic diameter of the cloud, i.e., $L_{\rm drive} = L_{\rm cloud}$, as,

$$\rho_{\rm crit} = \frac{\pi^2}{15} \rho_0 \alpha_{\rm vir,l} \mathcal{M}^2 , \quad (4.5)$$

where $\alpha_{\rm vir,l} = 5\sigma_l^2 L_{\rm cloud}/(2GM_{\rm cloud})$, the ratio of turbulent to gravitational energy. We note that these equations are only meaningful in the presence of a supersonic flow, as in our case.

In this simple stability picture, once the critical density is reached, the gas becomes unstable to gravitational collapse. Burkhart and Mocz (2019) related the critical density to a transition density between a piecewise lognormal and power law of the density distribution. A power-law density

[2]This expression assumes a line-width size relation with exponent of p=0.5, expected for supersonic turbulence

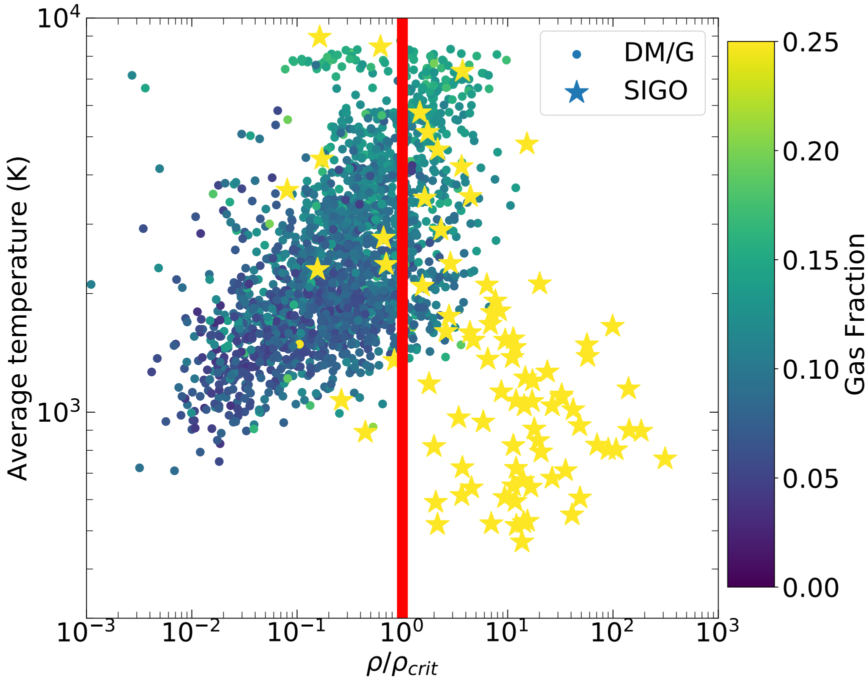

Figure 4.2: The average temperature in the stream velocity run as a function of $\rho/\rho_{\rm crit}$, at $z = 20$. The red vertical line indicates the $\rho = \rho_{\rm crit}$ line. To the right of the line we expect star formation to take place and to the left, star formation is suppressed. The color code depicts the gas fraction in the object. Recall that by definition SIGOs have gas fraction above 40%. Note the majority SIGOs are in the star forming regime.

PDF is the 1-point statistic's signature of gravitational collapse, regardless of the gas metallicity. A turbulent medium will have an initially lognormal density distribution, but once gravitational collapse sets in, the distribution can be described by a power law (Burkhart et al., 2017; Girichidis et al., 2014; Guszejnov et al., 2018). Thus, the transition density as a critical density for collapse is a natural consequence of the density distribution function. Below, we adopt this critical density threshold as a star formation indicator.

We apply the above star formation criterion to the objects found in the simulation. In Figure 4.1, we show the density of representative star forming SIGOs normalized to their critical density for star formation. To compute the critical density we need an estimate of the turbulence sonic scale, which is given by $L_{\rm cloud}/\mathcal{M}^2$ (e.g., Burkhart, 2018). Since SIGOs are ellipsoidal (e.g., Chiou et al., 2018), we assume $L_{\rm cloud} \sim 2R_{\rm max}$, because this is the maximum scale at which turbulence can be generated. We calculate the critical densities for each object type (i.e., DM/Gs and SIGOs) in our simulations following Equation (4.4). Considering first the DM/G objects we find that at $z = 20$, 19% (85%) of them have densities and temperatures that yield favorable conditions for star formation for the $2\sigma_{v_{\rm bc}}$ ($v_{\rm bc} = 0$) run. This difference between the stream velocity and no stream velocity case is expected since the stream velocity effect reduces the gas fraction of DM halos (e.g., Naoz et al., 2012; Tseliakhovich et al., 2011). In Figure 4.2 we show the temperatures and densities for the DM/G objects in the presence of stream velocity. As expected DM halos that host larger gas fractions are more likely to form stars, according to the $\rho_{\rm crit}$ criterion. Note that gas in the DM/G objects is expected to fragment into cooler clumps that will serve as star formation sites (e.g., Bromm et al., 1999; Greif et al., 2011).

Significantly, 88% of SIGOs may form stars for the $2\sigma_{v_{\rm bc}}$ run (there are ipso facto no SIGOs in the $v_{\rm bc} = 0$ run). As depicted in Figure 3.5, SIGOs have densities that are much higher than $\rho_{\rm crit}$ and are overall cool. *In other words, the majority of SIGOs have supercritical densities and are thus ripe sites for star formation.*

Note that since SIGOs are only marginally bound (Chiou et al., 2018), supernova feedback may disrupt the rest of the gas in them, thus suppressing further star formation. Indeed GCs tend to have multiple generations of stars, possibly from multiple star burst epochs. Subsequent star bursts may form during pericenter passage as a SIGO orbits the closest DM halo, if gas survived the supernova feedback or was able to accrete from the medium[3]. Here we focus on the first star formation episode and hence adopt a star burst formation model.

4.5 SIGO and DM/G Luminosity

For the SIGOs and DM/G, with pristine gas, we follow Schaerer (2003) and consider a star burst model with no metallicity at redshift $z = 20$ (his model “A”). This includes Lyman-α lines and the

[3]Here we adopt a semi-analytical approach for star formation, since detailed zoom-in simulations exploring the supernova feedback are beyond the scope of this chapter.

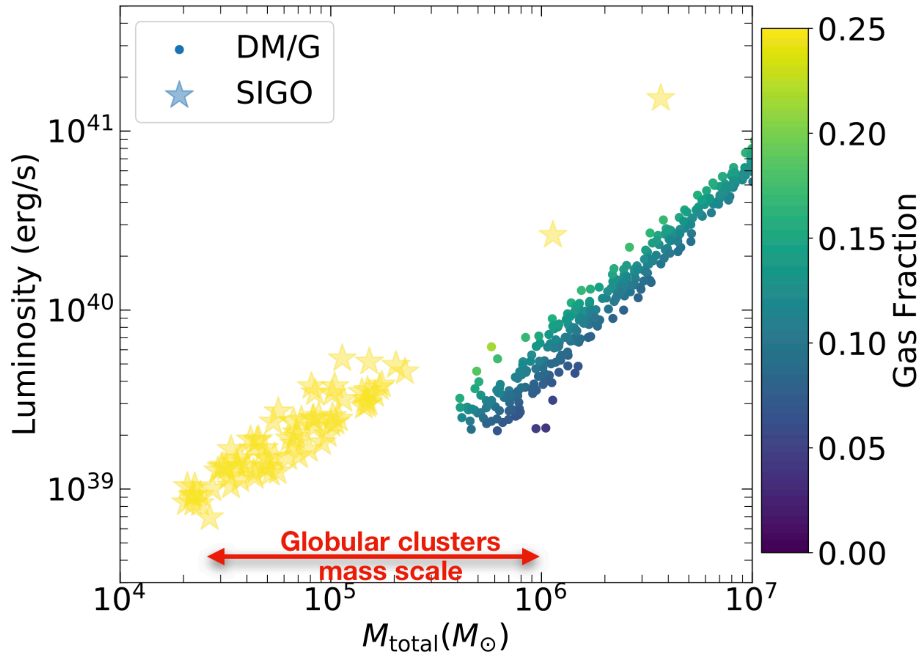

Figure 4.3: Luminosity as a function of mass for the $v_{\mathrm{bc}} = 2\sigma_{v_{\mathrm{bc}}}$ run at $z = 20$. The color code depicts the gas fraction in the object. The horizontal line represents a characteristic mass scale of present-day, local, globular clusters (e.g., Kimmig et al., 2015).

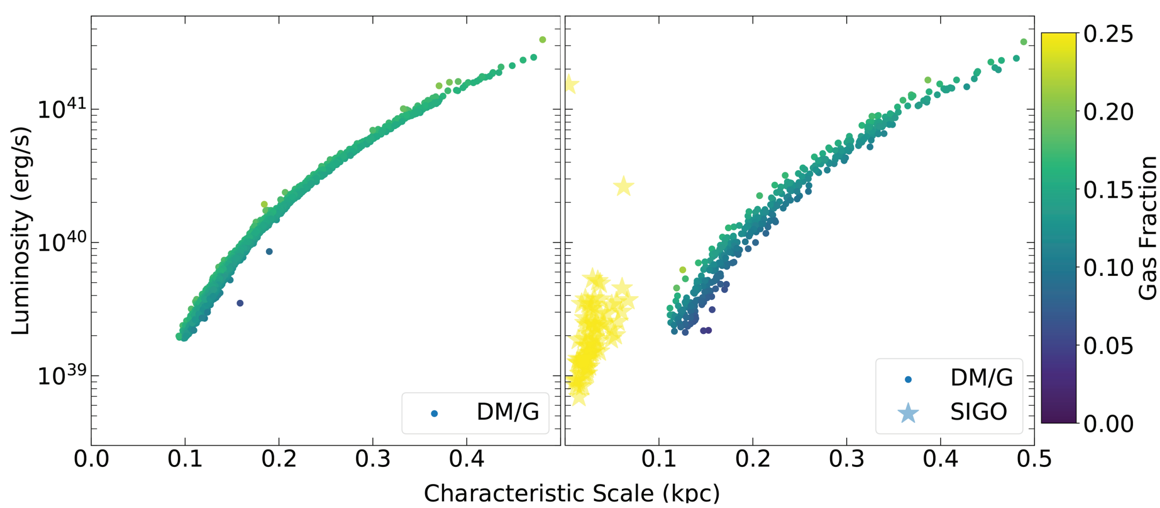

Figure 4.4: Luminosity as a function of the characteristic scale for $v_{\mathrm{bc}} = 0$ (left), $2\sigma_{v_{\mathrm{bc}}}$ (right). For the SIGOs, the characteristic scale chosen is the minimum ellipsoid axis. For DM/G objects, we adopt the virial radius. Only star-forming objects with $\rho > \rho_{\mathrm{crit}}$ are shown.

H ionizing photon flux, $Q(H)$. The luminosity is given by

$$L_l[\text{erg s}^{-1}] = c_l(1 - f_{\text{esc}})Q_i(t)[\text{s}^{-1}], \tag{4.6}$$

where Q_i is the ionizing photon flux[4], c_l is the line emission coefficient for Case B, and f_{esc} is the photon escape fraction. We assume a photon escape fraction of $f_{\text{esc}} = 0.5$ and that 10% of the gas mass of a SIGO or a classical object (DM/G) will be converted into stars.

With these relations at hand we estimate the luminosity-mass (Figure 4.3) and luminosity-radius (Figure 4.4) relation for the different objects. As it can be clearly seen in these Figures, the SIGOs and DM/G occupy different parts of the parameter space. Moreover, as shown in Figure 4.3, SIGOs cover the GC mass range.

As expected, and noted previously in the literature (e.g., Greif et al., 2011; Stacy et al., 2011), the stream velocity suppresses the abundance of DM/G objects and in particular the star-forming ones. In Figure 4.4, we display the results of the runs with and without stream velocity. The left panel corresponds to the no stream velocity case. Here, there are no SIGOs present and there is a fairly tight relation. With stream velocity, on the right panel, there are less DM/Gs and there is more scatter in the distribution.

Considering the SIGOs, they occupy a dimmer and more compact part of the parameter space. Since in general star formation would occur in high density peaks that are much smaller than the size of the SIGO, we consider the characteristic scale to be the smallest ellipsoid axis[5](whereas the characteristic scale for the DM/G is simply the virial radius). Indeed, it has been argued that GCs might form as the nuclei of a dwarf galaxy that dissolved (e.g., Searle and Zinn, 1978). Since luminosity is calculated based on the total gas mass of the object and SIGOs tend to be not be very massive, there is a separation in luminosity-mass space. As for luminosity-radius space, the prolate nature of SIGOs gives them a distribution of sizes and they tend to be less luminous in general than the DM/G.

[4]Note that following the model of (Schaerer, 2003), $Q_i(t)$ has a linear dependency on the mass of the object.

[5]Recall that we use $R_{\max}$ to calculate the the density threshold, because $R_{\max}$ describes the turbulence scale.

The mass and characteristic scale of the SIGOs seems to be consistent with Little Blue Dots (Elmegreen and Elmegreen, 2017) and the star forming dwarf detected recently by (Vanzella et al., 2019). The aforementioned observed objects have been suggested to be GCs progenitors, their similarity to SIGOs is uncanny and may suggest a strong link between high redshift, star-forming SIGOs and GCs progenitors. Future HST and JWST observations may yield stronger evidence.

4.6 Discussion

The supersonically induced gas objects (SIGOs) are expected to exists in patches of the Universe with non-negligible stream velocity (Chiou et al., 2018; Naoz and Narayan, 2014; Popa et al., 2016). We showed that these gas-rich objects, with little to no DM components, have high enough densities that can give rise to star formation. Thus, the early Universe is predicted to have two classes of star forming objects, the classical ones, i.e., high gas densities within DM halos (DM/G), as well as SIGOs.

We estimated the luminosity expected from star formation in these objects (both SIGOs and the classical objects). Due to the formation nature of SIGOs, they occupy different parts of the parameter space than the classical DM halos with gas. The SIGOs are dimmer than the classical objects at the same redshift. Note that, while the simulation snapshot here is associated with $z = 20$, we expect these objects to continue to form[6] and exist (at least before reionization), based on the agreement between the analytical calculations (Naoz and Narayan, 2014) and our simulations (Chiou et al., 2019, 2018; Popa et al., 2016).. Thus, future JWST observations may be able to disentangle star forming SIGOs from classical objects.

Moreover, we note that the recently observed Little Blue Dots (Elmegreen and Elmegreen, 2017), which are suggested to be star-forming progenitors of globular clusters, are consistent with with the mass and radius of SIGOs in the simulation. The star-forming dwarf found by Vanzella et al. (2019) has also a similar mass and size to our largest SIGOs. There may also be a connection

[6]Note that $\sim 10^6$ $M_\odot$ objects are expected to be fairly common (represent about a $1-\sigma$ fluctuation) at about $z \sim 6$ (e.g., Barkana, 2016; Fialkov et al., 2012; Naoz and Barkana, 2007).

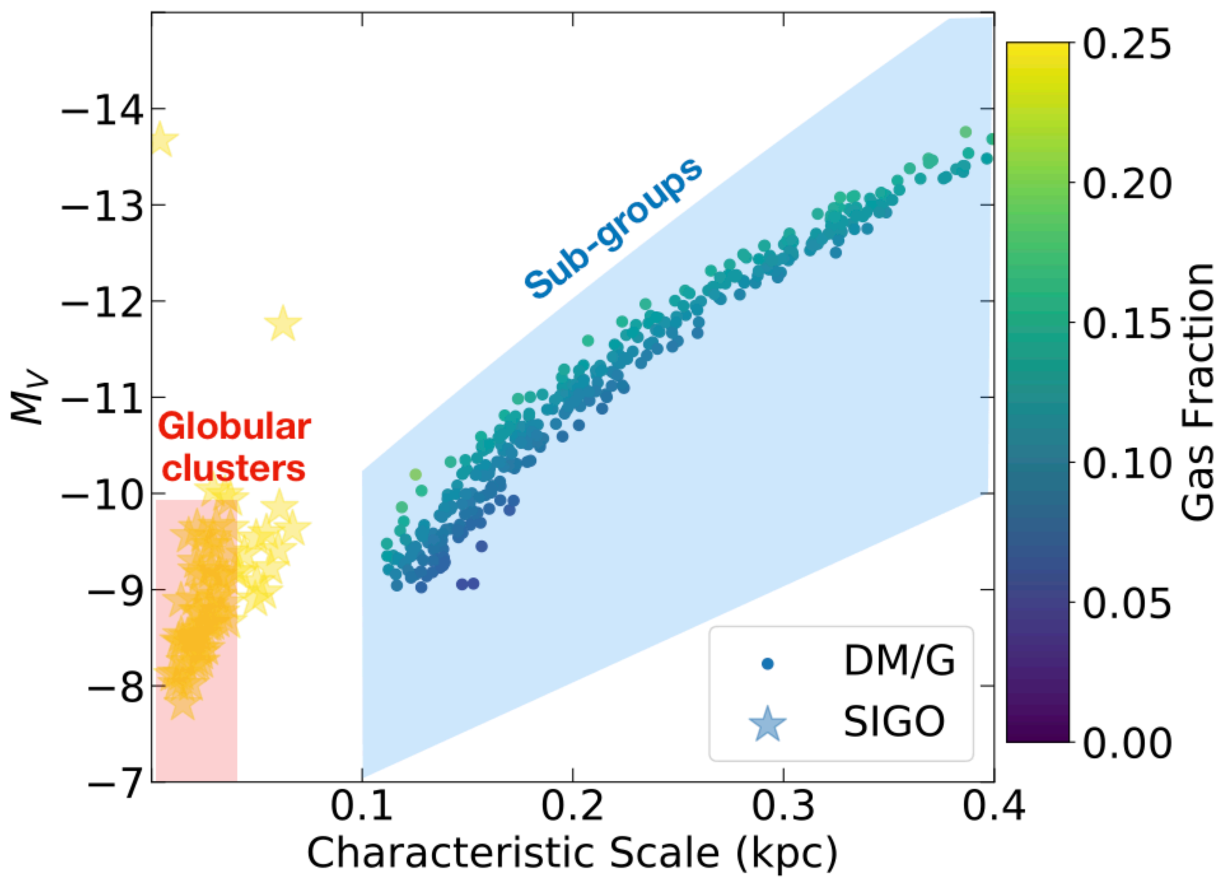

Figure 4.5: The speculated present-day, local, absolute visual magnitude as a function of characteristic scale of SIGOs and DM/G (see text for details). Over-plotted are object classes in the Local Group from (McConnachie, 2012).

between SIGOs and Giant HII Regions and HII Galaxies (Terlevich et al., 2018). Furthermore, we note that SIGOs that formed little to no stars may be connected to the starless dark HI objects predicted by Burkhart and Loeb (2016). Interestingly, the recent discoveries of two galaxies with little to no dark matter (Danieli et al., 2019; van Dokkum et al., 2019, 2018), share a striking resemblance to SIGOs. While the size estimation of these low redshift galaxies is somewhat larger (few kpc) than the SIGOs ($1-100$ pc), we speculate that these objects may be a result, in the local Universe, of a collections or mergers of SIGOs. Moreover, the 10 GCs identified around one of these galaxies (Danieli et al., 2019), are consistent with multiple high densities peaks we have found within our high redshift simulated SIGOs.

The separation of SIGOs and DM/G in the luminosity-radius parameter space (e.g., Figure 4.3) highly resembles the magnitude-radius separation parameter space of present-day, local, globular clusters and sub-groups separation (e.g., McConnachie, 2012, see their figure 6). Thus, we may speculate on how SIGOs and DM/G objects will be observed today. Assuming a burst-like star formation before reionization ($z = 10$), we adopt an initial mass function (IMF) for the objects. In particular, we adopt a top-heavy IMF for the SIGOs[7] following Decressin et al. (2007), and a Salpeter IMF for the DM/G. We then calculate the fraction of spectral types of stars that evolve along the main sequence. The majority of the stars that survive to present-day then will be G and K type stars, as well as red giants. Given this population, we subtract their various bolometric corrections. We can then roughly estimate each object's visual bolometric magnitude. We also estimate that the observed stellar cluster that formed within the SIGOs corresponding to the highest density peak which is, typically smaller than $R_{\rm max}$. Thus, we adopt the $R_{\rm min}$ for the observed value. Our order of magnitude estimations are presented in Figure 4.5. We also over-plot the region of the parameter space that is associated with globular clusters (red box) and Andromeda and the Milky Way sub groups (blue area) (McConnachie, 2012). Heuristically, the SIGOs are consistent with the absolute visual magnitudes of present-day, local, globular clusters. Although the SIGOS in this simulation only contain primordial gas, we speculate that some self-enrichment or second popula-

[7]Following Decressin et al. (2007), we use a piecewise IMF, with low mass end ($0.1M_\odot < M < 0.8M_\odot$) is given by a lognormal form and above $0.8M_\odot$ it is given by a top heavy power law with slope $x = 0.55$. Note that using a Salpeter slope for the SIGOs IMF did not significantly affect the results.

tion formation mechanism (such as pericenter passage of orbits about the nearest DM halo) may contribute to the nonzero metallicity in metal-poor GCs. Further simulations including explicit star formation (and the associated metal enrichment) are needed to address this. Nevertheless, the agreement between our rough estimates and the observations is very encouraging.

Finally, these results suggest that if this is the dominant formation mechanism of globular clusters, varying patches (on the order of few tens of Mpcs) in the Universe associated with different coherent $v_{\rm bc}$ values, will have significantly distinct abundances of globular clusters[8]. Indeed, about 39% of the Universe contains patches of stream velocity with $v_{\rm bc} \geq 1\sigma_{v_{\rm bc}}$ (Tseliakhovich et al., 2011). Thus, detailed HST and future JWST observations may allow to disentangle between different formation channels of globular clusters.

[8]From linear theory, the abundance of SIGOs on face value should follow the abundance of gas poor DM halos (e.g., Naoz and Narayan, 2014). Numerically, SIGOs undergo two body relaxation processes and numerically evaporate, (e.g., Chiou et al., 2018; Popa et al., 2016), thus, detailed abundance studies are challenging. Note that our choice of a larger σ_8 provides higher power that enables us to overcome some of the numerical challenges and can be viewed as a high-fluctuation patch in the Universe.

CHAPTER 5

Conclusion

5.1 Summary of Results

In this work, we have investigated the effects of the stream velocity between baryons and DM in the early Universe through the use of numerical simulations. In particular, we have focused on Supersonically Induced Gas Objects (SIGOs), that arise naturally due to the relative velocity between baryons and dark matter in the early Universe. Here we have paved the way towards progress in understanding a novel formation mechanism for globular clusters via SIGOs.

We began by studying how the stream velocity affects the spin morphologies of primordial objects via the spin parameter. This is an observable quantity that determines the rotational support of a object. We showed that with the inclusion of stream velocity, the spin parameter of DM halos follows lognormal distribution (as expected, e.g., Bullock et al., 2001), but the median spin parameter is larger. The misalignment angle between the angular momenta of gas and DM in a DM halo was shown to have a nearly isotropic distribution in contrast with the standard picture of galaxy formation which states that tidal torques endows the same initial angular momentum to both DM and baryons. This was the first time that analysis of the spin parameters of DM halos at the low mass range (10^{5-8} $M_{\odot}$) at high-redshift.

Focusing on the SIGOs, we studied their ellipsoidal morophology and showed that they differ from a standard NFW profile which describes classical DM halos and display a more cored inner profile. Since SIGOs themselves are not contained within a DM halo, we generalized the spin parameter to SIGOs by normalizing with respect to fiducial DM halo's mass which is $\sim 6M_{gas}$ contained in the SIGO. This generalized spin parameter also follows a log normal distribution and

SIGOs have higher spin parameters compared to the gas components of DM halos without stream velocity.

Further investigation of SIGOs requires the consideration of additional physical processes such as cooling and star formation. The simulations of Popa et al. (2016) only included adiabatic cooling due to the expansion of the Universe. To further connect SIGOs with globular clusters, we ran a new suite of simulations which included atomic cooling as well as stream velocity. Atomic cooling (as opposed to molecular cooling or metal-line cooling) was chosen since SIGOs form in the early Universe out of pristine gas. We showed that atomic cooling does not significantly alter SIGO properties such as overdensity, prolateness, and temperature. Since atomic cooling is inefficient below 10^4 K and most SIGOs with only adiabatic cooling already have temperatures lower than 10^4 K, this result is expected. Nevertheless, cooling does lead to a more diffuse environment around SIGOs. For DM/G however, we reproduced results that cooling does indeed decrease the temperature the hottest DM/G to below 10^4 K and also makes their structure more compact. Comparing the cold gas fractions, SIGOs have a higher cold gas fraction than DM halos. Cooling also further increases the scatter of the DM halo cold gas fraction as a function of mass.

To study the star formation in SIGOs from pristine gas, we employed a critical density for star formation based on the balance between gravity, thermal and turbulent pressure. Although the explicit details of formation of the first stars have been well studied in the literature, here we took a more global approach via this density threshold to study population statistics. We found that under this criteria, 88% of SIGOs form stars at $z = 20$ for a stream velocity of $v_{\rm bc} = 2\sigma_{{\rm v}bc}$. Then, we employed a starburst semi-analytic model to estimate the luminosity of star-forming SIGOs. SIGOs were found to occupy a distinct parameter space in the luminosity - radius diagram. We then evolved the stars along the main sequence and subtract bolometric corrections to obtain the visual magnitudes of present-day SIGOs. We showed that the SIGOs occupy a similar region to present day GC.

These results suggest that SIGOs may be a viable formation channel for modern day metal-poor GC. Indeed, the recently observed Little Blue Dots (Elmegreen and Elmegreen, 2017), which have been purported star-forming progenitors of GC are also consistent with the mass and size of

SIGOs in simulation. Furthermore, the observations of galaxies with little to no DM (Danieli et al., 2019; van Dokkum et al., 2019, 2018) also seem reminiscent of SIGOs, which also contain little to no DM. Although the sizes of these galaxies are larger, they may be a result of SIGO mergers. We leave the further investigation of detailed comparisons of SIGOs to observations to future work.

5.2 Future Work

It is important for any model of structure formation to predict the abundance of halos. Future work should calculate analytically the number density of the SIGOs and dark halos as a function of mass and redshift. The simple analytical model of Press and Schechter (1974), which is based on Gaussian random fields, assumes spherically symmetric collapse. It predicts that the abundance of halos depends on mass and redshift through the the two functions $\sigma(M, z)$ and $\delta_c(z)$, where $\sigma^2(M, z)$ is the variance (calculated from the power spectrum) as a function of halo mass at redshift z, and $\delta_c(z)$ is the critical collapse overdensity. Further work will study both the Zel'dovich approximation and the nonlinear evolution of over densities, as explained above. Using these results, one can calculate object abundances and compare them to results from simulations. This comparison will be used to disentangle the different physical processes that take place in the simulations and will allow us to better understand this formation scenario. The abundance of these halos is particularly important for comparisons with observations.

To further compare SIGOs to GC, the environments of the SIGOs and their clustering and abundances should be studied in-depth, which can be compared to present day GC abundances. Additional cooling channels such as molecular hydrogen can be explored to drive the temperatures down and densities up to further investigate the star forming potential of SIGOs. Higher resolution simulations are also favorable due to the numerical evaporation of SIGOs at low redshift (Popa et al., 2016).

Since SIGOs are only marginally bound (Chiou et al., 2018), an open question is to whether a first round of star formation and subsequent supernova will blow away all the gas and destroy the SIGO. Future simulations will include explicit star formation and feedback, though this remains challenging since the exact details of Population III star formation are still uncertain.

To follow SIGOs evolution to present day, future studies will employ a zoom-in method and to follow SIGOs to $z = 0$. This will allow us to directly compare our numerically results with the predictions presented in Naoz and Narayan (2014). This will allow us to quantify the survival of these objects up to present day, and will compare with linear analysis predictions.

Further connecting SIGOs to GC, we consider GC properties. In particular, observations show evidence for multiple stellar populations in GC (see e.g., Bastian and Lardo, 2018; Gratton et al., 2012, for a review). In Chiou et al. (2019), we have assumed a single star burst event in SIGOs and only primordial star formation. However, several close approaches of SIGOs in its orbit around a galaxy may correspond to further star formation episodes during accretion from pericenter passage. This may replenish gas and lead to a second round of star formation. Further work to study the in-depth time evolution and kinematics of SIGOs is necessary.

The upcoming *JWST* mission will be able to see deeper into Universe than ever before and uncover the mysteries of high redshift galaxies. SIGOs are a promising candidate to be found by this mission. Future studies and observations will further clarify the link between SIGOs and globular clusters.

BIBLIOGRAPHY

Abel, T., Bryan, G. L., and Norman, M. L. (2002). The Formation of the First Star in the Universe. *Science*, 295:93–98.

Ahn, K. (2016). How the Density Environment Changes the Influence of the Dark Matter-Baryon Streaming Velocity on Cosmological Structure Formation. *ApJ*, 830:68.

Asaba, S., Ichiki, K., and Tashiro, H. (2016). Effect of supersonic relative motion between baryons and dark matter on collapsed objects. *Phys. Rev. D*, 93(2):023518.

Ashman, K. M. and Zepf, S. E. (1992). The formation of globular clusters in merging and interacting galaxies. *ApJ*, 384:50–61.

Barkana, R. (2016). The rise of the first stars: Supersonic streaming, radiative feedback, and 21-cm cosmology. *Phys. Rep.*, 645:1–59.

Barkana, R. (2018). Possible interaction between baryons and dark-matter particles revealed by the first stars. *Nature*, 555:71 EP –.

Barkana, R. and Loeb, A. (2001). In the beginning: the first sources of light and the reionization of the universe. *Phys. Rep.*, 349:125–238.

Barkana, R., Outmezguine, N. J., Redigolo, D., and Volansky, T. (2018). Signs of Dark Matter at 21-cm? *ArXiv e-prints*.

Barnes, J. and Efstathiou, G. (1987). Angular momentum from tidal torques. *ApJ*, 319:575–600.

Bastian, N. and Lardo, C. (2018). Multiple Stellar Populations in Globular Clusters. *ARA&A*, 56:83–136.

Bekki, K. and Yong, D. (2012). On the origin of the stellar halo and multiple stellar populations in the globular cluster NGC 1851. *MNRAS*, 419:2063–2076.

Bittner, J. M. and Loeb, A. (2011). The imprint of the relative velocity between baryons and dark matter on the 21-cm signal from reionization. *ArXiv e-prints*.

Blumenthal, G. R., Faber, S. M., Primack, J. R., and Rees, M. J. (1984). Formation of galaxies and large-scale structure with cold dark matter. *Nature*, 311:517–525.

Böker, T., Sarzi, M., McLaughlin, D. E., van der Marel, R. P., Rix, H.-W., Ho, L. C., and Shields, J. C. (2004). A Hubble Space Telescope Census of Nuclear Star Clusters in Late-Type Spiral Galaxies. II. Cluster Sizes and Structural Parameter Correlations. *AJ*, 127:105–118.

Bonnor, W. B. (1956). Boyle's Law and gravitational instability. *MNRAS*, 116:351.

Bouwens, R. J., van Dokkum, P. G., Illingworth, G. D., Oesch, P. A., Maseda, M., Ribeiro, B., Stefanon, M., and Lam, D. (2017). Very low-luminosity galaxies in the early universe have observed sizes similar to single star cluster complexes. *ArXiv e-prints*.

Bovy, J. and Dvorkin, C. (2013). Low-mass Suppression of the Satellite Luminosity Function Due to the Supersonic Baryon-Cold-dark-matter Relative Velocity. *ApJ*, 768:70.

Boylan-Kolchin, M. (2018). The Little Engines That Could? Globular clusters contribute significantly to reionization-era star formation. *MNRAS*, 479:332–340.

Bradford, J. D., Geha, M., Muñoz, R. R., Santana, F. A., Simon, J. D., Côté, P., Stetson, P. B., Kirby, E., and Djorgovski, S. G. (2011). Structure and Dynamics of the Globular Cluster Palomar 13. *ApJ*, 743:167.

Bromm, V. (2013). Formation of the first stars. *Reports on Progress in Physics*, 76(11):112901.

Bromm, V. and Clarke, C. J. (2002). The Formation of the First Globular Clusters in Dwarf Galaxies before the Epoch of Reionization. *ApJ*, 566:L1–L4.

Bromm, V., Coppi, P. S., and Larson, R. B. (1999). Forming the First Stars in the Universe: The Fragmentation of Primordial Gas. *ApJ*, 527:L5–L8.

Bromm, V., Coppi, P. S., and Larson, R. B. (2002). The Formation of the First Stars. I. The Primordial Star-forming Cloud. *ApJ*, 564:23–51.

Brown, T. M., Tumlinson, J., Geha, M., Simon, J. D., Vargas, L. C., VandenBerg, D. A., Kirby, E. N., Kalirai, J. S., Avila, R. J., Gennaro, M., Ferguson, H. C., Munoz, R. R., Guhathakurta, P., and Renzini, A. (2014). The Quenching of the Ultra-Faint Dwarf Galaxies in the Reionization Era. *ArXiv e-prints*.

Bullock, J. S., Dekel, A., Kolatt, T. S., Kravtsov, A. V., Klypin, A. A., Porciani, C., and Primack, J. R. (2001). A Universal Angular Momentum Profile for Galactic Halos. *ApJ*, 555:240–257.

Burkert, A., Förster Schreiber, N. M., Genzel, R., Lang, P., Tacconi, L. J., Wisnioski, E., Wuyts, S., Bandara, K., Beifiori, A., Bender, R., Brammer, G., Chan, J., Davies, R., Dekel, A., Fabricius, M., Fossati, M., Kulkarni, S., Lutz, D., Mendel, J. T., Momcheva, I., Nelson, E. J., Naab, T., Renzini, A., Saglia, R., Sharples, R. M., Sternberg, A., Wilman, D., and Wuyts, E. (2016). The Angular Momentum Distribution and Baryon Content of Star-forming Galaxies at z ‘ 1-3. *ApJ*, 826:214.

Burkhart, B. (2018). The Star Formation Rate in the Gravoturbulent Interstellar Medium. *ApJ*, 863:118.

Burkhart, B. and Loeb, A. (2016). Predicted Sizes of Pressure-supported HI Clouds in the Outskirts of the Virgo Cluster. *ApJ*, 824:L7.

Burkhart, B. and Mocz, P. (2019). The Self-gravitating Gas Fraction and the Critical Density for Star Formation. *ApJ*, 879(2):129.

Burkhart, B., Stalpes, K., and Collins, D. C. (2017). The Razors Edge of Collapse: The Transition Point from Lognormal to Power-Law Distributions in Molecular Clouds. *ApJ*, 834:L1.

Chiou, Y. S., Naoz, S., Burkhart, B., Marinacci, F., and Vogelsberger, M. (2019). The Supersonic Project: Shining Light on SIGOs—A New Formation Channel for Globular Clusters. *ApJ*, 878(1):L23.

Chiou, Y. S., Naoz, S., Marinacci, F., and Vogelsberger, M. (2018). The Supersonic Project: rotational effects of supersonic motions on the first structures in the Universe. *MNRAS*, 481(3):3108–3117.

Christlieb, N., Bessell, M. S., Beers, T. C., Gustafsson, B., Korn, A., Barklem, P. S., Karlsson, T., Mizuno-Wiedner, M., and Rossi, S. (2002). A stellar relic from the early Milky Way. *Nature*, 419:904–906.

Conroy, C., Loeb, A., and Spergel, D. N. (2011). Evidence against Dark Matter Halos Surrounding the Globular Clusters MGC1 and NGC 2419. *ApJ*, 741:72.

Dalal, N., Pen, U.-L., and Seljak, U. (2010). Large-scale BAO signatures of the smallest galaxies. *JCAP*, 11:007.

Danieli, S., van Dokkum, P., Conroy, C., Abraham, R., and Romanowsky, A. J. (2019). Still Missing Dark Matter: KCWI High-resolution Stellar Kinematics of NGC1052-DF2. *ApJ*, 874:L12.

Davis, T. A., van de Voort, F., Rowlands, K., McAlpine, S., Wild, V., and Crain, R. A. (2019). Evolution of the cold gas properties of simulated post-starburst galaxies. *MNRAS*, 484(2):2447–2461.

Decressin, T., Charbonnel, C., and Meynet, G. (2007). Origin of the abundance patterns in Galactic globular clusters: constraints on dynamical and chemical properties of globular clusters. *A&A*, 475:859–873.

Diemer, B., Mansfield, P., Kravtsov, A. V., and More, S. (2017). The Splashback Radius of Halos from Particle Dynamics. II. Dependence on Mass, Accretion Rate, Redshift, and Cosmology. *ApJ*, 843:140.

Dolag, K., Borgani, S., Murante, G., and Springel, V. (2009). Substructures in hydrodynamical cluster simulations. *MNRAS*, 399:497–514.

Druschke, M., Schauer, A. T. P., Glover, S. C. O., and Klessen, R. S. (2019). Shape and Spin of Minihaloes. II: The Effect of Streaming Velocities. *arXiv e-prints*, page arXiv:1906.09845.

Ebert, R. (1955). Über die Verdichtung von H I-Gebieten. Mit 5 Textabbildungen. *ZAp*, 37:217.

Elmegreen, B. G., Malhotra, S., and Rhoads, J. (2012). Formation of Metal-poor Globular Clusters in Lyα Emitting Galaxies in the Early Universe. *ApJ*, 757:9.

Elmegreen, D. M. and Elmegreen, B. G. (2017). Little Blue Dots in the Hubble Space Telescope Frontier Fields: Precursors to Globular Clusters? *ApJ*, 851:L44.

Fall, S. M. and Efstathiou, G. (1980). Formation and rotation of disc galaxies with haloes. *MNRAS*, 193:189–206.

Fialkov, A. and Barkana, R. (2014). The rich complexity of 21-cm fluctuations produced by the first stars. *MNRAS*, 445(1):213–224.

Fialkov, A., Barkana, R., Tseliakhovich, D., and Hirata, C. M. (2012). Impact of the relative motion between the dark matter and baryons on the first stars: semi-analytical modelling. *MNRAS*, 424:1335–1345.

Gieles, M., Heggie, D. C., and Zhao, H. (2011). The life cycle of star clusters in a tidal field. *MNRAS*, 413:2509–2524.

Girichidis, P., Konstandin, L., Whitworth, A. P., and Klessen, R. S. (2014). On the Evolution of the Density Probability Density Function in Strongly Self-gravitating Systems. *ApJ*, 781:91.

Glover, S. (2013). The First Stars. In Wiklind, T., Mobasher, B., and Bromm, V., editors, *The First Galaxies*, volume 396 of *Astrophysics and Space Science Library*, page 103.

Glover, S. C. O. and Jappsen, A.-K. (2007). Star Formation at Very Low Metallicity. I. Chemistry and Cooling at Low Densities. *ApJ*, 666:1–19.

Gnedin, N. Y. (2000). Effect of Reionization on Structure Formation in the Universe. *ApJ*, 542:535–541.

Gnedin, O. Y., Ostriker, J. P., and Tremaine, S. (2014). Co-evolution of Galactic Nuclei and Globular Cluster Systems. *ApJ*, 785:71.

Gratton, R. G., Carretta, E., and Bragaglia, A. (2012). Multiple populations in globular clusters. Lessons learned from the Milky Way globular clusters. *A&A Rev.*, 20:50.

Greif, T. H., Springel, V., White, S. D. M., Glover, S. C. O., Clark, P. C., Smith, R. J., Klessen, R. S., and Bromm, V. (2011). Simulations on a Moving Mesh: The Clustered Formation of Population III Protostars. *ApJ*, 737:75.

Grillmair, C. J., Freeman, K. C., Irwin, M., and Quinn, P. J. (1995). Globular Clusters with Tidal Tails: Deep Two-Color Star Counts. *AJ*, 109:2553.

Gunn, J. E. (1980). The dynamics of galaxies and the 'missing mass' problem. *Philosophical Transactions of the Royal Society of London Series A*, 296:313–318.

Guszejnov, D., Hopkins, P. F., Grudić, M. Y., Krumholz, M. R., and Federrath, C. (2018). Isothermal Fragmentation: Is there a low-mass cut-off? *MNRAS*, 480:182–191.

Harris, W. E. and Pudritz, R. E. (1994). Supergiant molecular clouds and the formation of globular cluster systems. *ApJ*, 429:177–191.

Hartwig, T., Glover, S. C. O., Klessen, R. S., Latif, M. A., and Volonteri, M. (2015). How an improved implementation of H_2 self-shielding influences the formation of massive stars and black holes. *MNRAS*, 452:1233–1244.

Heggie, D. C. and Hut, P. (1996). Dark Matter in Globular Clusters. In Hut, P. and Makino, J., editors, *Dynamical Evolution of Star Clusters: Confrontation of Theory and Observations*, volume 174 of *IAU Symposium*, page 303.

Heitmann, K., Lukić, Z., Fasel, P., Habib, S., Warren, M. S., White, M., Ahrens, J., Ankeny, L., Armstrong, R., O'Shea, B., Ricker, P. M., Springel, V., Stadel, J., and Trac, H. (2008). The cosmic code comparison project. *Computational Science and Discovery*, 1(1):015003.

Hetznecker, H. and Burkert, A. (2006). The evolution of the dark halo spin parameters λ and λ' in a ΛCDM universe: the role of minor and major mergers. *MNRAS*, 370:1905–1914.

Hirano, S., Hosokawa, T., Yoshida, N., and Kuiper, R. (2017a). Supersonic gas streams enhance the formation of massive black holes in the early universe. *Science*, 357:1375–1378.

Hirano, S., Yoshida, N., Sakurai, Y., and Fujii, M. S. (2017b). Formation of the first star cluster and massive star binaries by fragmentation of filamentary primordial gas clouds. *ArXiv e-prints*.

Ibata, R., Nipoti, C., Sollima, A., Bellazzini, M., Chapman, S. C., and Dalessandro, E. (2013). Do globular clusters possess dark matter haloes? A case study in NGC 2419. *MNRAS*, 428:3648–3659.

Jeans, J. H. (1902). The Stability of a Spherical Nebula. *Philosophical Transactions of the Royal Society of London Series A*, 199:1–53.

Jiang, F., Dekel, A., Kneller, O., Lapiner, S., Ceverino, D., Primack, J. R., Faber, S. M., Macciò, A. V., Dutton, A., Genel, S., and Somerville, R. S. (2018). Is the dark-matter halo spin a predictor of galaxy spin and size? *ArXiv e-prints*.

Katz, N., Weinberg, D. H., and Hernquist, L. (1996). Cosmological Simulations with TreeSPH. *ApJS*, 105:19.

Kimmig, B., Seth, A., Ivans, I. I., Strader, J., Caldwell, N., Anderton, T., and Gregersen, D. (2015). Measuring Consistent Masses for 25 Milky Way Globular Clusters. *AJ*, 149:53.

Krauss, L. M. and Chaboyer, B. (2003). Age Estimates of Globular Clusters in the Milky Way: Constraints on Cosmology. *Science*, 299:65–70.

Kravtsov, A. V. and Gnedin, O. Y. (2005). Formation of Globular Clusters in Hierarchical Cosmology. *ApJ*, 623:650–665.

Kruijssen, J. M. D. (2015). Globular clusters as the relics of regular star formation in 'normal' high-redshift galaxies. *MNRAS*, 454:1658–1686.

Krumholz, M. R. and McKee, C. F. (2005). A General Theory of Turbulence-regulated Star Formation, from Spirals to Ultraluminous Infrared Galaxies. *ApJ*, 630:250–268.

Latif, M. A., Niemeyer, J. C., and Schleicher, D. R. G. (2014). Impact of baryonic streaming velocities on the formation of supermassive black holes via direct collapse. *MNRAS*, 440:2969–2975.

Liao, S., Gao, L., Frenk, C. S., Guo, Q., and Wang, J. (2017). The segregation of baryons and dark matter during halo assembly. *MNRAS*, 470:2262–2269.

Lithwick, Y. and Dalal, N. (2011). Self-similar Solutions of Triaxial Dark Matter Halos. *ApJ*, 734:100.

Liu, R.-Y. and Wang, X.-Y. (2011). Modeling the Broadband Emission of GRB 090902B. *ApJ*, 730:1.

Maio, U., Koopmans, L. V. E., and Ciardi, B. (2011). The impact of primordial supersonic flows on early structure formation, reionization and the lowest-mass dwarf galaxies. *MNRAS*, 412:L40–L44.

Maller, A. H. and Dekel, A. (2002). Towards a resolution of the galactic spin crisis: mergers, feedback and spin segregation. *MNRAS*, 335:487–498.

Mandelker, N., van Dokkum, P. G., Brodie, J. P., van den Bosch, F. C., and Ceverino, D. (2018). Cold Filamentary Accretion and the Formation of Metal-poor Globular Clusters and Halo Stars. *ApJ*, 861:148.

Mashchenko, S. and Sills, A. (2005). Globular Clusters with Dark Matter Halos. I. Initial Relaxation. *ApJ*, 619:243–257.

McConnachie, A. W. (2012). The Observed Properties of Dwarf Galaxies in and around the Local Group. *AJ*, 144:4.

McQuinn, M. and O'Leary, R. M. (2012). The Impact of the Supersonic Baryon-Dark Matter Velocity Difference on the z ˜ 20 21 cm Background. *ApJ*, 760:3.

Mo, H. J., Mao, S., and White, S. D. M. (1998). The formation of galactic discs. *MNRAS*, 295:319–336.

Mocz, P. and Burkhart, B. (2018). Star formation from dense shocked regions in supersonic isothermal magnetoturbulence. *MNRAS*, 480:3916–3927.

Mocz, P., Vogelsberger, M., Robles, V. H., Zavala, J., Boylan-Kolchin, M., Fialkov, A., and Hernquist, L. (2017). Galaxy formation with BECDM - I. Turbulence and relaxation of idealized haloes. *MNRAS*, 471:4559–4570.

Moore, B. (1996). Constraints on the Global Mass-to-Light Ratios and on the Extent of Dark Matter Halos in Globular Clusters and Dwarf Spheroidals. *ApJ*, 461:L13.

More, S., Diemer, B., and Kravtsov, A. V. (2015). The Splashback Radius as a Physical Halo Boundary and the Growth of Halo Mass. *ApJ*, 810:36.

Muñoz, J. B. (2019). Robust velocity-induced acoustic oscillations at cosmic dawn. *Phys. Rev. D*, 100(6):063538.

Muratov, A. L. and Gnedin, O. Y. (2010). Modeling the Metallicity Distribution of Globular Clusters. *ApJ*, 718:1266–1288.

Naoz, S. and Barkana, R. (2005a). Growth of linear perturbations before the era of the first galaxies. *MNRAS*, 362:1047–1053.

Naoz, S. and Barkana, R. (2005b). Growth of linear perturbations before the era of the first galaxies. *MNRAS*, 362:1047–1053.

Naoz, S. and Barkana, R. (2007). The formation and gas content of high-redshift galaxies and minihaloes. *MNRAS*, 377:667–676.

Naoz, S., Barkana, R., and Mesinger, A. (2009). Gas in simulations of high-redshift galaxies and minihaloes. *MNRAS*, 399:369–376.

Naoz, S. and Narayan, R. (2013). Generation of Primordial Magnetic Fields on Linear Overdensity Scales. *Physical Review Letters*, 111(5):051303.

Naoz, S. and Narayan, R. (2014). Globular Clusters and Dark Satellite Galaxies through the Stream Velocity. *ApJ*, 791:L8.

Naoz, S., Noter, S., and Barkana, R. (2006). The first stars in the Universe. *MNRAS*, 373:L98–L102.

Naoz, S., Yoshida, N., and Barkana, R. (2011a). The non-linear evolution of baryonic overdensities in the early universe: initial conditions of numerical simulations. *MNRAS*, 416:232–241.

Naoz, S., Yoshida, N., and Barkana, R. (2011b). The non-linear evolution of baryonic overdensities in the early universe: initial conditions of numerical simulations. *MNRAS*, 416(1):232–241.

Naoz, S., Yoshida, N., and Gnedin, N. Y. (2012). Simulations of Early Baryonic Structure Formation with Stream Velocity. I. Halo Abundance. *ApJ*, 747:128.

Naoz, S., Yoshida, N., and Gnedin, N. Y. (2013). Simulations of Early Baryonic Structure Formation with Stream Velocity. II. The Gas Fraction. *ApJ*, 763:27.

Navarro, J. F., Frenk, C. S., and White, S. D. M. (1996). The Structure of Cold Dark Matter Halos. *ApJ*, 462:563.

Odenkirchen, M., Grebel, E. K., Dehnen, W., Rix, H.-W., Yanny, B., Newberg, H. J., Rockosi, C. M., Martínez-Delgado, D., Brinkmann, J., and Pier, J. R. (2003). The Extended Tails of Palomar 5: A $10\deg$ Arc of Globular Cluster Tidal Debris. *AJ*, 126:2385–2407.

O'Leary, R. M. and McQuinn, M. (2012). The Formation of the First Cosmic Structures and the Physics of the z ˜ 20 Universe. *ApJ*, 760:4.

Padmanabhan, T. (2002). *Theoretical Astrophysics*. Cambridge University Press.

Park, H., Ahn, K., Yoshida, N., and Hirano, S. (2020). First Structure Formation under the Influence of Gas-Dark Matter Streaming Velocity and Density: Impact of the Baryons-trace-dark matter Approximation. *arXiv e-prints*, page arXiv:2004.00863.

Peebles, P. J. E. (1969). Origin of the Angular Momentum of Galaxies. *ApJ*, 155:393.

Peebles, P. J. E. (1984). Dark matter and the origin of galaxies and globular star clusters. *ApJ*, 277:470–477.

Popa, C., Naoz, S., Marinacci, F., and Vogelsberger, M. (2016). Gas-rich and gas-poor structures through the stream velocity effect. *MNRAS*, 460:1625–1639.

Press, W. H. and Schechter, P. (1974). Formation of Galaxies and Clusters of Galaxies by Self-Similar Gravitational Condensation. *ApJ*, 187:425–438.

Reed, D. S., Bower, R., Frenk, C. S., Gao, L., Jenkins, A., Theuns, T., and White, S. D. M. (2005). The first generation of star-forming haloes. *MNRAS*, 363:393–404.

Rees, M. J. and Ostriker, J. P. (1977). Cooling, dynamics and fragmentation of massive gas clouds - Clues to the masses and radii of galaxies and clusters. *MNRAS*, 179:541–559.

Renaud, F., Agertz, O., and Gieles, M. (2017). The origin of the Milky Way globular clusters. *MNRAS*, 465:3622–3636.

Richardson, M. L. A., Scannapieco, E., and Thacker, R. J. (2013). Hybrid Cosmological Simulations with Stream Velocities. *ApJ*, 771:81.

Rodriguez-Gomez, V., Sales, L. V., Genel, S., Pillepich, A., Zjupa, J., Nelson, D., Griffen, B., Torrey, P., Snyder, G. F., Vogelsberger, M., Springel, V., Ma, C.-P., and Hernquist, L. (2017). The role of mergers and halo spin in shaping galaxy morphology. *MNRAS*, 467:3083–3098.

Saitoh, T. R., Koda, J., Okamoto, T., Wada, K., and Habe, A. (2006). Tidal Disruption of Dark Matter Halos around Proto-Globular Clusters. *ApJ*, 640:22–30.

Sarmento, R., Scannapieco, E., and Cohen, S. (2018). Following the Cosmic Evolution of Pristine Gas. II. The Search for Pop III-bright Galaxies. *ApJ*, 854:75.

Schaal, K. and Springel, V. (2015). Shock finding on a moving mesh - I. Shock statistics in non-radiative cosmological simulations. *MNRAS*, 446:3992–4007.

Schaerer, D. (2003). The transition from Population III to normal galaxies: Lyalpha and He II emission and the ionising properties of high redshift starburst galaxies. *A&A*, 397:527–538.

Schaerer, D. and Charbonnel, C. (2011). A new perspective on globular clusters, their initial mass function and their contribution to the stellar halo and the cosmic reionization. *MNRAS*, 413:2297–2304.

Schauer, A. T. P., Glover, S. C. O., Klessen, R. S., and Ceverino, D. (2019). The influence of streaming velocities on the formation of the first stars. *MNRAS*, 484(3):3510–3521.

Schauer, A. T. P., Regan, J., Glover, S. C. O., and Klessen, R. S. (2017). The formation of direct collapse black holes under the influence of streaming velocities. *MNRAS*, 471:4878–4884.

Schaye, J., Crain, R. A., Bower, R. G., Furlong, M., Schaller, M., Theuns, T., Dalla Vecchia, C., Frenk, C. S., McCarthy, I. G., Helly, J. C., Jenkins, A., Rosas-Guevara, Y. M., White, S. D. M., Baes, M., Booth, C. M., Camps, P., Navarro, J. F., Qu, Y., Rahmati, A., Sawala, T., Thomas, P. A., and Trayford, J. (2015). The EAGLE project: simulating the evolution and assembly of galaxies and their environments. *MNRAS*, 446:521–554.

Schneider, M. D., Frenk, C. S., and Cole, S. (2012). The shapes and alignments of dark matter halos. *JCAP*, 5:030.

Searle, L. and Zinn, R. (1978). Compositions of halo clusters and the formation of the galactic halo. *ApJ*, 225:357–379.

Seljak, U. and Zaldarriaga, M. (1996). A Line-of-Sight Integration Approach to Cosmic Microwave Background Anisotropies. *ApJ*, 469:437.

Sharma, S. and Steinmetz, M. (2005). The Angular Momentum Distribution of Gas and Dark Matter in Galactic Halos. *ApJ*, 628:21–44.

Sheth, R. K., Mo, H. J., and Tormen, G. (2001). Ellipsoidal collapse and an improved model for the number and spatial distribution of dark matter haloes. *MNRAS*, 323:1–12.

Sijacki, D., Vogelsberger, M., Kereš, D., Springel, V., and Hernquist, L. (2012). Moving mesh cosmology: the hydrodynamics of galaxy formation. *MNRAS*, 424:2999–3027.

Silk, J. (1977). On the fragmentation of cosmic gas clouds. I - The formation of galaxies and the first generation of stars. *ApJ*, 211:638–648.

Somerville, R. S., Behroozi, P., Pandya, V., Dekel, A., Faber, S. M., Fontana, A., Koekemoer, A. M., Koo, D., Pérez-González, P. G., Primack, J. R., Santini, P., Taylor, E. N., and van der Wel, A. (2017). The Relationship between Galaxy and Dark Matter Halo Size from z˜3 to the present. *ArXiv e-prints*.

Springel, V. (2005). The cosmological simulation code GADGET-2. *MNRAS*, 364:1105–1134.

Springel, V. (2010a). E pur si muove: Galilean-invariant cosmological hydrodynamical simulations on a moving mesh. *MNRAS*, 401:791–851.

Springel, V. (2010b). Smoothed Particle Hydrodynamics in Astrophysics. *ARA&A*, 48:391–430.

Stacy, A., Bromm, V., and Loeb, A. (2011). Effect of Streaming Motion of Baryons Relative to Dark Matter on the Formation of the First Stars. *ApJ*, 730:L1.

Tanaka, T. L. and Li, M. (2014). The formation of massive black holes in z 30 dark matter haloes with large baryonic streaming velocities. *MNRAS*, 439:1092–1100.

Tanaka, T. L., Li, M., and Haiman, Z. (2013). The effect of baryonic streaming motions on the formation of the first supermassive black holes. *MNRAS*, 435:3559–3567.

Taylor, M. A., Puzia, T. H., Gomez, M., and Woodley, K. A. (2015). Observational Evidence for a Dark Side to NGC 5128's Globular Cluster System. *ApJ*, 805:65.

Teklu, A. F., Remus, R.-S., Dolag, K., Beck, A. M., Burkert, A., Schmidt, A. S., Schulze, F., and Steinborn, L. K. (2015). Connecting Angular Momentum and Galactic Dynamics: The Complex Interplay between Spin, Mass, and Morphology. *ApJ*, 812:29.

Terlevich, E., Fernández-Arenas, D., Terlevich, R., Gieles, M., Chávez, R., and González-Morán, A. L. (2018). From Giant H II regions and H II galaxies to globular clusters and compact dwarf ellipticals. *MNRAS*, 481:268–276.

Trenti, M., Padoan, P., and Jimenez, R. (2015). The Relative and Absolute Ages of Old Globular Clusters in the LCDM Framework. *ApJ*, 808:L35.

Tseliakhovich, D., Barkana, R., and Hirata, C. M. (2011). Suppression and spatial variation of early galaxies and minihaloes. *MNRAS*, 418:906–915.

Tseliakhovich, D. and Hirata, C. (2010). Relative velocity of dark matter and baryonic fluids and the formation of the first structures. *Phys. Rev. D*, 82(8):083520.

van den Bosch, F. C., Abel, T., Croft, R. A. C., Hernquist, L., and White, S. D. M. (2002). The Angular Momentum of Gas in Protogalaxies. I. Implications for the Formation of Disk Galaxies. *ApJ*, 576:21–35.

van Dokkum, P., Danieli, S., Abraham, R., Conroy, C., and Romanowsky, A. J. (2019). A Second Galaxy Missing Dark Matter in the NGC 1052 Group. *ApJ*, 874:L5.

van Dokkum, P., Danieli, S., Cohen, Y., Merritt, A., Romanowsky, A. J., Abraham, R., Brodie, J., Conroy, C., Lokhorst, D., Mowla, L., O'Sullivan, E., and Zhang, J. (2018). A galaxy lacking dark matter. *Nature*, 555:629–632.

Vanzella, E., Calura, F., Meneghetti, M., Castellano, M., Caminha, G. B., Mercurio, A., Cupani, G., Rosati, P., Grillo, C., Gilli, R., Mignoli, M., Fiorentino, G., Arcidiacono, C., Lombini, M., and Cortecchia, F. (2019). Massive star cluster formation under the microscope at z = 6. *MNRAS*, 483:3618–3635.

Vanzella, E., Calura, F., Meneghetti, M., Mercurio, A., Castellano, M., Caminha, G. B., Balestra, I., Rosati, P., Tozzi, P., De Barros, S., Grazian, A., D'Ercole, A., Ciotti, L., Caputi, K., Grillo, C., Merlin, E., Pentericci, L., Fontana, A., Cristiani, S., and Coe, D. (2017). Paving the way for the JWST: witnessing globular cluster formation at z 3. *MNRAS*, 467:4304–4321.

Vanzella, E., De Barros, S., Cupani, G., Karman, W., Gronke, M., Balestra, I., Coe, D., Mignoli, M., Brusa, M., Calura, F., Caminha, G.-B., Caputi, K., Castellano, M., Christensen, L., Comastri, A., Cristiani, S., Dijkstra, M., Fontana, A., Giallongo, E., Giavalisco, M., Gilli, R., Grazian, A., Grillo, C., Koekemoer, A., Meneghetti, M., Nonino, M., Pentericci, L., Rosati, P., Schaerer, D., Verhamme, A., Vignali, C., and Zamorani, G. (2016). High-resolution Spectroscopy of a Young, Low-metallicity Optically Thin L = 0.02L* Star-forming Galaxy at z = 3.12. *ApJ*, 821:L27.

Velliscig, M., Cacciato, M., Schaye, J., Hoekstra, H., Bower, R. G., Crain, R. A., van Daalen, M. P., Furlong, M., McCarthy, I. G., Schaller, M., and Theuns, T. (2015). Intrinsic alignments of galaxies in the EAGLE and cosmo-OWLS simulations. *MNRAS*, 454:3328–3340.

Visbal, E., Barkana, R., Fialkov, A., Tseliakhovich, D., and Hirata, C. M. (2012). The signature of the first stars in atomic hydrogen at redshift 20. *Nature*, 487:70–73.

Vogelsberger, M., Genel, S., Sijacki, D., Torrey, P., Springel, V., and Hernquist, L. (2013). A model for cosmological simulations of galaxy formation physics. *MNRAS*, 436:3031–3067.

Vogelsberger, M., Genel, S., Springel, V., Torrey, P., Sijacki, D., Xu, D., Snyder, G., Bird, S., Nelson, D., and Hernquist, L. (2014a). Properties of galaxies reproduced by a hydrodynamic simulation. *Nature*, 509:177–182.

Vogelsberger, M., Genel, S., Springel, V., Torrey, P., Sijacki, D., Xu, D., Snyder, G., Nelson, D., and Hernquist, L. (2014b). Introducing the Illustris Project: simulating the coevolution of dark and visible matter in the Universe. *MNRAS*, 444:1518–1547.

Vogelsberger, M., Mohayaee, R., and White, S. D. M. (2011). Non-spherical similarity solutions for dark halo formation. *MNRAS*, 414:3044–3051.

Vogelsberger, M., Sijacki, D., Kereš, D., Springel, V., and Hernquist, L. (2012). Moving mesh cosmology: numerical techniques and global statistics. *MNRAS*, 425(4):3024–3057.

Walcher, C. J., Böker, T., Charlot, S., Ho, L. C., Rix, H.-W., Rossa, J., Shields, J. C., and van der Marel, R. P. (2006). Stellar Populations in the Nuclei of Late-Type Spiral Galaxies. *ApJ*, 649:692–708.

Walcher, C. J., van der Marel, R. P., McLaughlin, D., Rix, H.-W., Böker, T., Häring, N., Ho, L. C., Sarzi, M., and Shields, J. C. (2005). Masses of Star Clusters in the Nuclei of Bulgeless Spiral Galaxies. *ApJ*, 618:237–246.

Wang, L., Dutton, A. A., Stinson, G. S., Macciò, A. V., Gutcke, T., and Kang, X. (2017). NIHAO VII: predictions for the galactic baryon budget in dwarf to Milky Way mass haloes. *MNRAS*, 466(4):4858–4867.

White, S. D. M. and Rees, M. J. (1978). Core condensation in heavy halos - A two-stage theory for galaxy formation and clustering. *MNRAS*, 183:341–358.

Whitmore, B. C. and Schweizer, F. (1995). Hubble space telescope observations of young star clusters in NGC-4038/4039, 'the antennae' galaxies. *AJ*, 109:960–980.

Whitmore, B. C., Zhang, Q., Leitherer, C., Fall, S. M., Schweizer, F., and Miller, B. W. (1999). The Luminosity Function of Young Star Clusters in "the Antennae" Galaxies (NGC 4038-4039). *AJ*, 118:1551–1576.

Wise, J. H. (2012). First Light: A Brief Review. *arXiv e-prints*, page arXiv:1201.4820.

Xu, H., Norman, M. L., O'Shea, B. W., and Wise, J. H. (2016). Late Pop III Star Formation During the Epoch of Reionization: Results from the Renaissance Simulations. *ApJ*, 823:140.

Yoo, J., Dalal, N., and Seljak, U. (2011). Supersonic relative velocity effect on the baryonic acoustic oscillation measurements. *JCAP*, 7:18.

Yoshida, N., Omukai, K., Hernquist, L., and Abel, T. (2006). Formation of Primordial Stars in a ΛCDM Universe. *ApJ*, 652:6–25.

Zavala, J., Frenk, C. S., Bower, R., Schaye, J., Theuns, T., Crain, R. A., Trayford, J. W., Schaller, M., and Furlong, M. (2016). The link between the assembly of the inner dark matter halo and the angular momentum evolution of galaxies in the EAGLE simulation. *MNRAS*, 460:4466–4482.

Zjupa, J. and Springel, V. (2017). Angular momentum properties of haloes and their baryon content in the Illustris simulation. *MNRAS*, 466:1625–1647.